B- and D-meson decay constants from three-flavor lattice QCD

A. Bazavov, C. Bernard, C. M. Bouchard, C. DeTar, M. Di Pierro, A. X. El-Khadra, R. T. Evans, E. D. Freeland, E. Gámiz, Steven Gottlieb, U. M. Heller, J. E. Hetrick, R. Jain, A. S. Kronfeld, J. Laiho, L. Levkova, P. B. Mackenzie, E. T. Neil, M. B. Oktay, J. N. Simone, R. Sugar, D. Toussaint, and R. S. Van de Water (Fermilab Lattice and MILC Collaborations)

Phys. Rev. D **85**, 114506 — Published 8 June 2012

DOI: 10.1103/PhysRevD.85.114506

FERMILAB-PUB-11/651-T

B- and *D*-meson decay constants from three-flavor lattice QCD

A. Bazavov,[1] C. Bernard,[2] C.M. Bouchard,[3,4,5] C. DeTar,[6] M. Di Pierro,[7] A.X. El-Khadra,[3] R.T. Evans,[3] E.D. Freeland,[3,8] E. Gámiz,[4,9] Steven Gottlieb,[10] U.M. Heller,[11] J.E. Hetrick,[12] R. Jain,[3] A.S. Kronfeld,[4] J. Laiho,[13] L. Levkova,[6] P.B. Mackenzie,[4] E.T. Neil,[4] M.B. Oktay,[6] J.N. Simone,[4] R. Sugar,[14] D. Toussaint,[15] and R.S. Van de Water[1,*]

(Fermilab Lattice and MILC Collaborations)

[1] *Physics Department, Brookhaven National Laboratory, Upton, NY, USA*
[2] *Department of Physics, Washington University, St. Louis, Missouri, USA*
[3] *Physics Department, University of Illinois, Urbana, Illinois, USA*
[4] *Fermi National Accelerator Laboratory, Batavia, Illinois, USA*
[5] *Department of Physics, The Ohio State University, Columbus, OH, USA*
[6] *Physics Department, University of Utah, Salt Lake City, Utah, USA*
[7] *School of Computing, DePaul University, Chicago, Illinois, USA*
[8] *Department of Physics, Benedictine University, Lisle, Illinois, 60532, USA*
[9] *CAFPE and Departamento de Física Teórica y del Cosmos, Universidad de Granada, Granada, Spain*
[10] *Department of Physics, Indiana University, Bloomington, Indiana, USA*
[11] *American Physical Society, Ridge, New York, USA*
[12] *Physics Department, University of the Pacific, Stockton, California, USA*
[13] *SUPA, School of Physics and Astronomy, University of Glasgow, Glasgow, UK*
[14] *Department of Physics, University of California, Santa Barbara, California, USA*
[15] *Department of Physics, University of Arizona, Tucson, Arizona, USA*

We calculate the leptonic decay constants of $B_{(s)}$ and $D_{(s)}$ mesons in lattice QCD using staggered light quarks and Fermilab bottom and charm quarks. We compute the heavy-light meson correlation functions on the MILC asqtad-improved staggered gauge configurations which include the effects of three light dynamical sea quarks. We simulate with several values of the light valence- and sea-quark masses (down to $\sim m_s/10$) and at three lattice spacings ($a \approx 0.15$, 0.12, and 0.09 fm) and extrapolate to the physical up and down quark masses and the continuum using expressions derived in heavy-light meson staggered chiral perturbation theory. We renormalize the heavy-light axial current using a mostly nonperturbative method such that only a small correction to unity must be computed in lattice perturbation theory and higher-order terms are expected to be small. We use the two finer lattice spacings for our central analysis and use the third to help estimate discretization errors. We obtain $f_{B^+} = 196.9(9.1)$ MeV, $f_{B_s} = 242.0(10.0)$ MeV, $f_{D^+} = 218.9(11.3)$ MeV, $f_{D_s} = 260.1(10.8)$ MeV, and the SU(3) flavor-breaking ratios $f_{B_s}/f_B = 1.229(26)$ and $f_{D_s}/f_D = 1.188(25)$, where the numbers in parentheses are the total statistical and systematic uncertainties added in quadrature.

PACS numbers: 12.38.Gc, 13.20.Fc, 13.20.He
Keywords: Lattice QCD, leptonic decays of mesons, chiral perturbation theory

* E-mail contact: ruthv@bnl.gov

I. INTRODUCTION

Leptonic decays of B and D mesons, in which the hadron annihilates weakly to a W boson, are important probes of heavy-to-light quark flavor-changing interactions. When combined with a nonperturbative lattice QCD calculation of the heavy-light pseudoscalar meson decay constant, f_B or f_D, a precise experimental measurement of the leptonic decay width allows the determination of the Cabibbo-Kobayashi-Maskawa (CKM) quark-mixing matrix element $|V_{ub}|$ or $|V_{cd}|$. Conversely, if the relevant CKM matrix element is known from an independent process such as semileptonic decay or from CKM-unitarity constraints, a comparison of the decay constant from lattice QCD simulations with that measured by experiment provides a straightforward test of the Standard Model. As the lattice and experimental determinations become more precise, this test will become more sensitive and may ultimately reveal, through the appearance of a discrepancy, the presence of new physics in the quark flavor sector.

Improved determinations of the B meson decay constant f_B are of particular importance given the current, approximately 3-σ tension in the CKM unitarity triangle that may indicate the presence of new physics in B_d-mixing or $B \to \tau\nu$ decay [1–4]. The experimental uncertainty in the branching fraction $\mathcal{B}(B \to \tau\nu)$ is at present $\sim 30\%$ [5, 6], but this error is expected to be reduced to $\sim 10\%$ at next-generation B factories KEK-B [7] with the Belle II detector [8] and Super$B$ in Italy [9, 10] in as little as five or six years, at which point even modest improvements in the determination of f_B will significantly help constrain the apex of the CKM unitarity triangle and isolate the source of new physics [11].

Because leptonic decays are "gold-plated" processes in numerical lattice QCD simulations (they have a single stable hadron in the initial state and no hadrons in the final state [12]), they can be determined accurately using present lattice methods. Currently all lattice calculations of $f_{D_{(s)}}$ and $f_{B_{(s)}}$ that include the effects of three light dynamical quarks use staggered lattice fermions [13, 14] for the up, down, and strange quarks. Because staggered fermions are computationally cheaper than other lattice fermion formulations, they allow for QCD simulations with dynamical quarks as light as $0.05m_s$, several lattice spacings, down to $a \approx 0.045$ fm, large physical volumes, and high statistics. This enables lattice determinations of many light-light and heavy-light meson quantities with controlled systematic uncertainties. The results of staggered lattice calculations are largely in excellent numerical agreement with experimental results [12]. This includes both postdictions, such as the pion and kaon decay constants [15], and predictions, as in the case of the B_c meson mass [16]. Such successes give confidence that further calculations using the same methods are reliable. This is essential if lattice QCD calculations of hadronic weak matrix elements are to be used to test the Standard Model and search for new physics.

The staggered dynamical quark simulations used here employ the fourth-root procedure ("rooting") for eliminating unwanted extra quark degrees of freedom that arise from lattice fermion doubling. The rooting method is not standard quantum field theory, and at nonzero lattice spacing it leads to violations of unitarity [17–20] that can be considered nonlocal [21]. Nevertheless, there are strong arguments [22, 23] that the desired local, unitary theory of QCD is reproduced by the rooted staggered lattice theory in the continuum limit. Further, one can show [18, 24] that the unitarity-violating lattice artifacts in the pseudo-Goldstone boson sector can be described, and hence removed, using rooted staggered chiral perturbation theory (rSχPT), which is a low-energy effective description of the rooted staggered lattice theory [25–27]. When coupled with other analytical and numerical evidence (see Refs. [28–31] for reviews and Ref. [32] for a recent study), this gives us confidence that the rooting procedure is valid. Indeed, the validity of the rooted staggered lattice simulations is of critical importance to flavor physics phenomenology, since a majority of the unquenched, three-flavor lattice results for hadronic weak matrix elements used to determine CKM matrix elements and as inputs to constraints on the CKM unitarity triangle come from such simulations [33].

In this paper, we present new results for the leptonic decay constants of heavy-light mesons containing bottom and charm quarks. We use the "2+1" flavor asqtad-improved gauge configurations made publicly-available by the MILC Collaboration [34]. These ensembles include the effects of three light, dynamical sea-quark flavors: one with mass m_h near m_s (the physical strange-quark mass) and the other two with mass m_l as small as $0.1m_h$. We generate light valence quarks for the B and D mesons using the same staggered action as in the sea sector, and generate heavy bottom and charm quarks using the clover action [35] with the Fermilab interpretation [36]. Because the Fermilab method uses knowledge of the heavy-quark limit of QCD to systematically eliminate heavy-quark discretization errors, exploiting ideas of Symanzik [37, 38] and of heavy-quark effective theory (HQET) [39–41], it is well-suited for both bottom and charm quarks. We simulate with many values for the light up/down quark mass (the mass of our lightest pion in both the sea and valence sectors is ≈ 250 MeV), and at three lattice spacings $a \approx 0.09$ fm, $a \approx 0.12$ fm, and $a \approx 0.15$ fm. We then extrapolate our numerical lattice data to the physical up and down quark masses and continuum guided by expressions derived in staggered chiral perturbation theory for heavy-light mesons (HMSχPT) [42–44]. We try several fits of this type. Our most reliable results come from the data at $a \approx 0.09$ fm and $a \approx 0.12$ fm only. We use fits including all three lattices as part of our error analysis.

We match the heavy-light axial current to continuum QCD with a mostly nonperturbative approach, computing the flavor-diagonal (heavy-heavy and light-light) renormalization factors nonperturbatively and then calculate the

remaining flavor off-diagonal correction factor ($\rho_{A^4_{Qq}}$) in lattice perturbation theory [40, 45, 46]. This procedure has the advantage that $\rho_{A^4_{Qq}}$ is close to unity. Furthermore, tadpole diagrams cancel in the ratio needed to obtain $\rho_{A^4_{Qq}}$, thereby improving the convergence of the perturbative series. Empirically, the size of the 1-loop contribution to $\rho_{A^4_{Qq}}$ is found to be small.

Our results for the charmed-meson decay constants improve upon our published results for f_D and f_{D_s} in Ref. [47] in several ways. The coarsest lattices used in this work have a smaller lattice spacing ($a \approx 0.15$ fm) than those used in our previous work ($a \approx 0.18$ fm). The number of configurations in the two most chiral ensembles with $a \approx 0.12$ fm has been increased, approximately by factors of 1.4 (sea $m_l = 0.1m_h$) and 1.7 (sea $m_l = 0.14m_h$). We have added new data on a new $a \approx 0.09$ fm sea-quark ensemble with a light quark mass of $0.1m_h$. We now obtain our results from a combined analysis of our entire data set (all partially-quenched mass combinations and lattice spacings). Furthermore, we now compute the bottom meson decay constants f_B and f_{B_s}. We have presented reports on this project at several conferences [48–52]; in our final analysis of this data set we also improve upon bottom and charm quark mass-tuning, with increased statistics and a more sophisticated analysis of heavy-quark discretization effects.

This paper is organized as follows. In Sec. II, we present an overview of the calculation, including the gluon and light-quark actions used in generating the gauge configurations and the light- and heavy-quark actions used in constructing the heavy-light meson correlators. We also introduce the mostly nonperturbative method for matching the lattice heavy-light current to the continuum, and the treatment of heavy-quark discretization errors from the Fermilab action within our chiral-continuum extrapolation. Next, in Sec. III, we describe the details of our numerical simulations and we present the parameters used, such as the light-quark masses and lattice spacings. We also describe the procedure for tuning the hopping parameter in the clover action so that it corresponds to b and c quarks. In Sec. IV, we define the two-point correlation functions used to extract the decay constant at each value of the light-quark mass and lattice spacing. We use two different fitting procedures to obtain the decay constants that differ in their treatment of the statistical errors, choice of fit ranges and number of states, and choice of input correlators. We include the difference between the two in our estimate of the fitting systematic uncertainty. Next, we present the numerical details of the calculation of the heavy-light axial-current renormalization factor in Section V. Putting the results of the two previous sections together, in Sec. VI, we extrapolate the renormalized decay constant data at unphysical quark masses and nonzero lattice spacing to the physical light quark masses and zero lattice spacing using HMSχPT. In Sec. VII, we estimate the contributions of the various systematic uncertainties to the decay constants, discussing each item in our error budget separately. We present the final results for the decay constants in Sec. VIII, and compare them to other lattice QCD calculations and to experiment. We describe the impact of our results for current flavor physics phenomenology and then conclude by discussing the ongoing improvements to our calculations, and their future impact on searches for new physics in the quark flavor sector.

Appendix A applies HQET to the Fermilab action to obtain explicit expressions for heavy-quark discretization effects. Appendix B contains the complete set of fit results for the heavy-light pseudoscalar meson mass and renormalized decay constant for all combinations of sea-quark mass, light valence-quark mass, and heavy-quark mass used in the chiral-continuum extrapolation. These results will be included as an EPAPS attachment upon publication.

II. METHODOLOGY

The decay rate for a charged pseudoscalar meson H (with flavor content Q and $\bar{q}$) to leptons is, in the Standard Model,

$$\Gamma(H \to \ell\nu) = \frac{M_H}{8\pi} f_H^2 \left| G_F V_{Qq}^* m_\ell \right|^2 \left(1 - \frac{m_\ell^2}{M_H^2}\right)^2, \tag{2.1}$$

where M_H is the mass of the meson H, G_F is the Fermi constant, and V_{Qq} is the pertinent element of the CKM matrix. The decay constant f_H parameterizes the pseudoscalar-to-vacuum matrix element of the axial vector current,

$$\langle 0|\mathcal{A}^\mu|H(p)\rangle = ip^\mu f_H, \tag{2.2}$$

where p^μ is the 4-momentum of the pseudoscalar meson. The flavor contents of the associated vector current and CKM matrix element are given in Table I. Note that the neutral B_s decays to a charged lepton pair with an amplitude proportional to f_{B_s}; hence the CKM factor in the decay rate involves more than one CKM matrix element. Because this process is loop-suppressed in the Standard Model, it is potentially sensitive to new physics effects. These formulas hold for all pseudoscalar mesons; in the normalization convention used here, $f_\pi(|V_{ud}|/0.97425) = 130.41 \pm 0.20$ MeV [53].

TABLE I. Flavor content of the axial vector current and associated CKM matrix element.

H	$\mathcal{A}^\mu$	V
D	$\bar{d}\gamma^\mu\gamma^5 c$	V_{cd}^*
D_s	$\bar{s}\gamma^\mu\gamma^5 c$	V_{cs}^*
B	$\bar{b}\gamma^\mu\gamma^5 u$	V_{ub}
B_s	$\bar{b}\gamma^\mu\gamma^5 s$	—

In Eq. (2.2), the 1-particle state assumes the relativistic normalization convention. For mesons containing a heavy quark, however, it is more convenient to pull out factors of M_H to ensure a smooth $M_H \to \infty$ limit:

$$\langle 0|\mathcal{A}^\mu|H(p)\rangle\,(M_H)^{-1/2} = i(p^\mu/M_H)\phi_H. \tag{2.3}$$

In lattice QCD, the normalization of states on the left-hand side falls out of correlation functions more naturally. Thus, most of our analysis, including error analysis, focuses on ϕ_H. We then obtain $f_H = \phi_H/\sqrt{M_H}$ using the experimentally measured value of the meson mass [54].

To compute the decay constants with lattice gauge theory, we must choose a discretization for the heavy quark, the light quark, and the gluons. As in previous work [47, 55–58], we choose the Fermilab method for heavy quarks [36] and staggered quarks with the asqtad action [59] for the light (valence) quark. The gauge action is Symanzik improved, with couplings chosen to remove order $\alpha_s a^2$ errors from gluon loops [60], but not those from quark loops [61] (which became available only after the gauge-field generation was well underway).

For heavy bottom and charm quarks, we use the Sheikholeslami-Wohlert (SW) clover action [35] with the Fermilab interpretation [36], which connects to the continuum limit as $am_Q \to 0$. This is an extension of the Wilson action [62], which retains the Wilson action's smooth limit as $am_Q \to \infty$ and also remains well behaved for $m_Q a \approx 1$. Because this lattice action respects heavy-quark spin-flavor symmetry, one can apply HQET to organize the discretization effects. In essence, one uses HQET to develop the $1/m_Q$ expansion both for continuum QCD and for lattice gauge theory (LGT) [39–41]. Discretization effects are then captured order-by-order in the heavy-quark expansion by the difference of the short-distance coefficients in the descriptions of QCD and LGT. Thus, in principle, the lattice heavy-quark action can be improved to arbitrarily high orders in $1/m_Q$ by adjusting a sufficiently large number of parameters in the lattice action. (See Ref. [63] for details at dimension 6 and 7. In principle, the adjustment can be done nonperturbatively, such as in the scheme of Ref. [64].) In practice, we tune the hopping parameter κ and the clover coefficient $c_{\rm SW}$ of the SW action, to remove discretization effects through order $1/m_Q$ in the heavy-quark expansion.

The HQET analysis of cutoff effects could be applied to any lattice action with heavy-quark symmetry, such as the action of lattice NRQCD [65]. In the latter case, it is simply a different perspective on the usual approach to lattice NRQCD, which derives the heavy-quark Lagrangian formally, and then replaces derivatives with difference operators. A key feature of the Wilson, SW, Fermilab and OK [63] actions is their well-behaved continuum limit, which is especially important for charm. For $m_Q a < 1$, one can analyze the cutoff effects in a complementary way with the Symanzik effective action [37, 38]. This two-pronged attack shows that the difference of short-distance coefficients, mentioned above, vanishes as a suitable power of lattice spacing a. In this paper, we shall use our knowledge of this behavior to constrain heavy-quark discretization effects in several steps of our analysis. See Secs. III B, VI, and Appendix A for details.

The lattice and continuum currents are related by a matching factor Z_{A^μ} [40]:

$$Z_{A^\mu} A^\mu \doteq \mathcal{A}^\mu + \mathrm{O}\left(\alpha_s a\Lambda f_i(m_Q a)\right) + \mathrm{O}\left(a^2\Lambda^2 f_j(m_Q a)\right), \tag{2.4}$$

where $\doteq$ denotes equality of matrix elements, and the functions $f_{i,j}$ that depend on $m_Q a$ stem from the difference in the HQET short-distance coefficients. In the Fermilab method, they remain of order 1 for all values of $m_Q a$ [36, 63], and they are given explicitly in Appendix A. In this work, we compute Z_{A^μ} mostly nonperturbatively [45] and partly in one-loop perturbation theory. As shown in the analysis of Ref. [40], many of the Feynman diagrams in the perturbative expansion of $Z_{A^4_{Qq}}$ are common or similar to those in the flavor-conserving renormalization factors $Z_{V^4_{QQ}}$ and $Z_{V^4_{qq}}$, which can be computed nonperturbatively. Therefore, we define $\rho_{A^4_{Qq}}$ by

$$Z_{A^4_{Qq}} = \rho_{A^4_{Qq}} \sqrt{Z_{V^4_{qq}} Z_{V^4_{QQ}}}, \tag{2.5}$$

evaluating only $\rho_{A^4_{Qq}}$ in lattice perturbation theory.

TABLE II. The MILC three-flavor lattices and valence asqtad quark masses used in this work. All of the valence masses were used in version II of the correlator fits (Sec IV C), while only the ones in bold print were used in version I (Sec IV B).

$\approx a$ [fm]	am_h	am_l	u_0	r_1/a	$n_{\rm conf}\times$	$n_{\rm src}$	valence am_q
0.09	0.031	0.0031	0.8779	3.69	435×	4	**0.0031**, 0.0037, 0.0042, **0.0044**, 0.0052, **0.0062**, **0.0087**, **0.0124**, **0.0186**, **0.0272**, **0.031**
		0.0062	0.8782	3.70	557×	4	**0.0031**, 0.0037, **0.0044**, 0.0052, **0.0062**, **0.0087**, **0.0124**, **0.0186**, **0.0272**, **0.031**
		0.0124	0.8788	3.72	518×	4	**0.0031**, **0.0042**, **0.0062**, **0.0087**, **0.0124**, **0.0186**, **0.0272**, **0.031**
0.12	0.05	0.005	0.8678	2.64	678×	4	**0.005**, 0.006, **0.007**, 0.0084, **0.01**, 0.012, **0.014**, 0.017, **0.02**, 0.024, **0.03**, **0.0415**
		0.007	0.8678	2.63	833×	4	**0.005**, 0.006, **0.007**, 0.0084, **0.01**, 0.012, **0.014**, 0.017, **0.02**, 0.024, **0.03**, **0.0415**
		0.01	0.8677	2.62	592×	4	**0.005**, 0.006, **0.007**, 0.0084, **0.01**, 0.012, **0.014**, 0.017, **0.02**, 0.024, **0.03**, **0.0415**
		0.02	0.8688	2.65	460×	4	**0.005**, 0.006, **0.007**, 0.0084, **0.01**, 0.012, **0.014**, 0.017, **0.02**, 0.024, **0.03**, **0.0415**
		0.03	0.8696	2.66	549×	4	**0.005**, 0.006, **0.007**, 0.0084, **0.01**, 0.012, **0.014**, 0.017, **0.02**, 0.024, **0.03**, **0.0415**
0.15	0.0484	0.0097	0.8604	2.13	631×	4	**0.0048**, **0.007**, **0.0097**, 0.013, **0.0194**, 0.0242, **0.029**, 0.0387, **0.0484**
		0.0194	0.8609	2.13	631×	4	**0.0048**, **0.007**, **0.0097**, 0.013, **0.0194**, 0.0242, **0.029**, 0.0387, **0.0484**
		0.029	0.8614	2.13	576×	4	**0.0048**, **0.007**, **0.0097**, 0.013, **0.0194**, 0.0242, **0.029**, 0.0387, **0.0484**

The flavor-conserving factors account for most of the value of the heavy-light renormalization factor $Z_{A^4_{Qq}}$. They are obtained by enforcing the normalization condition, at zero momentum transfer,

$$1 = Z_{V^4_{qq}} \langle H_q | V^4_{qq} | H_q \rangle, \tag{2.6}$$

where H_q is a hadron containing a single quark of flavor q, and V^μ_{qq} is the lattice version of the degenerate vector current. This condition holds for all discretizations and quark masses and, hence, the heavy quark (*i.e.*, $Z_{V^4_{QQ}}$) as well. The remaining correction factor $\rho_{A^4_{Qq}}$ is close to unity due to the cancellation of most of the radiative corrections including tadpole graphs. Although such cancellations have only been explicitly shown at 1-loop in lattice perturbation theory [40, 46], we expect similar cancellations to persist at higher orders. Therefore, the perturbative truncation error in the heavy-light renormalization factor is subdominant.

III. LATTICE SIMULATION DETAILS

A. Parameters

Table II lists the subset of the ensembles of lattice gauge fields generated by the MILC Collaboration [31] used in this analysis. We now describe each entry in the table.

We analyze data at three lattice spacings: $a \approx 0.15$ fm, $a \approx 0.12$ fm, and $a \approx 0.09$ fm. The ensembles contain 2+1 flavors of sea quarks, using the asqtad-improved staggered action [59], and the square (fourth) root of the staggered determinant for the two degenerate light sea quarks (one strange sea quark). The sea contains one flavor with mass m_h close to the physical strange quark mass and two degenerate lighter flavors of mass m_l. The tadpole improvement factor u_0 is a parameter of the gauge and asqtad staggered (sea) quark action and is determined from the fourth root of the average plaquette. We calculate the two-point correlation functions on each ensemble from an average over four different time sources.

TABLE III. Table of clover coefficients and κ values for charm and bottom used in heavy-light two-point simulations.

			κ_{sim}	
$\approx a$ [fm]	am_l/am_h	$c_{\rm SW}$	charm	bottom
0.09	0.0031/0.031	1.478	0.127	0.0923
	0.0062/0.031	1.476		
	0.0124/0.031	1.473		
0.12	0.005/0.05	1.72	0.122	0.086
	0.007/0.05	1.72		
	0.01/0.05	1.72		
	0.02/0.05	1.72		
	0.03/0.05	1.72		
0.15	0.0097/0.0484	1.570	0.122	0.076
	0.0194/0.0484	1.567		
	0.0290/0.0484	1.565		

The relative lattice scale is determined by calculating r_1/a on each ensemble, where r_1 is related to the force between static quarks, $r_1^2 F(r_1) = 1.0$ [66, 67]. Table II lists r_1/a values for each of the ensembles that result from fitting the calculated r_1/a to a smooth function [68], as explained in Eqs. (115) and (116) of Ref. [31].

In order to fix the absolute lattice scale, one must compute a physical quantity which can be compared directly to experiment. The combination of the PDG's value of f_π with MILC's 2009 determination of $r_1 f_\pi$ [69] yields $r_1 = 0.3117(6)(^{+12}_{-31})$ fm. From an average of three methods for scale setting, including one based on Υ splittings, the HPQCD collaboration obtains $r_1 = 0.3133(23)(3)$ fm [70], consistent with MILC. Symmetrizing MILC's error range gives $r_1 = 0.3108(21)$ fm, and a straightforward average with the HPQCD result then yields $r_1 = 0.3120(16)$ fm. This average omits likely correlations, due to the use of MILC sea-quark configurations by both groups. Conservatively assuming a 100% correlation, we inflate the error to 0.0022 fm. Finally, for convenience, we also shift the central value slightly, back to the 2009 MILC central value. We thus take $r_1 = 0.3117(22)$ fm in this paper.

The complete list of light (asqtad) valence quark masses m_q simulated in this analysis is also given in Table II. The mass values are selected to be roughly logarithmically spaced, but to also include the set of light sea quark masses simulated at each lattice spacing. We use a multimass solver to compute the valence quark propagators. The marginal numerical cost of including masses heavier than our lightest $m_q \sim 0.1 m_s$ is small and logarithmic spacing is designed to constrain the chiral logarithms.

In Table III, we show the coefficient of the Sheikholeslami-Wohlert term $c_{\rm SW}$ of the clover action and the κ values used to compute heavy-light two-point functions. The coefficient of the clover term is set to the tadpole-improved tree-level value $c_{\rm SW} = u_0^{-3}$. For the $a \approx 0.09$ and 0.15 ensembles the tadpole coefficient is taken from the average plaquette. We note, however, that at lattice spacing $a \approx 0.12$ fm the tadpole coefficient u_0 appearing in both the valence asqtad action and the heavy quark clover action is taken from the average of the Landau link evaluated on the $am_l/am_h = 0.01/0.05$ ensemble. Hence, in our $a \approx 0.12$ fm lattice data there is a mismatch between light valence and sea quark mass definitions. As discussed in Sec. VII, this (inadvertent) choice leads to a small error in the decay constants. We have remedied this mismatch by using the plaquette u_0 everywhere in new runs started while this analysis was underway.

The charm and bottom kappa values listed in Table III are based on our initial kappa tuning analysis using about one fourth of our final statistics. We then used a larger data set to refine our determination of the κ values corresponding to bottom and charm as described in the next subsection. We adjust our data post-facto to correspond to tuned values of $\kappa_{\rm c}$ and $\kappa_{\rm b}$ using the measured value of the derivative $\delta\phi/\delta\kappa$.

B. Input quark masses m_c and m_b

Our method for tuning κ for charm and bottom quarks closely follows that of Ref. [58], where further details can be found. We start with the dispersion relation for a heavy particle on the lattice [36]

$$E^2(\boldsymbol{p}) = M_1^2 + \frac{M_1}{M_2}\boldsymbol{p}^2 + \frac{1}{4}A_4\,(a\boldsymbol{p}^2)^2 + \frac{1}{3}A_{4'}a^2\sum_{j=1}^{3}|p_j|^4 + \ldots, \tag{3.1}$$

TABLE IV. Hopping-parameter values used to compute the dispersion relation.

		κ_Q	
$\approx a$ [fm]	$n_{\rm conf} \times n_{\rm src}$	charm	bottom
0.09	1912×4	0.1240, 0.1255, 0.1270	0.090, 0.092, 0.094
0.12	592×4	0.114, 0.117, 0.119, 0.122, 0.124	0.074, 0.086, 0.093, 0.106
0.15	631×8	0.100, 0.115, 0.122, 0.125	0.070, 0.076, 0.080, 0.090

TABLE V. Hopping parameter values $\kappa_{\rm c}$ and $\kappa_{\rm b}$ corresponding to charm and bottom. The outputs of the tuning are labeled $\kappa_{\rm tuned}$, where the first error is from statistics and the second is from r_1, which enters through matching to the experimentally-measured D_s and B_s meson masses. The derivative $d\phi/d\kappa$ is used to correct the values of ϕ obtained with the simulated values $\kappa_{\rm sim}$ listed in Table III to the tuned values given below.

	charm		bottom	
$\approx a$ [fm]	$\kappa_{\rm tuned}$	$d\phi/d\kappa$	$\kappa_{\rm tuned}$	$d\phi/d\kappa$
0.09	0.12691(18)(13)	−21.66	0.0959(13)(3)	−7.41
0.12	0.12136(37)(19)	−18.23	0.0856(19)(3)	−6.82
0.15	0.12093(36)(24)	−15.40	0.0788(11)(3)	−6.07

where

$$M_1 \equiv E(\mathbf{0}) \tag{3.2}$$

is called the rest mass, and the kinetic mass is given by

$$M_2^{-1} \equiv \left.\frac{\partial E(\boldsymbol{p})}{\partial p_j^2}\right|_{\boldsymbol{p}=\mathbf{0}}. \tag{3.3}$$

These meson masses differ from corresponding quark masses, m_1 and m_2, by binding-energy effects. The bare mass or, equivalently, the hopping parameter κ must be adjusted so that these masses reproduce an experimental charmed or b-flavored meson mass. When they differ, as they do when $m_Q a \ll 1$, one must choose. Decay constants are unaffected by the heavy-quark rest mass m_1 [39], so it does not make sense to adjust the bare mass to M_1. We therefore focus on M_2, adjusting κ to the strange pseudoscalars D_s and B_s, both because the signal degrades for lighter spectator masses and because this avoids introducing an unnecessary systematic uncertainty due to a chiral extrapolation.

The first step is to compute the correlator $C_2^{(S_1S_2)}(t,\boldsymbol{p})$ in Eq. (4.8) (below) for several 3-momenta $\boldsymbol{p}$ and several values of κ and light quark mass, bracketing charm and bottom, and strange, respectively. We use all momenta such that $|\boldsymbol{p}| \le 4\pi/L$. Second, we fit the time dependence of the multichannel correlation matrix $C_2^{(S_1S_2)}$ to a sum of exponentials—including the usual staggered-fermion oscillating terms—and extract the ground state energy $aE(\boldsymbol{p})$ by minimization of an augmented χ^2 [58, 71, 72]. Third, we fit the energies to the dispersion relation given in Eq. (3.1), through $\mathrm{O}(p_i^4)$. The output of this fit is aM_1, M_1/M_2, A_4, and $A_{4'}$, all as functions of κ. Fourth, we form $M_2(\kappa)$ from the first two fit outputs and r_1/a, propagating the error with a single-elimination jackknife. Finally, we obtain our tuned $\kappa_{\rm c}$ and $\kappa_{\rm b}$ by interpolating in κ so that $M_2(\kappa)$ matches the experimentally known D_s and B_s masses. The κ values used to compute M_2 are listed in Table IV. For each of the lattice spacings listed, we used the ensemble with light-to-strange sea-quark mass ratio $am_l/am_h = 0.2$. The resulting tuned values of $\kappa_{\rm c}$ and $\kappa_{\rm b}$ are shown with errors in Table V.

We constrain the coefficients A_4 and $A_{4'}$ with Gaussian priors derived from the HQET theory of cutoff effects, adding the contribution of the priors to the χ^2 in the minimization procedure [71, 72]. (In principle, we could include such priors for M_1 and M_1/M_2 too, but in practice we take priors so wide that these fit parameters are solely data-driven.) Neglecting binding energies, we have exact tree-level expressions for a_4 and $a_{4'}$, the quark analogs of A_4 and $A_{4'}$. The differences $A_4 - a_4^{[0]}$ and $A_{4'} - a_{4'}^{[0]}$ stem from both perturbative and nonperturbative effects. The asymptotics of the former can be estimated along the lines of Appendix A 3, and the latter can be deduced following the methods of Refs. [39, 73]. Briefly, we constrain $A_n(\kappa)$, $n \in \{4, 4'\}$, to a Gaussian with central value

$$a_n^{[0]}(m_0 a) + \alpha_s a_n^{[1]}(m_0 a) + \bar{\Lambda} a\, A_n'(m_0 a). \tag{3.4}$$

Here $a_n^{[0]}$ is the exact tree-level contribution, $a_n^{[1]}$ is an estimate of the one-loop contribution, and A'_n is an expression for the binding-energy contribution. The width of the Gaussian is determined by combining in quadrature the chosen widths of the separate contributions, as outlined in Appendix A 3.

The details of the κ_c and κ_b determination differ from that of Ref. [58] in two respects. First, we use the pseudoscalar meson masses rather than the spin average of pseudoscalar and vector meson masses, leading to a modest reduction of the statistical error. Second, we include the quartic terms in Eq. (3.1), allowing us to fold discretization effects directly into the dispersion-relation fit. Although we consider these two changes improvements, the change in the tuned κ values as compared to Ref. [58] stems primarily from the substantial increase in statistics on key ensembles.

The computations of the correlation functions needed to extract ϕ_D and ϕ_B have been carried out using the fiducial values listed in Table III. These simulation κ's were obtained near the beginning of the project, but while the runs were in progress, we redetermined the hopping parameters utilizing increased statistics and reflecting an updated value of r_1 [69]. The resulting improved determinations of κ_c and κ_b differ slightly from the simulation values. In order to adjust ϕ from the simulated value $\kappa_{\rm sim}$ to the tuned value $\kappa_{\rm tuned}$, we write

$$\phi_{\rm tuned} = \phi_{\rm sim} + \frac{d\phi}{d\kappa}(\kappa_{\rm tuned} - \kappa_{\rm sim}), \tag{3.5}$$

where the derivatives $d\phi/d\kappa$ listed in Table V are obtained from tuning runs with nearby κ values. As explained in Sec. VII, these derivatives are also used to propagate to the decay constants the statistical and scale uncertainties on $\kappa_{\rm tuned}$ listed in Table V.

IV. TWO-POINT CORRELATOR FITS

We obtain the unrenormalized decay amplitude for every combination of heavy-quark mass, light-quark mass, and sea-quark ensemble by fitting the heavy-light meson two-point correlation functions, described in Sec. IV A. We use two independent fitting procedures, which we refer to as "Analysis I" and "Analysis II". These procedures differ in several respects. In Analysis I, we use a jackknife procedure for estimating errors, while in Analysis II, we use a bootstrap procedure. The two analyses also differ in their methods for handling autocorrelations in the data and in their choices of fit ranges, priors for masses and amplitudes, and numbers of states included. In the end, we use Analysis I (Sec. IV B) to obtain central values, and use differences from fits with different distance ranges and/or number of states included, and from Analysis II (Sec. IV C) to estimate the systematic error due to choices made in the fit procedure.

A. Lattice correlators

The lattice axial-vector current is given by

$$A_a^4(x) = [\bar{\Psi}(x)\gamma^4\gamma^5\Omega(x)]_a\chi(x), \tag{4.1}$$

where $\chi(x)$ is the one-component field appearing in the staggered action, and $\Omega(x) = \gamma_1^{x_1/a}\gamma_2^{x_2/a}\gamma_3^{x_3/a}\gamma_4^{x_4/a}$ is the transformation connecting naive and staggered fields [74]. The heavy-quark field Ψ is a four-component (Dirac) spinor field, and the remaining free Dirac index is interpreted as a taste label.

To remove tree-level discretization errors in the lattice axial current, the heavy-quark field Ψ is "rotated":

$$\Psi = [1 + ad_1\boldsymbol{\gamma}\cdot\boldsymbol{D}]\psi, \tag{4.2}$$

where ψ is the field appearing in the clover action. Tree-level improvement is obtained when

$$d_1 = \frac{1}{2+m_0a} - \frac{1}{2(1+m_0a)}, \tag{4.3}$$

where

$$m_0a = \frac{1}{u_0}\left(\frac{1}{2\kappa} - \frac{1}{2\kappa_{\rm crit}}\right) \tag{4.4}$$

is the tapdole-improved bare mass. The critical hopping parameter $\kappa_{\rm crit}$ is the one for which the clover-clover pion mass vanishes.

As usual in lattice gauge theory, we obtain the matrix element in (2.3) from two-point correlation functions. We introduce pseudoscalar operators

$$\mathcal{O}_a^{(S)}(x) = \sum_y [\bar{\psi}(y) S(y,x) \gamma^5 \Omega(x)]_a \chi(x), \tag{4.5}$$

depending on a "smearing" function S. In this work, we use two functions, the local (or unsmeared) source $S(x,y) = \delta_{xy}$, and the smeared source (in Coulomb gauge)

$$S(x,y) = \delta_{x_4 y_4} S(\boldsymbol{x} - \boldsymbol{y}), \tag{4.6}$$

where $S(\boldsymbol{r})$ is the $1S$ solution of the Richardson potential for the quarkonium systems [75]. We obtain $S(\boldsymbol{x} - \boldsymbol{y})$ by scaling the radial Richardson wavefunction to lattice units, interpolating it to lattice sites, and then using it as the spatial source for the heavy-quark propagators [76].

We introduce two-point correlation functions

$$\Phi_2^{(S)}(t) = \sum_{a=1}^{4} \sum_{\boldsymbol{x}} \left\langle {A_a^4}^\dagger(t,\boldsymbol{x}) \mathcal{O}_a^{(S)}(0) \right\rangle, \tag{4.7}$$

$$C_2^{(S_1 S_2)}(t,\boldsymbol{p}) = \sum_{a=1}^{4} \sum_{\boldsymbol{x}} e^{i\boldsymbol{p}\cdot\boldsymbol{x}} \left\langle {\mathcal{O}_a^{(S_1)}}^\dagger(t,\boldsymbol{x}) \mathcal{O}_a^{(S_2)}(0) \right\rangle, \tag{4.8}$$

where $\langle \bullet \rangle$ now represents the ensemble average. For large time separations, $\Phi_2^{(S)}$ is proportional to the matrix element ϕ_H, and the proportionality is determined from $C_2^{(SS)}(t,\boldsymbol{0})$. Each two-point function is constructed from a staggered quark propagator with local (δ) sources and sinks. We compute C_2 functions for all (four) combinations $S_1, S_2 = \delta$ and 1S, requiring heavy clover quark propagators with all combinations of 1S smeared and local sources and sinks. Only the local sink clover propagators are needed to compute the Φ_2 functions. With the sum over tastes in Eqs. (4.7) and (4.8), the correlation functions Φ_2 and C_2 can also be cast in a heavy-naive formalism [77].

The staggered light quarks in the axial-current and pseudoscalar two-point correlation functions lead to the presence of opposite-parity states that oscillate in time as $(-1)^t$. Hence the two-point functions take the following forms:

$$\begin{aligned} \Phi_2^{(S)}(t) = {} & A_\Phi^{(S)} \left(e^{-Mt} + e^{-M(T-t)} \right) + \widetilde{A}_\Phi^{(S)} (-1)^t \left(e^{-\widetilde{M}t} + e^{-\widetilde{M}(T-t)} \right) \\ & + A_\Phi'^{(S)} \left(e^{-M't} + e^{-M'(T-t)} \right) + \ldots, \end{aligned} \tag{4.9}$$

$$\begin{aligned} C_2^{(S_1 S_2)}(t, \vec{p}=0) = {} & A^{(S_1)} A^{(S_2)} \left(e^{-Mt} + e^{-M(T-t)} \right) + \widetilde{A}^{(S_1)} \widetilde{A}^{(S_2)} (-1)^t \left(e^{-\widetilde{M}t} + e^{-\widetilde{M}(T-t)} \right) \\ & + A'^{(S_1)} A'^{(S_2)} \left(e^{-M't} + e^{-M'(T-t)} \right) + \ldots, \end{aligned} \tag{4.10}$$

where a prime denotes a standard excited state of the same parity and a tilde denotes the mass or amplitude of an opposite-parity state. The oscillating behavior is visible throughout the entire lattice temporal extent, and must be included in fits to extract the ground-state mass and amplitudes.

We then obtain the renormalized decay amplitude in lattice units from the ratio

$$a^{3/2} \phi_H = \sqrt{2} \frac{Z_{A^4_{Qq}} A_\Phi^{(S)}}{A^{(S)}}, \tag{4.11}$$

where $A_\Phi^{(S)}$ and $A^{(S)}$ are the amplitudes of the ground state exponentials defined in Eqs. (4.9) and (4.10), and the renormalization factor $Z_{A^4_{Qq}}$ is discussed in Sec. V.

B. Analysis I

Our primary analysis of two-point correlation functions $\Phi_2^{(S)}$ and $C_2^{(S_1 S_2)}$—"Analysis I"—proceeds as follows. The amplitudes $A_\Phi^{(S)}$ and $A^{(S)}$ in Eq. (4.11) are determined from fits to multiple correlators using the full data correlation matrix. In Analysis I, we start by fitting combinations A, B, C and D in Table VI. We find combination A, which uses the axial-current correlator with a $1S$ smeared source and the pseudoscalar correlator with a $1S$ smeared source

TABLE VI. Combinations of two-point functions that can be used to extract $a^{3/2}\phi_H$. All combinations of two and three correlators are shown. Additional combinations of four or more correlators are not enumerated.

two-point function	fit combination A	B	C	D	E	F
$\Phi_2^{(1S)}(t)$	•		•	•	•	•
$\Phi_2^{(\delta)}(t)$		•	•	•	•	•
$C_2^{(1S,1S)}(t)$	•				•	•
$C_2^{(\delta,\delta)}(t)$		•			•	
$C_2^{(\delta,1S)}(t)$			•			•
$C_2^{(1S,\delta)}(t)$				•		

TABLE VII. Numbers of states and time ranges used in two-point Analysis I. In the number of states, "1+1" means one simple exponential and one oscillating state (opposite parity). The fits in columns two through five were used for the central values, while the fits in columns six through nine were used in estimating systematic errors from the choice of fit ranges (see Sec. VII C).

	central fits				alternate fits			
	charm		bottom		charm		bottom	
$\approx a$ [fm]	n_{states}	t range	n_{states}	t range	n_{states}	t range	n_{states}	t range
0.15	1+1	11–23	2+1	4–20	1+1	12–23	1+1	9–20
0.12	1+1	14–31	2+1	5–22	1+1	16–31	1+1	12–22
0.09	1+1	21–47	2+1	7–30	1+1	23–47	1+1	16–30

and sink, to be suitable. The extra complexity of combinations of three correlators (C and D) give little benefit, and the errors from combination A are somewhat smaller than those from combination B.

For fits to charm-light meson correlators, we include just one simple exponential (the desired state) and one oscillating exponential, which we call a "1+1 state fit". We choose the minimum distance, t_{min}, such that contributions from excited states are small compared to our statistical errors. Because we fit two propagators simultaneously while imposing the constraint that the masses be equal, this is a six parameter fit: two amplitudes for each propagator and a common mass for each of the simple and oscillating exponentials. To help stabilize the fit, the amplitudes and mass of the oscillating state are weakly constrained by Gaussian priors, which are incorporated as additional terms in χ^2 in the fitting procedure [71, 72]. The central values for these priors are determined by a trial fit where the prior for the opposite parity mass is set to 500 ± 250 MeV above the ground state mass,[1] and the amplitudes are unconstrained. Then the jackknife fits use central values for the opposite parity state amplitudes and mass determined by the trial fit, with Gaussian widths that are typically 3–10 times the error estimates on these parameters, so in the end the priors make a negligible contribution to χ^2. We have checked, by varying the prior widths for three of the 0.09 fm ensembles, that such wide priors are still narrow enough to ensure stable fits. We propagate the uncertainties in the correlator fits to the subsequent chiral-continuum extrapolation with a jackknife procedure. In the jackknife resamples, we center the priors at the values found in the fit to the full ensemble, again with widths that are typically three to ten times the error estimates on these parameters.

The bottom meson correlators fall off much more rapidly with t, so it is difficult to take a large enough minimum distance to insure that excited state contributions are negligible. Therefore we use a fit with two simple exponentials and one oscillating exponential or a "2+1 state fit". The mass of this excited state is also weakly constrained by priors in the same way that the opposite parity mass is, except that the width of the prior on the excited state mass is set to 200 MeV.

Figure 1 shows the heavy-light pseudoscalar mass as a function of the minimum time used in the fit. The left-hand plots show sample fits to bottom correlators, while the right-hand plots show sample fits to charm correlators. We select fitting ranges to give reasonable fits for all sea-quark ensembles and all valence-quark masses. We quantify the goodness-of-fit with the "p value" [54], which is the probability that a fit with this number of degrees of freedom would have a χ^2 larger than this value. Table VII gives the fit ranges for charm-light and bottom-light correlators on the three lattice spacings, both for the fits used for the central values and for alternate fits used in estimating

[1] Although 500 MeV is a reasonable guess for the mass gap to the first excited state of the meson, we actually expect that this excited state in the fit approximates the contributions of a number of physical states, likely including both single and multiparticle channels.

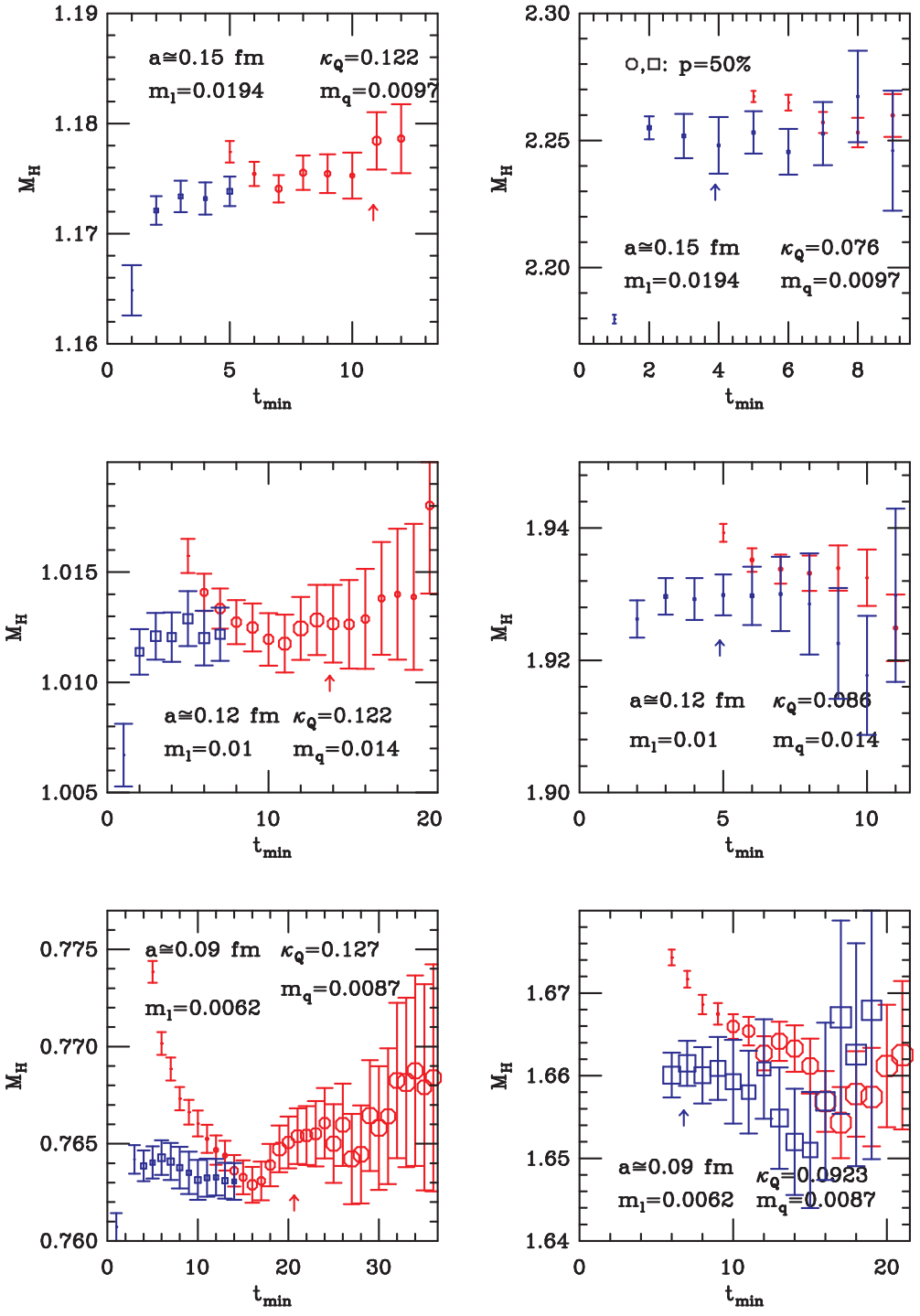

FIG. 1. Ground-state rest mass M_H versus minimum distance $t_{\rm min}$ included in the fit. For each lattice spacing, we show an ensemble with the dynamical light-quark mass m_l in the middle of the range. Similarly, we show correlators with a valence quark mass m_V in the center of the ranges used. The top two panels are at $a \approx 0.15$ fm, the middle two at $a \approx 0.12$ fm and the bottom two at $a \approx 0.09$ fm. In each row the left panel shows results for charm and the right-panel shows results for bottom. The size of each plot symbol is proportional to the p value (confidence level) of the fit, with the symbol size in the legends of the upper right panel corresponding to $p = 50\%$. The red octagons are for fits including one state of each parity ("1+1 fits") and the blue squares are for fits including an excited state of the same parity as the ground state ("2+1 fits"). In each panel, the arrow indicates the fit that is used in Sec. VI.

systematic errors from choices of fit parameters. The meson masses, $a^{3/2}\phi_H$ values, and p values for the data set used in Analysis I are tabulated in Appendix B.

The decay amplitude $a^{3/2}\phi_H$ is highly correlated among different light valence-quark masses on the same ensemble. To propagate the correlations among the different valence masses to the subsequent chiral-continuum extrapolation, in Sec. VI, we use a single-elimination jackknife procedure to estimate the covariance matrix of $a^{3/2}\phi_H$ for the selected valence quark masses. This is done by computing the covariance matrix of the single elimination jackknife samples, and multiplying by $(N-1)^2$, where N is the number of configurations in the ensemble. In fact, when all valence quark masses are kept, the covariance matrices are close enough to singular to be unmanageable. This reflects the fact that the correlators for intermediate valence masses can be very accurately predicted from the correlators for nearby masses, so some of the correlators provide very little new information. Therefore, we omit some valence quark masses, using only those set in bold in Table II.

We use a single elimination jackknife rather than an omit-J jackknife because a large number of samples are needed to compute a reliable covariance matrix. Successive configurations in the ensemble are not independent, however, so we must take autocorrelations into account. We do so by repeating the calculation after first blocking the data by a factor of four. (This block size of four is determined from tests on the $a \approx 0.12$ fm lattices using fit Analysis II, for which it gives a reasonable compromise between suppressing autocorrelations and leaving enough data points for the statistical analysis.) We then compute, for each valence-quark mass i, the ratio R_i of the diagonal element of the covariance matrix with a block size of four to the same element of the unblocked covariance matrix:

$$R_i = \sigma_{ii}^{(4)}/\sigma_{ii}, \tag{4.12}$$

where the superscript denotes the block size. The rescaled covariance matrix for $a^{3/2}\phi_H$ is given by

$$C_{ij}^{(4)} = C_{ij}\sqrt{R_i R_j}, \tag{4.13}$$

which preserves the eigenvalue structure of the covariance matrix, whereas simply using the covariance matrix of the blocked data would be more likely to produce spurious small eigenvalues. The rescaling factors R_i themselves have errors, and in many cases turn out to be less than one. In such cases, we do not replace the R_i by one, despite the fact that this would likely be a better estimate of the individual R_i. Doing so would yield a covariance matrix with a bias toward larger errors, and could produce misleading estimates of goodness-of-fit in the later analysis.

Finally, we combine the covariance matrices from all of the individual ensembles into larger covariance matrices, one each for the charm and bottom $a^{3/2}\phi_H$. Since different ensembles are statistically independent, these large covariance matrices are block diagonal, with each block containing the correlations among different light valence-quark masses on a single sea-quark ensemble.

C. Analysis II

Analysis II is a second, independent analysis of the two-point correlators that uses the bootstrap method to propagate correlated errors from the two-point analysis through to the chiral extrapolations. In Analysis II, we block average the two-point correlator data over four sequential configurations (which themselves are spaced by more than four trajectories) before the analysis. In the bootstrap procedure, we resample the data (with replacement), taking the number of sampled configurations to be equal to the number of blocked configurations in each bootstrap ensemble. For each bootstrap ensemble, we recompute the covariance matrix. During the bootstrap process, we randomly draw from a gaussian distribution new prior mean values of each constrained parameter belonging to an excited state while keeping the widths fixed. The ground state parameters are given loose priors so that the fitted values are determined by the data. To help stabilize the fits, the ground state prior means are not randomized in the bootstrap. Prior values for the energy splittings are taken from a chiral quark model calculation for the D and B meson systems [78]. Prior widths are taken to be about 200 MeV for excited states. Excited state amplitudes $\log(A^{(S)})$ have a prior width $\sigma_{\log A} = 2$.

On each gauge ensemble, the same sequence of gauge resamplings is taken for all valence m_q to preserve correlations among $a^{3/2}\phi_H$ values. Our final results are based upon 4,000 bootstrap replications of the data. We use the central values of $a^{3/2}\phi_H$ from the fits to the entire ensemble in the chiral-continuum extrapolation, and use the bootstrap values to obtain the covariance matrix.

To optimize the determination of $a^{3/2}\phi_H$, we compare simultaneous fits of up to six two-point functions; the various combinations of up to four functions are listed in Table VI. At a minimum, one axial-current correlator must be paired with one propagator (combinations A or B in Table VI) to extract $a^{3/2}\phi_H$. Combination A, using smeared operators, is used in Analysis I, described above. Because fits of four or more two-point functions over a wide time range can lead to a poorly determined data covariance matrix having large rank relative to the number of available configurations, we

focus on combinations having two or three correlators. Unlike combination A, combination B does not take advantage of smeared sources and the ratio does not show convincing plateaus over the range of times with decent signal to noise. Comparing combination C to D, the smeared source in C is less noisy than the smeared sink in D.

Given these considerations, for fits to charm correlators, we use two-point function combination C to obtain $a^{3/2}\phi_H$ which uses both of the axial current functions. We look for stability of the ground-state mass and amplitude when varying $t_{\rm min}$, $t_{\rm max}$, and the number of excited states included in the fit. We also compare fit results from other combinations of correlators to check that we have isolated the correct ground-state energy and matrix element. Our final results come from fits accounting for two pseudoscalar states and two (oscillating) opposite-parity states.

For fits to bottom correlators, we use combination B for our final results; this is the same set used in Analysis I. Combination C gives fits with rather low confidence levels for the B meson and tends to result in larger errors for $a^{3/2}\phi_H$. Again, we examine fits varying the time range; we also try fits with up to three pseudoscalar states plus three oscillating opposite parity states. We use these fits and fits to alternate combinations of two-point correlators as a consistency check.

The fit results from the two different analyses are consistent with each other for most cases, but there are a few cases where they differ by a standard deviation or more (see Figure 11). The $a^{3/2}\phi_H$ results from the two analyses are propagated through the chiral-continuum extrapolations in Secs. VI B and VI C. The resulting differences in the extrapolated results in turn provide the basis for our systematic error analysis due to fit choices given in Sec. VII C.

V. HEAVY-LIGHT CURRENT MATCHING

In this section, we discuss in more detail the ingredients of Eq. (2.5), which allow a "mostly nonperturbative" matching procedure [45].

A. Perturbative calculation of $\rho_{A^4_{Qq}}$

The perturbative expansion of $\rho_{A^4_{Qq}}$ can be written as

$$\rho_{A^4_{Qq}} = 1 + \alpha_s(q^*)\rho^{[1]}_{A^4}(m_Q a, m_q a) + \ldots . \tag{5.1}$$

where α_s is the strong coupling and $\rho^{[1]}_{A^4}$ is the one-loop coefficient. The one-loop coefficient is calculated in Ref. [46] using lattice perturbation theory, where we see explicitly that $\rho^{[1]}_{A^4}$ is small because most of the one-loop corrections cancel. The self-energy contributions cancel exactly (to all orders, in fact), and, in practice, we are in a region where $\rho^{[1]}_{A^4}(m_Q a, m_q a)$, viewed as a function of $m_Q a$, has two zeroes. Therefore the renormalization factor $\rho_{A^4_{Qq}}$ is close to unity for both bottom and charm.

The perturbative calculation of $\rho_{A^4_{Qq}}$ in Eq. (5.1) proceeds as follows. We use $\alpha_s(q^*)$ defined in the V scheme [79] as determined in Ref. [80], and take $q^* = 2/a$, which is close to the optimal choice of Refs. [79, 81] for a wide range of quark masses. The one-loop coefficients $\rho^{[1]}_{A^4}$ are computed for light-quark masses $am_q = 0.001, 0.01, 0.04$ to cover the range used in this analysis. From these we obtain $\rho_{A^4_{Qq}}$ at other light-quark masses by linear interpolation in am_q. For illustration, Table VIII lists $\rho_{A^4_{bq}}$ and $\rho_{A^4_{cq}}$ evaluated at the light valence mass $am_q = 0.01$ for the eleven sea-quark ensembles used in this work. Note that the sea-quark mass dependence is indirect, via the plaquette used to determine $\alpha_s(q^*)$. The dependence on the light-quark mass in the current is very mild: for bottom, $\rho_{A^4_{bq}}$ changes with am_q by 0.07–0.2%, depending on lattice spacing, and for charm, $\rho_{A^4_{cq}}$ changes by around 0.1%. On the fine ensembles, the am_q dependence is almost as large as the total one-loop correction because the overall cancellation, especially in $\rho_{A^4_{cq}}$, is so fortuitously good.

B. Nonperturbative computation of $Z_{V^4_{qq}}$ and $Z_{V^4_{QQ}}$

The nonperturbative part of the matching factor $Z_{A^4_{Qq}}$ is obtained from the temporal components of the clover-clover and staggered-staggered vector currents. At zero-momentum transfer, the (correctly normalized) vector current simply counts flavor-number, so it is possible to obtain Z_{V^4} nonperturbatively for any discretization and any mass [45].

TABLE VIII. The perturbative correction factor $\rho_{A^4_{Qq}}$ for the heavy-light current A^4 at the simulated charm and bottom heavy quark κ values given in Table III and at $am_q = 0.01$ for the different sea-quark ensembles. The statistical errors associated with the numerical integration are negligible.

$\approx a$ [fm]	am_l/am_h	$\rho_{A^4_{bq}}$	$\rho_{A^4_{cq}}$
0.09	0.0031/0.031	1.0026	1.0000
	0.0062/0.031	1.0026	1.0000
	0.0124/0.031	1.0026	1.0000
0.12	0.005/0.05	1.0081	0.9959
	0.007/0.05	1.0081	0.9959
	0.010/0.05	1.0081	0.9959
	0.020/0.05	1.0080	0.9960
	0.030/0.05	1.0079	0.9961
0.15	0.0097/0.0484	1.0270	0.9937
	0.0194/0.0484	1.0267	0.9938
	0.0290/0.0484	1.0265	0.9938

For the staggered-staggered current, we compute

$$C_3^{(S_1S_2)}(t_2,0,t_1) = \sum_{ab}\sum_{\boldsymbol{x},\boldsymbol{y}} \left\langle \mathcal{O}_a^{(S_1)}(t_2,\boldsymbol{y}) V^4_{ab}(0) {\mathcal{O}_b^{(S_2)}}^\dagger(t_1,\boldsymbol{x}) \right\rangle, \tag{5.2}$$

where, as in Eq. (4.5), $\mathcal{O}_a^{(S)}$ is a smeared or local clover-staggered meson operator with mass chosen to optimize the signal, and

$$V^4_{ab}(x) = \bar{\chi}(x)[\Omega^\dagger(x)\gamma^4\Omega(x)]_{ab}\chi(x) \tag{5.3}$$

is the temporal component of the staggered-staggered vector current. The three-point functions C_3 are computed from the same staggered quarks used for the clover-staggered two point functions. The staggered quark is transformed into an improved naive quark by applying the Ω matrix; this naive quark at time t_1 is then used as the source term when computing the charm propagator. We smear the source at t_1 so that $S_1 = S_2$.

We compute $Z_{V^4_{qq}}$ using a D_q meson [*cf.* Eq. (4.5)], which provides a good signal. The three-point function $C_3^{(S_1S_2)}(t_2,0,t_1)$ contains states of both the desired and the opposite parity, with the latter carrying oscillating $(-1)^t$ dependence. We construct $C_3^{(S_1S_2)}(t_2,0,t_1)$ with local sources $S_1 = S_2 = \delta$ and compute it at multiple even and odd values of t_1 and t_2 in order to disentangle the ground-state amplitude from the other contributions.

Within the time range $t_1 < 0 < t_2$ and in the limit of large separations, $|t_1|, t_2 \gg a$,

$$\begin{aligned} C_3^{(\delta,\delta)}(t_2,0,t_1) = {} & Z^{-1}_{V^4_{qq}} A^2 \exp\left(-E(t_2-t_1)\right) \\ & + Z'AB\left[(-1)^{t_1}\exp\left(E't_1 - Et_2\right) + (-1)^{t_2}\exp\left(Et_1 - E't_2\right)\right] \\ & + Z''B^2(-1)^{(t_1+t_2)}\exp\left(-E'(t_2-t_1)\right) + \ldots, \end{aligned} \tag{5.4}$$

neglecting contributions from excited states. We extract $Z_{V^4_{qq}}$ from a minimum χ^2 fit to the three-point function using the right-hand side of Eq. (5.4) as the model function. The fit is linear in the free parameters $Z^{-1}_{V^4_{qq}}$, Z'' and Z', while we fix the ground-state energies E and E', and the operator overlaps A and B to the values determined by fitting the two-point function $C_2^{(\delta)}(t,\mathbf{0})$. We use a single-elimination jackknife procedure to compute the data covariance matrix.

Table IX presents our results for $Z_{V^4_{qq}}$ on the ensembles used in this work. The three-point functions for the $Z_{V^4_{qq}}$ calculation are generated at a single source time, $t_{\rm src} = 0$ (instead of the four used for two-point functions $\Phi_2^{(S)}$ and $C_2^{(S_1S_2)}$). At $a \approx 0.12$ fm we have results at two values of the sea quark masses which are consistent within errors. At $a \approx 0.09$ and 0.15 fm we have results for several values of m_q. We do not see evidence for a dependence upon m_q with current statistics. The errors, however, increase at smaller quark mass. Hence, we use the $Z_{V^4_{qq}}$ corresponding to $m_q \sim m_s$ in Eq. (4.11). In the table, they are set in **bold**.

TABLE IX. Light-light vector current renormalization factor $Z_{V^4_{qq}}$. Values in bold are used in computing the heavy-light current renormalizations. With our conventions, the tree-level value of $Z_{V^4_{qq}}$ is 2. A colon is used to represent the range of time values included in the fit.

$\approx a$ [fm]	am_l/am_h	$n_{\rm conf}$	$-t_1$	t_2	am_q	$Z_{V^4_{qq}}$
0.09	0.0124/0.031	518	23:12	11:13	0.0272	**1.868(49)**
			23:12	11:13	0.0124	1.883(69)
0.12	0.01/0.05	592	15:9	7:11	0.03	**1.853(45)**
	0.007/0.05	523	20:7	7:12	0.03	1.882(56)
0.15	0.0097/0.0484	631	20:5	4:12	0.0484	**1.704(34)**
			20:5	4:12	0.029	1.709(40)
			20:5	4:12	0.0242	1.711(42)
			20:5	4:12	0.0194	1.707(45)
			20:5	4:12	0.0097	1.662(55)

For the clover-clover current, we compute

$$\widetilde{C}_3^{(S_1S_2)}(t_2,t_1,0)=\sum_{\boldsymbol{x},\boldsymbol{y}}\left\langle\widetilde{\mathcal{O}}^{(S_1)\dagger}(t_2,\boldsymbol{y})V^4_{QQ}(t_1,\boldsymbol{x})\widetilde{\mathcal{O}}^{(S_2)}(0)\right\rangle, \tag{5.5}$$

where

$$V^4_{QQ}(x)=\bar{\Psi}(x)\gamma^4\Psi(x) \tag{5.6}$$

is the temporal component of the (rotated) clover-clover vector current. The clover-clover bilinear

$$\widetilde{\mathcal{O}}^{(S)}(x)=\sum_y\bar{\psi}(y)S(x,y)\gamma^5 s(x) \tag{5.7}$$

consists of a heavy-quark field corresponding to charm or bottom, as the case may be, and a light clover-quark field s with mass chosen to provide a good signal. At large time separations, these three-point functions are proportional to $Z^{-1}_{V^4_{QQ}}$, with the proportionality coming from

$$\widetilde{C}_2^{(S_1S_2)}(t)=\sum_{\boldsymbol{x}}\left\langle\widetilde{\mathcal{O}}^{(S_1)\dagger}(t,\boldsymbol{x})\widetilde{\mathcal{O}}^{(S_2)}(0)\right\rangle. \tag{5.8}$$

We compute $Z_{V^4_{QQ}}$ using a $\bar{Q}s$ meson, where the strange quark is simulated with the clover action to circumvent oscillating opposite-parity states [*cf.* Eq. (5.7)]. We restrict our calculation of $\widetilde{C}_{2,3}$ to $S=S_1=S_2$ using both local and 1S smearing functions. The function $\widetilde{C}_2$ combines a local-local clover quark with mass around m_s and a heavy clover quark propagator with source and sink S. The function $\widetilde{C}_3$ requires the same heavy- and light-quark propagators as needed in $\widetilde{C}_2$. An additional heavy-quark propagator originating from t_2 has as its source the light quark propagator restricted to t_2, multiplied by γ_5 and convolved with smearing function S.

In Eq. (5.7), we use a random color wall source with three dilutions for both the heavy and light spectator quarks that originate from $t=0$. We generate two- and three-point functions for both local-local and smeared-smeared source-sink combinations where the smearing is applied to the heavy quark. We compute the 2- and 3-point functions at several values of κ spanning a range from around the charm quark to the bottom quark. We determine $Z_{V^4_{QQ}}$ from a fit to the plateaus in the jackknifed ratio of the three-point and two-point functions. Our results are summarized in Table X.

In order to properly normalize the derivative $d\phi/d\kappa_Q$ (see Eq. (3.5)), we need values of $Z_{V^4_{QQ}}$ at κ values other than those used in the $Z_{V^4_{QQ}}$ simulations. We therefore fit the simulation results to the interpolating quartic polynomial

$$Z_{V^4_{QQ}}(\kappa)=1+\sum_{j=1}^{4}c_j\kappa^j \tag{5.9}$$

which reproduces the infinite mass limit $Z_{V^4_{QQ}}\to 1$. Our codes employ the hopping parameter version of the action; so, at tree level $c_1=-6u_0$ and for $j>1$, $c_j=0$. We constrain the interpolation parameters to the tree-level values

TABLE X. Heavy-heavy vector current renormalization factor $Z_{V^4_{QQ}}$ computed at several κ values, covering the charm and bottom quark masses, for three lattice spacings.

$\approx a$ [fm]	am_l/am_h	$n_{\rm conf} \times n_{\rm src}$	κ_Q	$Z_{V^4_{QQ}}$
0.09	0.0062/0.031	1912×2	0.1283	0.2749(4)
			0.127	0.2830(4)
			0.110	0.3856(6)
			0.0950	0.4730(8)
			0.0931	0.4840(9)
0.12	0.007/0.05	2110×2	0.124	0.2899(4)
			0.122	0.3028(4)
			0.116	0.3410(5)
			0.098	0.4507(7)
			0.086	0.5209(10)
			0.074	0.5894(15)
0.15	0.0194/0.0484	631×2	0.122	0.3195(14)
			0.118	0.3440(16)
			0.088	0.5195(48)
			0.076	0.5898(81)

TABLE XI. Heavy-heavy vector current renormalization factor $Z_{V^4_{QQ}}$ corresponding to the charm and bottom $\kappa_{\rm sim}$ values used in the decay constant simulations.

	charm		bottom	
$\approx a$ [fm]	κ_Q	$Z_{V^4_{QQ}}$	κ_Q	$Z_{V^4_{QQ}}$
0.09	0.127	0.2829(4)	0.0923	0.4891(9)
0.12	0.122	0.3029(4)	0.086	0.5216(10)
0.15	0.122	0.3199(14)	0.076	0.5868(81)

taking $\sigma_j = 4$ as the widths. Table XI shows values for $Z_{V^4_{QQ}}$ interpolated to the nominal charm and bottom $\kappa_{\rm sim}$ used in our decay constant runs. Figure 2 plots the data in Table X together with the interpolation of Eq. (5.9). To aid perturbative intuition, the values of $Z_{V^4_{QQ}}$ in the figure are scaled by the tree-level expression $1 - 6u_0\kappa$; the relation between κ and $m_0a/(1 + m_0a)$ can be inferred from Eq. (4.4).

VI. CHIRAL AND CONTINUUM EXTRAPOLATION

In this section, we present the combined chiral and continuum extrapolations used to obtain the physical values of the $B_{(s)}$ and $D_{(s)}$ meson decay constants. We first discuss the use of $SU(3)$ chiral perturbation theory for heavy-light mesons in Sec. VI A, giving the formulas used for the chiral fits and describing our method for incorporating heavy-quark and light-quark discretization effects into the extrapolation. We then show the chiral fits for the D system in Sec. VI B, and for the B system in Sec. VI C.

A. Chiral Perturbation Theory framework

The errors introduced by the chiral and (light-quark) continuum extrapolations are controlled with rooted staggered chiral perturbation theory (rSχPT) [25, 26] applied to heavy-light mesons. In Ref. [42], the heavy-light decay constant was calculated to one-loop in rSχPT at leading order in the heavy-quark expansion [$(1/M_H)^0$], where M_H is a generic heavy-light meson mass. A replica trick is used in rSχPT to take into account the effect of the fourth root of the staggered determinant [18, 24].

In addition to using the form calculated in Ref. [42], we also use a chiral fit form that includes, in the loops, the effects of hyperfine splittings (*e.g.*, $M_B^* - M_B$) and flavor splittings (*e.g.*, $M_{B_s} - M_B$). These splittings are ~ 100

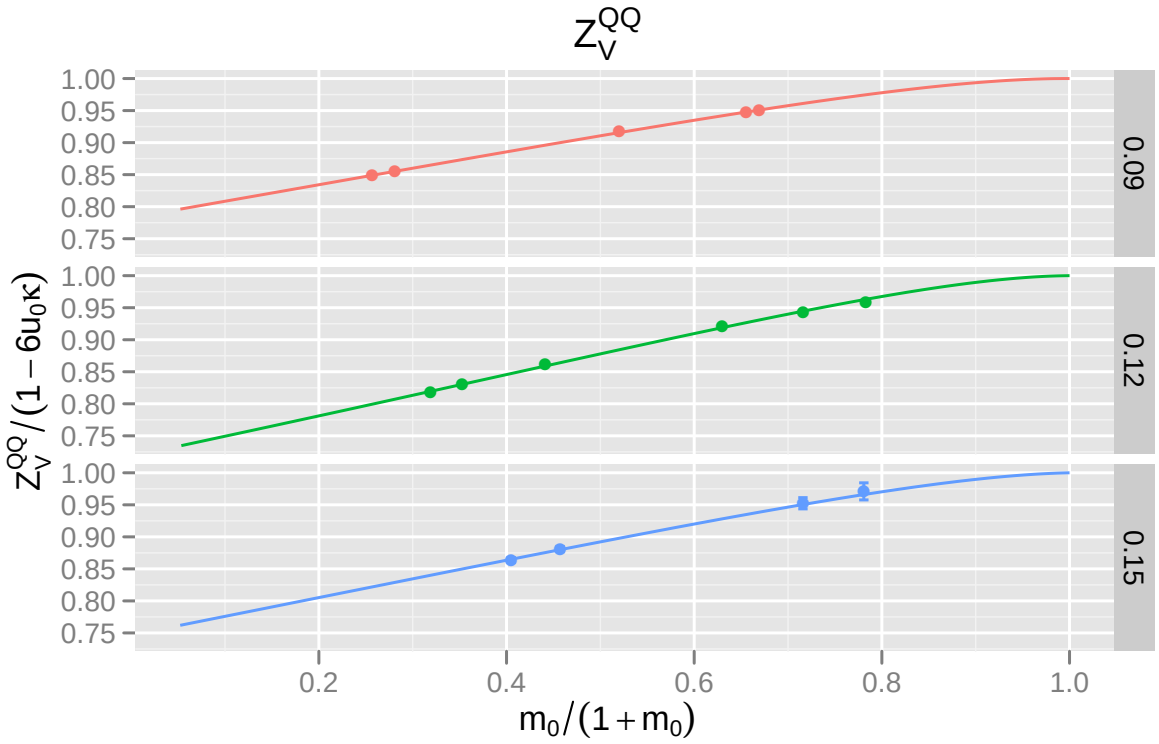

FIG. 2. Plot of $Z_{V^4_{QQ}}/(1-6u_0\kappa)$ *vs.* $m_0a/(1+m_0a)$ for the three lattice spacings.

MeV, and so not much smaller than M_π, despite the fact that they are formally of order $1/M_H$. Since the lightest pseudoscalar meson masses in our simulations are $\sim$ 225 MeV, it is not immediately obvious that including the splittings is necessary or useful. Their inclusion is motivated, first of all, by the observation of Arndt and Lin [82] that finite-volume effects in the one-loop diagrams can be substantially larger with the splittings present. This is mainly due to the fact that accidental cancellations in finite volume effects between different diagrams at $(1/M_H)^0$ disappear once splittings are included. As described below, it is not difficult to include the splitting effects into the calculation of Ref. [42]. We also discuss the extent to which including the splittings, but not other effects that could occur at order $1/M_H$, is a systematic approximation. In practice, we do fits both including and omitting the splittings, and use the difference as one estimate of the chiral extrapolation error. For central values, we include the splittings, because this yields a more conservative estimate of finite-volume effects.

With staggered quarks, the (squared) pseudoscalar meson masses are

$$M^2_{ab,\xi} = B_0(m_a + m_b) + a^2\Delta_\xi, \tag{6.1}$$

where m_a and m_b are quark masses, B_0 is a parameter of χPT, and the representation of the meson under the taste symmetry group is labeled by $\xi = P, A, T, V, I$ [25]. The exact non-singlet chiral symmetry of staggered quarks as $m_a, m_b \to 0$ ensures that $\Delta_P = 0$. All of these pseudoscalars appear in the "pion" cloud around the heavy-light meson in the simulation, and all of them therefore affect the decay constant.

Working at leading order $[(1/M_H)^0]$ in the heavy-quark expansion and at one loop, or next-to-leading order (NLO),

in the chiral expansion, the rSχPT expression for the decay constant with light valence quark q takes the form [42]

$$\phi_{H_q} = \phi_H^0 \Bigg[1 + \frac{1}{16\pi^2 f^2} \frac{1+3g_\pi^2}{2} \Bigg\{ -\frac{1}{16} \sum_{e,\xi} \ell(M_{eq,\xi}^2) - \frac{1}{3} \sum_{j \in \mathcal{M}_I^{(2,q)}} \frac{\partial}{\partial M_{Q,I}^2} \left[R_j^{[2,2]}(\mathcal{M}_I^{(2,q)}; \mu_I^{(2)}) \ell(M_j^2) \right] - \left(a^2 \delta_V' \sum_{j \in \hat{\mathcal{M}}_V^{(3,q)}} \frac{\partial}{\partial M_{Q,V}^2} \left[R_j^{[3,2]}(\hat{\mathcal{M}}_V^{(3,q)}; \mu_V^{(2)}) \ell(M_j^2) \right] + [V \to A] \right) \Bigg\} + p(m_q, m_l, m_h, a^2) \Bigg], \tag{6.2}$$

where m_q is the light valence-quark mass, e runs over the sea quarks, the lighter two of which have masses m_l, and the heavier, m_h.[2] The parameter ϕ_H^0 is independent of the light masses, and p is an analytic function. We fit the charm and bottom systems separately, so ϕ_H^0 depends, in practice, on the heavy-quark mass. The meson mass $M_{Q,\xi}$ is similar to $M_{ab,\xi}$ in Eq. (6.1), but constructed from a valence quark-antiquark, $q\bar{q}$. The light-meson decay constant $f \approx f_\pi \cong 130.4$ MeV and the H-H^*-π coupling g_π controls the size of the one-loop effects. Taste-violating hairpin diagrams, which arise only at non-zero lattice spacing, are parameterized by δ_A' and δ_V'. The residue functions $R_j^{[n,k]}(\{M\},\{\mu\})$ are defined in Ref. [26]. Chiral logarithms are written in terms of the functions $\ell(M^2)$ [83]:

$$\ell(M^2) = M^2 \ln \frac{M^2}{\Lambda_\chi^2} \qquad \text{[infinite volume]}, \tag{6.3}$$

$$\ell(M^2) = M^2 \left(\ln \frac{M^2}{\Lambda_\chi^2} + \delta_1(ML) \right) \qquad \text{[spatial volume } L^3\text{]}, \tag{6.4}$$

$$\delta_1(ML) \equiv \frac{4}{ML} \sum_{\boldsymbol{r} \neq \boldsymbol{0}} \frac{K_1(|\boldsymbol{r}|ML)}{|\boldsymbol{r}|}. \tag{6.5}$$

Here Λ_χ is the chiral scale, K_1 the Bessel function of imaginary argument, and $\boldsymbol{r}$ any non-zero three-vector with integer components. The mass sets in the residue functions of Eq. (6.2) are

$$\mu^{(2)} = \{M_U^2, M_S^2\}, \tag{6.6}$$

$$\mathcal{M}^{(2,q)} = \{M_Q^2, M_\eta^2\}, \tag{6.7}$$

$$\hat{\mathcal{M}}^{(3,q)} = \{M_Q^2, M_\eta^2, M_{\eta'}^2\}, \tag{6.8}$$

where M_U (M_S) is the mass of the pseudoscalar $l\bar{l}$ ($h\bar{h}$) meson.

The salient feature of the chiral extrapolation of ϕ_{H_q} is that the chiral logs have a characteristic curvature as $m_q \to 0$ [84]. At non-zero lattice spacing, the presence of the additive splittings $a^2\Delta_\xi$ in the meson masses reduces the curvature of the chiral logarithms. The characteristic curvature returns, however, as the continuum limit is approached.

To combine data from several lattice spacings into one chiral extrapolation, it is necessary to convert lattice units to (some sort of) physical units. As mentioned in Sec. III A, we convert in two steps, first by canceling lattice units with the appropriate power of r_1/a. In particular, pseudoscalar meson masses [*cf.* Eq. (6.1)] become $r_1^2 M_{ab,\xi}^2 = (r_1/a)^2 (aM_{ab,\xi})^2$, and the decay constant [*cf.* Eq. (6.2)] becomes $r_1^{3/2}\phi_H = (r_1/a)^{3/2}(a^{3/2}\phi_H)$, with $a^{3/2}\phi_H$ determined from Analyses I or II (*cf.* Sec. IV). Strictly speaking, one must take the quark mass dependence of r_1 into account, either separately or by modifying the right-hand side of Eq. (6.2) accordingly. At the present level of accuracy, we ignore this subtlety, canceling units ensemble-by-ensemble with the computed r_1/a. Since r_1 is expected to depend smoothly on m_l and m_h, we are unlikely to introduce an uncontrolled error into the extrapolated decay constants. (After completing the chiral-continuum extrapolation in r_1 units, we then use $r_1 = 0.3117(22)$ fm (*cf.* Sec. III A) to convert to MeV.)

---

[2] The physical values of the average up-down quark mass and of the strange-quark mass are denoted by $\hat{m} = (m_u + m_d)/2$ and m_s, respectively.

To quantify the size of NLO (and higher) corrections to χPT, it is useful to define dimensionless parameters x_q, x_l and x_h proportional to the quark masses m_q, m_l and m_h:

$$x_{q,l,h} \equiv \frac{(r_1 B_0)(r_1/a)(2am_{q,l,h})}{8\pi^2 f_\pi^2 r_1^2} \ .$$

Since the splittings $a^2\Delta_\xi$ are added to the quark mass terms in Eq. (6.1), it is similarly useful to define

$$x_{\Delta_\xi} \equiv \frac{r_1^2 a^2 \Delta_\xi}{8\pi^2 f_\pi^2 r_1^2}, \tag{6.9}$$

$$x_{\bar{\Delta}} \equiv \frac{r_1^2 a^2 \bar{\Delta}}{8\pi^2 f_\pi^2 r_1^2}, \tag{6.10}$$

where $\bar{\Delta}$ is the average pion splitting

$$\bar{\Delta} = \tfrac{1}{16}(\Delta_P + 4\Delta_A + 6\Delta_T + 4\Delta_V + \Delta_I). \tag{6.11}$$

The x_i are in "natural" units for χPT, in the sense that one expects that chiral corrections, when written as series in the x_i, have coefficients [or low-energy constants (LECs)] that are of order 1.

We then take the analytic function p in Eq. (6.2) to have the following form at NLO

$$L_{\rm val}(x_q + x_{\Delta_{\rm val}}) + L_{\rm sea}(2x_l + x_h + 3x_{\Delta_{\rm sea}}) + L_a \frac{a^2}{16\pi^2 f_\pi^2 r_1^4}, \tag{6.12}$$

where $L_{\rm val}$, $L_{\rm sea}$ and L_a are quark-mass-independent LECs that we fit from our data, and we define

$$x_{\Delta_{\rm val}} \equiv \frac{9}{5} x_{\bar{\Delta}} - \frac{4}{5} x_{\Delta_I}, \tag{6.13}$$

$$x_{\Delta_{\rm sea}} \equiv \frac{9}{11} x_{\bar{\Delta}} + \frac{2}{11} x_{\Delta_I}, \tag{6.14}$$

The low-energy constants $L_{\rm val}$, $L_{\rm sea}$ and L_a depend implicitly on the chiral scale Λ_χ, so that the complete expression, Eq. (6.2), is independent of Λ_χ. As in Ref. [42], we choose to include the a^2 dependent terms $x_{\Delta_{\rm sea}}$ and $x_{\Delta_{\rm val}}$ in the coefficients of $L_{\rm val}$ and $L_{\rm sea}$ so that these coefficients represent those combinations of meson masses that arise naturally under a change of Λ_χ in the chiral logarithms.

The LEC L_a arises from analytic taste-violating effects; it serves as a counterterm to absorb changes proportional to the taste-violating hairpins δ'_A and δ'_V under a change in chiral scale. As such, we take the a^2 coefficient of L_a in Eq. (6.12) to vary with lattice spacing like $x_{\Delta_{\rm val}}$. As long as L_a then appears as an independent fit parameter, the introduction of the $x_{\Delta_{\rm sea}}$ and $x_{\Delta_{\rm val}}$ terms in the coefficients of $L_{\rm val}$ and $L_{\rm sea}$ in Eq. (6.12) has a negligible effect on the results from the chiral fits. However, we find that the introduction of these terms significantly reduces the magnitude of L_a; in other words, most of the discretization error from the light quarks appears to be due to the a^2 dependence of the light meson masses in the chiral loops. We leave $L_{\rm val}$, $L_{\rm sea}$ and L_a unconstrained in the fits that determine central values; their size is of O(1) as expected (and is in fact ≤ 0.6).

In the region of the strange-quark mass, the data for the decay constants show some curvature, and at least some quadratic terms in the quark masses (NNLO effects) must in general be added in order to obtain acceptable ($p > 0.01$) fits. There are four such LECs, giving a NNLO contribution to p of the form

$$Q_1 x_q^2 + Q_2(2x_l + x_h)^2 + Q_3 x_q(2x_l + x_h) + Q_4(2x_l^2 + x_h^2). \tag{6.15}$$

Fits omitting the Q_1 and Q_3 terms give poor confidence levels and are rejected; adding the Q_2 and Q_4 terms does not change the fit results much, but increases over-all errors by up to 30%. To be conservative, we include all four terms in fits for central values; other acceptable fits (for example, fixing Q_2 or Q_4 or both to zero) are included among the alternatives used to estimate the systematic error of the chiral extrapolation.

For the central-value fits, the Q_i are mildly constrained by Gaussian priors with central value 0 and width 0.5, since that is roughly the expected size in natural units. After fitting, the posterior values satisfy $|Q_i| \leq 0.5$, and Q_1 and Q_3 have errors ≈ 0.05 (much less than the prior width), indicating that they are constrained by the data. Q_2 and Q_4 have errors ~ 0.5, indicating that they are largely constrained by the priors. Changing the prior widths for the Q_i to 1.0 has a negligible effect on central values and errors of the decay constants, although the posterior Q_2 and Q_4 typically increase in size and error, as expected.

While the chiral form introduced so far gives acceptable simultaneous fits to our data from all available lattice spacings, we still need to estimate the size of heavy-quark and generic light-quark discretization errors. Following the Bayesian approach advocated in Refs. [71, 72], we add constrained lattice-spacing-dependent terms to the fit function until the statistical errors of the results cease to increase appreciably. For the heavy quark, we take up to six such terms, $f_E(m_0a)$, $f_X(m_0a)$, $f_Y(m_0a)$, $f_B(m_0a)$, $f_3(m_0a)$, and $f_2(m_0a)$, where m_0 is the heavy quark bare mass. Details about the origin and form of these six functions are given in Appendix A. These functions estimate fractional (not absolute) errors, and as such are included within the square brackets in Eq. (6.2) (or its equivalent, Eq. (6.20) below). The first three are $O(a^2)$ corrections and are added to the fit with coefficients $z_i\,(a\Lambda)^2$, $i \in \{E, X, Y\}$, where Λ is a scale characteristic of the heavy-quark expansion, and the z_i are parameters with prior value 0 and prior width 1 (for f_Y) or $\sqrt{2}$ (for f_E and f_X, since they each appear twice in the analysis of Appendix A). The next two terms are $O(\alpha_s a)$ corrections, added with coefficients $z_i\,\alpha_s a\Lambda$, $i \in \{B, 3\}$, with z_i taken to have prior value 0 and prior width 1 (for f_B) or $\sqrt{2}$ (for f_3, again because it appears twice). The final term arises from the propagation to the decay constants of heavy-quark errors in the tuning of the heavy-quark hopping parameter, κ. It comes in with coefficient $z_2\,(a\Lambda)^3$, with z_2 having prior value 0 and prior width 1. We take a large value $\Lambda = 700$ MeV, which provides conservatively wide priors, especially for the first five terms. Once one of each of the first two types of terms is added, the errors already reach $\sim$80% of their values with all six added.

Similar terms representing generic light-quark errors, which are not automatically included in the fit function (unlike taste-violating terms), may also be added. With the asqtad staggered action, generic discretization effects are of $O(\alpha_s a^2)$. We allow the physical LECs ϕ_H^0, $L_{\rm val}$, $L_{\rm sea}$, Q_1, Q_2, Q_3, and Q_4, to have small relative variations with lattice spacing with coefficients $C_i\alpha_s(a\Lambda)^2$, where i stands for any of the seven physical LECs, Λ is again taken to be 700 MeV, and the C_i have prior value 0 with prior width 1. This corresponds to a maximum of about a 3% difference for a given LEC between the $a \approx 0.12$ fm and the $a \approx 0.09$ fm ensembles. Once several heavy-quark discretization terms have been introduced, these light-quark terms further increase the total error of individual decay constants by less than 10%. However, the errors on the decay constant ratios f_{D_s}/f_{D^+} and f_{B_s}/f_{B^+} are significantly increased by light-quark discretization effects, because the heavy-quark effects on the ratios cancel to first approximation. For our central values, we include all six heavy-quark and all seven light-quark terms, so the total error from a given fit should estimate all (taste-conserving) discretization errors, as well as normal statistical effects. To estimate "heavy-quark" and "light-quark" discretization effects separately, we set to zero the light- or heavy-quark discretization terms, respectively, and then subtract the statistical errors in quadrature. Such separate errors are not relevant to any final results quoted below, but are included as separate lines in the error budget for informational purposes.

As mentioned above, our preferred fit form modifies Eq. (6.2) by including the effects of hyperfine and flavor splittings of the heavy-light mesons in one-loop diagrams. We now briefly describe how one may adjust the results of Ref. [42] to include these splittings. In Eq. (6.2), the contributions proportional to g_π^2 come from diagrams with internal H^* propagators, namely the left-hand diagrams in Fig. 5 of Ref. [42]. Contributions with no factor of g_π^2 come from diagrams with light-meson tadpoles, namely the right-hand diagrams in Fig. 5 of Ref. [42]. The latter have no internal heavy-light propagators, so are unaffected by any heavy-light splittings. The splittings in the former diagrams depend on whether the light-meson line is connected (Fig. 5a, left, of Ref. [42]), or disconnected (Fig. 5b, left). In the disconnected case, the H^* in the loop always has the same flavor (q) as the external H_q, so there is no flavor splitting between the two, only a hyperfine splitting. In the connected case, the H^* in the loop has the flavor of the virtual sea quark loop (which we labeled by e in Eq. (6.2)), so there is flavor splitting with the external H_q, in addition to the hyperfine splitting.

Let Δ^* be the (lowest-order) hyperfine splitting, and δ_{eq} be the flavor splitting between a heavy-light meson with light quark of flavor e and one of flavor q. At lowest order, δ_{eq} is proportional to the quark-mass difference (or light-meson squared mass difference), which can be written in terms of a parameter λ_1:

$$\delta_{eq} \cong 2\lambda_1 B_0(m_e - m_q) \cong \lambda_1(M_E^2 - M_Q^2), \tag{6.16}$$

where M_E is the mass of an $e\bar{e}$ light meson. Here we have used the notation of Arndt and Lin [82] and included a factor of B_0 in the middle expression; B_0 is omitted in the notation of Ref. [85], Eq. (16), and of Ref. [42], Eq. (45).

By convention, the mass of the external H is removed in the heavy quark effective theory, so the mass shell is at $\boldsymbol{k} = \boldsymbol{0}$, where $\boldsymbol{k}$ is the external three-momentum. When there is no splitting, the internal H^* has its pole at the same place, which makes the integrals particularly simple, giving the chiral log function $\ell(M^2)$, Eq. (6.3). If a splitting Δ is present, the integrals involve a significantly more complicated function, which we denote

$$J(M, \Delta) = (M^2 - 2\Delta^2)\log(M^2/\Lambda^2) + 2\Delta^2 - 4\Delta^2 F(M/\Delta) \qquad \text{[infinite volume]}. \tag{6.17}$$

Here the function F is most simply expressed [86, 87]

$$F(1/x) = \begin{cases} -\frac{\sqrt{1-x^2}}{x}\left[\frac{\pi}{2} - \tan^{-1}\frac{x}{\sqrt{1-x^2}}\right], & \text{if } |x| \le 1, \\ \frac{\sqrt{x^2-1}}{x}\ln(x + \sqrt{x^2-1}), & \text{if } |x| \ge 1, \end{cases} \tag{6.18}$$

which is valid for all x.

It is then straightforward to write down the generalization of Eq. (6.2) to include splittings. The basic rule is to replace

$$\ell(M^2) \to J(M, \Delta) \tag{6.19}$$

in the terms proportional to g_π^2. It is not hard to show that $J(M, 0) = \ell(M^2)$, so this replacement is consistent with the original result neglecting the splittings. In making the replacements, one must choose the correct value of the splitting Δ in each term. As mentioned above, in terms that come from the diagram with a disconnected light-meson propagator, one must put $\Delta = \Delta^*$. But in terms that come from the diagram with a connected light-meson propagator, one must put $\Delta = \Delta^* + \delta_{eq}$, because the internal heavy-light meson is a H_e^*, while the external meson is an H_q. The result for the heavy-light meson decay amplitude including the splittings is then

$$\begin{aligned}
\phi_{H_q} = \phi_H^0 \Bigg[1 + \frac{1}{16\pi^2 f^2} \frac{1}{2} \Bigg\{ & -\frac{1}{16} \sum_{e,\Xi} \ell(M_{eq,\Xi}^2) \\
& - \frac{1}{3} \sum_{j \in \mathcal{M}_I^{(2,x)}} \frac{\partial}{\partial M_{X,I}^2} \left[R_j^{[2,2]}(\mathcal{M}_I^{(2,x)}; \mu_I^{(2)}) \ell(M_j^2) \right] \\
& - \left(a^2 \delta_V' \sum_{j \in \hat{\mathcal{M}}_V^{(3,x)}} \frac{\partial}{\partial M_{X,V}^2} \left[R_j^{[3,2]}(\hat{\mathcal{M}}_V^{(3,x)}; \mu_V^{(2)}) \ell(M_j^2) \right] + [V \to A] \right) \\
& - 3 g_\pi^2 \frac{1}{16} \sum_{e,\Xi} J(M_{eq,\Xi}, \Delta^* + \delta_{eq}) \\
& - g_\pi^2 \sum_{j \in \mathcal{M}_I^{(2,x)}} \frac{\partial}{\partial M_{X,I}^2} \left[R_j^{[2,2]}(\mathcal{M}_I^{(2,x)}; \mu_I^{(2)}) J(M_j, \Delta^*) \right] \\
& - 3 g_\pi^2 \left(a^2 \delta_V' \sum_{j \in \hat{\mathcal{M}}_V^{(3,x)}} \frac{\partial}{\partial M_{X,V}^2} \left[R_j^{[3,2]}(\hat{\mathcal{M}}_V^{(3,x)}; \mu_V^{(2)}) J(M_j, \Delta^*) \right] + [V \to A] \right) \Bigg\} \\
& + p(m_q, m_l, m_h, a^2) \Bigg].
\end{aligned} \tag{6.20}$$

It is also straightforward to include finite-volume effects into Eq. (6.20). One simply replaces

$$J(M, \Delta) \to J(M, \Delta) + \delta J(M, \Delta, L), \tag{6.21}$$

where $\delta J(M, \Delta, L)$ is the finite-volume correction in a spatial volume L^3. The correction can be written in terms of functions defined in Refs. [44, 82]:

$$\delta J(M, \Delta, L) = \frac{M^2}{3} \delta_1(ML) - 16\pi^2 \left[\frac{2\Delta}{3} J_{FV}(M, \Delta, L) + \frac{\Delta^2 - M^2}{3} K_{FV}(M, \Delta, L) \right] , \tag{6.22}$$

with

$$K_{FV}(M, \Delta, L) \equiv \frac{\partial}{\partial \Delta} J_{FV}(M, \Delta, L), \tag{6.23}$$

and $\delta_1(ML)$ as given in Eq. (6.5).

Before turning to the fit details and results, we briefly discuss the extent to which including the splittings as in Eq. (6.20), and not other possible $1/M_H$ effects, is a systematic improvement on Eq. (6.2). In fact, in a parametric sense within the power counting introduced by Boyd and Grinstein [85], this is a systematic improvement, as long as we make some further specifications as to how Eq. (6.20) should be applied. As we detail below, however, the power counting of Ref. [85] is only marginally applicable to our data. For that reason we ultimately fit to both Eq. (6.20) and Eq. (6.2) and take the difference as one measure of the chiral extrapolation error.

For the following discussion, let Δ be a generic splitting (Δ^* or δ_{eq} or a linear combination of the two), and M be a generic light pseudoscalar mass. The power counting introduced in Ref. [85] takes

$$\frac{\Delta^2,\ \Delta M,\ M^2}{M_H} \ll \Delta \sim M. \tag{6.24}$$

For our data, treating Δ and M as the same size is not dangerous, even though Δ is significantly smaller than our simulation M values—at worst this means that we include some terms unnecessarily. The condition $M^2/M_H \ll \Delta$, which is necessary to drop other $1/M_H$ contributions as still higher order, is marginally valid, however. For the D system, $M_K^2/M_D \approx 130$ MeV, which is roughly of the same size as Δ^* and δ_{sd}. For the B system, $M_K^2/M_B \approx 47$ MeV, of the same size as Δ^* but somewhat less than δ_{sd}. For the purposes of the chiral extrapolation, however, what matters is the applicability of the power counting at the lowest simulated light meson masses, not its applicability at M_K.[3] For our lightest simulated pions with mass $\sim M_K/2$, we can reduce the left hand side of the inequality in Eq. (6.24) by a factor of four, at which point it becomes reasonably applicable.

Having tentatively accepted the power counting of Eq. (6.24), it is clear that $F(M/\Delta)$ in Eq. (6.17) should be treated as O(1). Then the difference between $J(M,\Delta)$ and the chiral logarithm it replaces, $\ell(M^2)$ is of the same order as $\ell(M^2)$ itself, so including the splittings becomes mandatory at the one-loop order to which we are working. The next question is whether Eq. (6.2) includes *all* effects to this order. As discussed by Boyd and Grinstein, the key issue is whether operators with two or more derivatives (two or more powers of residual momentum $\boldsymbol{k}$) on the heavy fields can contribute. Such operators are suppressed by $1/M_H$ relative to the leading-order heavy-light Lagrangian, which has a single derivative. Since we are keeping Δ^*, which is also in principle a $1/M_H$ effect, one might worry that such operators could contribute at the same order. The power counting implies, however, that the relevant diagrams pick up a factor of $(\Delta, M)/M_H$ relative to the terms being kept in Eq. (6.20). The reason for the difference is that the explicit extra factor of $\boldsymbol{k}$ turns into Δ or M—the only dimensional constants available—after integration. In the term that generates the hyperfine splitting itself, in contrast, the dimensional quantity balanced against $1/M_H$ is Λ—a heavy-quark QCD scale—rather than M. The power counting in Eq. (6.24) effectively treats Λ as larger than M (so that $\Delta \sim \Lambda^2/M_H \sim M$). Similarly, the term that generates the flavor splittings has a single factor of m_q and no residual momentum, and Eq. (6.24) effectively takes $m_q \sim \boldsymbol{k}$ in such terms.

Boyd and Grinstein do find some other contributions at the same order as Eq. (6.20), but most come from terms that are simply Λ/M_H times terms in the leading-order heavy-light Lagrangian or current, and thus give simply an overall factor times the result without them. The exceptions are the terms multiplied by g_2 in Eq. (15) of Ref. [85] and by ρ_2 in Eq. (18) of Ref. [85]. These are operators that have the same dimension as the original Lagrangian current operators, but that violate heavy-quark spin symmetry, and therefore give different contributions to the pseudoscalar and vector meson decay constants at this order. Since we are only looking at pseudoscalar meson decay constants here, however, and since these effects are flavor-independent, we can also absorb all of the $1/M_H$ effects into (1) the effects of the splittings in the loop, described by Eq. (6.20), and (2) an overall factor in front of the full one-loop result.

The overall factor in Eq. (6.20) is $1/(16\pi^2 f^2)$. Since f is not fixed at one loop, one should in any case allow it to vary over a reasonable range, which we take to be f_π to f_K. We allow such variations even when we fit to the form without splittings, Eq. (6.2). The difference between using f_π and f_K corresponds to a 45% change in the size of the one-loop coefficient, but produces only a 1 to 3 MeV change in the decay constants.[4] We therefore assume that any further $1/M_H$ uncertainty in $1/(16\pi^2 f^2)$ has negligible effects on our results.

Finally, there is a question of whether terms coming from taste violations contribute something new at the same order in which we include splittings. Since taste-violating terms in the Lagrangian can enter just like light-quark masses, this is a possibility in principle. Corresponding to the terms in the quark masses that generate flavor splittings of heavy-light mesons (*cf.* Eq. (45) of Ref. [42]), there are taste-violating terms given in Eq. (51) of that paper. Just as for the quark-mass terms, however, we are only interested here in contributions that change the heavy-light meson mass, not ones coupling the mesons to pion fields. When the pion fields are set to zero, all the terms in Eq. (51) of Ref. [42] just give a constant heavy-light meson mass term proportional to a^2 that contributes equally to the H and H^* masses of all valence flavors. Terms that produce a hyperfine splitting would have to also violate heavy quark spin symmetry, and hence be of order $a^2\Lambda/M_H$. Similarly, terms that produce flavor splitting would need to violate flavor symmetry, and hence be of order $a^2 m_q/\Lambda_\chi$. Both such contributions are higher order in our power-counting. Since there is no splitting, there is no contribution to the decay constants because the effect will vanish when we put the external B or D meson on mass shell.

In our chiral fits, we take the physical light-quark masses, as well as the parameters B_0, $a^2\Delta_\xi$, δ'_A, and δ'_V, from the MILC Collaboration's results of rSχPT fits to light pseudoscalars masses and decay constants [15, 88] on ensembles that include lattice spacing $a \approx 0.15$ fm through $a \approx 0.06$ fm. Table XII shows the values used. In general, we use older MILC determinations since newer versions, *e.g.*, those in Ref. [69], do not cover the full range of lattice spacings employed here (but are consistent where they overlap). The exceptions are the values of the taste-violating

[3] We assume here that the fit to the data is good over the full mass range simulated. It is not important for the chiral extrapolation that the fit be systematic in the region around M_K, but it must describe the data in that range so that we can correctly interpolate to the physical kaon mass. In Sec. VII, we check that the inclusion of points around M_K in the fit does not significantly affect the chiral extrapolation to light quark mass.

[4] Most of the change in the size of the overall coefficient is compensated by a change in the LECs that come from the fit to our data.

TABLE XII. Inputs to our heavy-light chiral fits taken from the MILC Collaboration's light-meson chiral fits [15, 88]. The physical bare-quark masses m_u, m_d, $\hat{m} \equiv (m_u + m_d)/2$, and m_s are determined by demanding that the charged pion and kaons take their physical masses after the removal of electromagnetic effects. Errors in the masses are due to statistics, chiral extrapolation systematics, scale determination, and (for m_d and m_u) the estimate of electromagnetic effects, respectively. "Continuum" values are found from chiral fits that have been extrapolated to the continuum, but masses are still in units of the "fine" ($a \approx 0.09$ fm) lattice spacing, and with the fine-lattice value of the mass renormalization. Values for $r_1^2 a^2 \delta'_A$ and $r_1^2 a^2 \delta'_V$ take into account newer MILC analyses [69] as noted in the text. The light-meson analysis determining these quantities assumes that they scale like the taste-violating splittings Δ_ξ and are larger by a factor of 1.68 on the 0.15 fm lattices than on the 0.12 fm lattices, and smaller by a factor 0.35 on the 0.09 fm lattices than on the 0.12 fm lattices. The statistical and systematic errors on $r_1 B_0$ and $r_1^2 a^2 \Delta_\xi$ are not given here; such errors have negligible effect on the heavy-light decay constants.

Quantity	Lattice spacing			
	$a \approx 0.15$ fm	$a \approx 0.12$ fm	$a \approx 0.09$ fm	"continuum"
$am_s \times 10^2$	4.29(1)(8)(6)	3.46(1)(10)(5)	2.53(0)(6)(4)	2.72(1)(7)(4)
$a\hat{m} \times 10^3$	1.55(0)(3)(2)	1.25(0)(4)(2)	0.927(2)(27)(13)	0.997(2)(32)(14)
$am_d \times 10^3$	2.20(0)(4)(3)(5)	1.78(0)(6)(3)(4)	1.31(0)(4)(2)(3)	1.40(0)(5)(2)(3)
$am_u \times 10^4$	8.96(2)(17)(13)(49)	7.31(2)(23)(10)(40)	5.47(1)(16)(8)(30)	5.90(1)(19)(9)(32)
$r_1 B_0$	6.43	6.23	6.38	6.29
$r_1^2 a^2 \Delta_A$	0.351	0.205	0.0706	0
$r_1^2 a^2 \Delta_T$	0.555	0.327	0.115	0
$r_1^2 a^2 \Delta_V$	0.721	0.439	0.152	0
$r_1^2 a^2 \Delta_I$	0.897	0.537	0.206	0
$r_1^2 a^2 \delta'_A$	—	−0.28(6)	—	0
$r_1^2 a^2 \delta'_V$	—	0.00(7)	—	0

hairpin parameters $r_1^2 a^2 \delta'_A$ and $r_1^2 a^2 \delta'_V$. For them, the newer analysis including two-loop chiral logarithms gives larger systematic errors and a changed sign of the central value of $r_1^2 a^2 \delta'_V$, which has always been consistent with zero. For these parameters, we therefore use the wider ranges listed in Table XII, which encompasses both types of analyses. For comparison, the results of the analysis of Ref. [88] were $r_1^2 a^2 \delta'_A = -0.30(1)(4)$ and $r_1^2 a^2 \delta'_V = -0.05(2)(4)$.

In order to fit Eq. (6.20) to our lattice data, it is also necessary to input values for the hyperfine splitting Δ^* and for λ_1 in Eq. (6.16). For B mesons, we have [54]

$$\Delta^* = M_{B^*} - M_B \approx 45.8 \text{ MeV}, \tag{6.25}$$

$$\delta_{sd} = M_{B_s} - M_B \approx 87.0 \text{ MeV}, \tag{6.26}$$

$$\lambda_1 \approx 0.192 \text{ GeV}^{-1}, \tag{6.27}$$

where we use $M_E = M_S = 0.6858(40)$ GeV [70] and $M_Q = M_{\pi^0} \approx 135.0$ MeV to obtain λ_1 from the experimental data. Similarly, for D mesons, we have

$$\Delta^* = M_{D_0^*} - M_{D_0} \approx 142.1 \text{ MeV}, \tag{6.28}$$

$$\delta_{sd} = M_{D_s} - M_{D_\pm} \approx 98.9 \text{ MeV}, \tag{6.29}$$

$$\lambda_1 \approx 0.219 \text{ GeV}^{-1}. \tag{6.30}$$

In the chiral fit, we input the relevant physical Δ^* and λ_1 from either Eqs. (6.25)–(6.27) or (6.28)–(6.30), and then use Eq. (6.16) with the actual m_e and m_q from each data point, and B_0 the slope for a given ensemble, from Table XII. We emphasize here that B_0 comes from a simple tree-level chiral fit of light meson masses to Eq. (6.1). This is adequate for our purposes, since the resulting meson masses are only used within the one-loop chiral logarithms.

We can now present the actual chiral fits and show how we extract results and systematic errors from them. Recall that we compute ϕ_{H_q} for many combinations of the valence and light sea-quark masses, and at three lattice spacings: $a \approx 0.15$, 0.12, and 0.09 fm. We fit all the decay constant data to the form given either by Eq. (6.20) or by Eq. (6.2). One-loop finite-volume effects are included through Eq. (6.21) or Eq. (6.4). There are four unconstrained free parameters in our fits: the LO parameter ϕ_H^0, and the one-loop LECs $L_{\rm val}$, $L_{\rm sea}$, L_a [Eq. (6.12)]. The central fit fixes the chiral coupling f at f_π, but a range of couplings are considered in alternative fits, as described in more detail in Sec. VII. Similarly, the H-H^*-π coupling g_π, which is poorly constrained by our data, is taken in the range 0.51 ± 0.20. This encompasses a range of phenomenological and lattice determinations [86, 89–94], as discussed in Ref. [56]. In the central fit, g_π is held fixed at 0.51, while it is varied in alternative fits described in Sec. VII. Although

changing g_π is equivalent to changing f when splittings are omitted [*cf.* Eq. (6.2)], the effects are inequivalent when splittings are included [*cf.* Eq. (6.20)]. This is especially true of the finite-volume effects, for which the splittings have the potential to produce significant changes [82].

Some additional parameters constrained by Bayesian priors are also included in the chiral fits, as discussed above. The taste-violating hairpin parameters δ'_V and δ'_A are given by the ranges in Table XII. In addition, up to six heavy-quark and up to seven light-quark lattice-spacing dependent terms, are added for investigation of discretization effects. Except where otherwise noted, all twelve such terms are included in the fits plotted below: this gives errors that include true statistical errors plus our estimate of discretization effects from the heavy quarks and generic (taste non-violating) discretization errors from the light quarks. In addition, some or all of the (mildly) constrained NNLO LECs, $Q_1, \ldots, Q_4$, are included. Again, unless otherwise noted, the fits below include all four such parameters; such fits tend to give larger (and hence more conservative) errors than fits that restrict the number of these parameters. In total, there are 23 fit parameters in the central fits: the 19 constrained parameters listed in this paragraph, and the 4 unconstrained parameters listed in the previous paragraph.

B. Chiral fits and extrapolations for the D system

Figure 3 shows our central chiral fit to $r_1^{3/2}\phi_{D^+}$ and $r_1^{3/2}\phi_{D_s}$. Data from ensembles at $a \approx 0.15$ fm, $a \approx 0.12$ fm and $a \approx 0.09$ fm are shown, but the $a \approx 0.15$ fm ensembles are not included in the fit. The points and covariance matrix are obtained from Analysis I (Sec. IV B) of the two-point functions. For clarity, only the unitary (full QCD) points are shown for ϕ_D (and approximately unitary for ϕ_{D_s}), but the fit is to all the partially-quenched data on the $a \approx 0.12$ fm and $a \approx 0.09$ fm ensembles. The fit properly takes into account the covariance of the data; χ^2/dof and the p value (goodness of fit) are reasonable, as shown. The points in Fig. 3 are plotted as a function of mass m_x, where, for ϕ_{D^+}, the light valence mass m_q and the light sea mass m_l are given by $m_q = m_l = m_x$. For ϕ_{D_s}, only

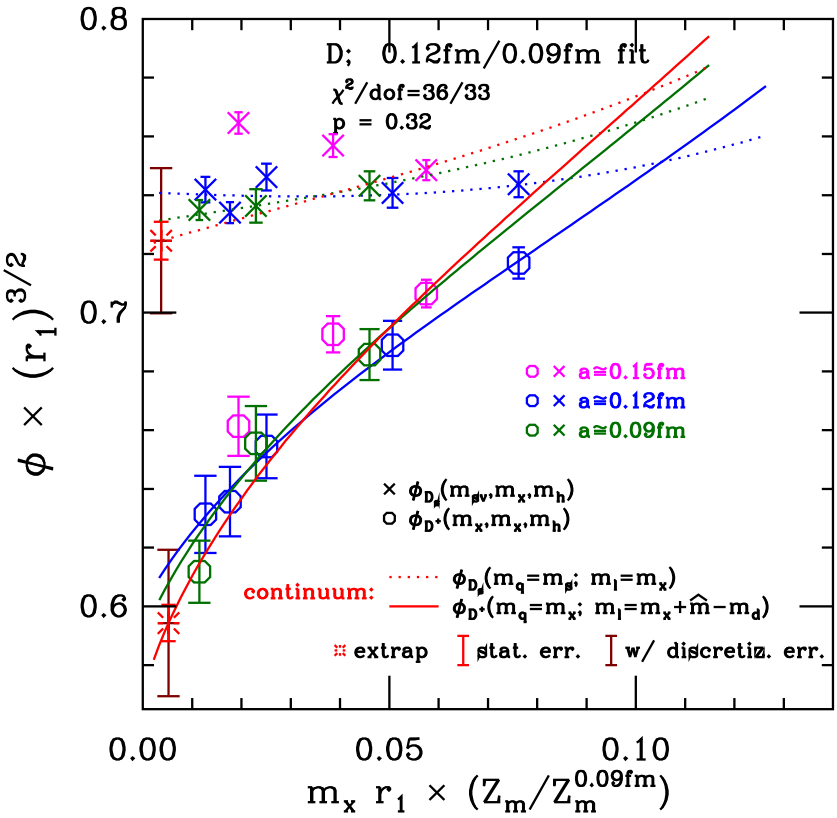

FIG. 3. Central chiral fit for the D system, based on Analysis I of the fits to 2-point correlators. Only (approximately) unitary points are shown. Data from ensembles at $a \approx 0.15$ fm, $a \approx 0.12$ fm and $a \approx 0.09$ fm are shown, but the $a \approx 0.15$ fm ensembles are not included in the fit. The bursts show extrapolated values for ϕ_{D_s} and ϕ_{D^+}, with the purely statistical errors in bright red and the statistical plus discretization errors in darker red. The physical strange-quark mass corresponds to an abscissa value of $m_x \approx 0.1$.

$m_l = m_x$ varies, while m_q is held fixed at the value m_{s_v} near the physical strange mass m_s.[5] In order to be able to compare ensembles at different lattice spacings, we have adjusted the bare quark masses by the ratio $Z_m/Z_m^{0.09\,\mathrm{fm}}$, where Z_m is the (one-loop) mass renormalization constant [95], and $Z_m^{0.09\,\mathrm{fm}}$ is its value on the $a \approx 0.09$ fm ensembles.

The continuum extrapolation is carried out by taking the fitted parameters and setting $a^2 = 0$ in all taste-violating terms (parameterized by Δ_ξ, δ'_A, δ'_V, and L_a), all heavy-quark discretization effects (parameterized by z_E, z_X, z_Y, z_B, z_3, and z_2) and all generic light-quark discretization effects (parameterized by C_i). The red lines (solid for ϕ_{D^+}, dotted for ϕ_{D_s}) show the effect of extrapolating to the continuum and setting the strange quark mass (both sea, m_h, and valence, m_{s_v}) to the physical value m_s.

Finally, the bursts give the result after the chiral extrapolation in the continuum, *i.e.*, setting $m_x = m_d$ for ϕ_{D^+}, and $m_x = \hat{m}$ for ϕ_{D_s}. The larger, dark red, error bars on the bursts show the total error from the fit, which includes heavy-quark and generic light-quark discretization errors using Bayesian priors, as described above. The smaller, bright red error bars, show purely statistical errors, which are computed by a fit with all the discretization prior functions turned off. In plotting the red line for ϕ_{D^+}, the light sea mass is shifted slightly ($m_l = m_x + \hat{m} - m_d$) so that it takes its proper mass when $m_x = m_d$. (We neglect isospin violations in the sea.) The small mass differences between $\hat{m}$ and m_d (and the corresponding difference between $\hat{m}$ and m_u for the B^+) produce changes in ϕ that are much smaller than our current errors, but we include them here with an eye to future work, where the precision will improve.

The trend of the data for the coarsest lattice spacing ($a \approx 0.15$ fm, the magenta points in Fig. 3) tends to be rather different than for the finer lattice spacings, especially for the D_s, which is why we exclude the $a \approx 0.15$ fm data from the central fit. This trend is even more exaggerated for the B system, but with particularly large statistical errors; see Fig. 6 below. Nevertheless, the effect of including the $a \approx 0.15$ fm points in the fit is a rough indication of the size of discretization errors. Figure 4 shows what happens to the fit when these points are included: ϕ_{D^+} and ϕ_{D_s} each move up an amount comparable to (but less than) the size of the larger (dark red) error bars, which represent

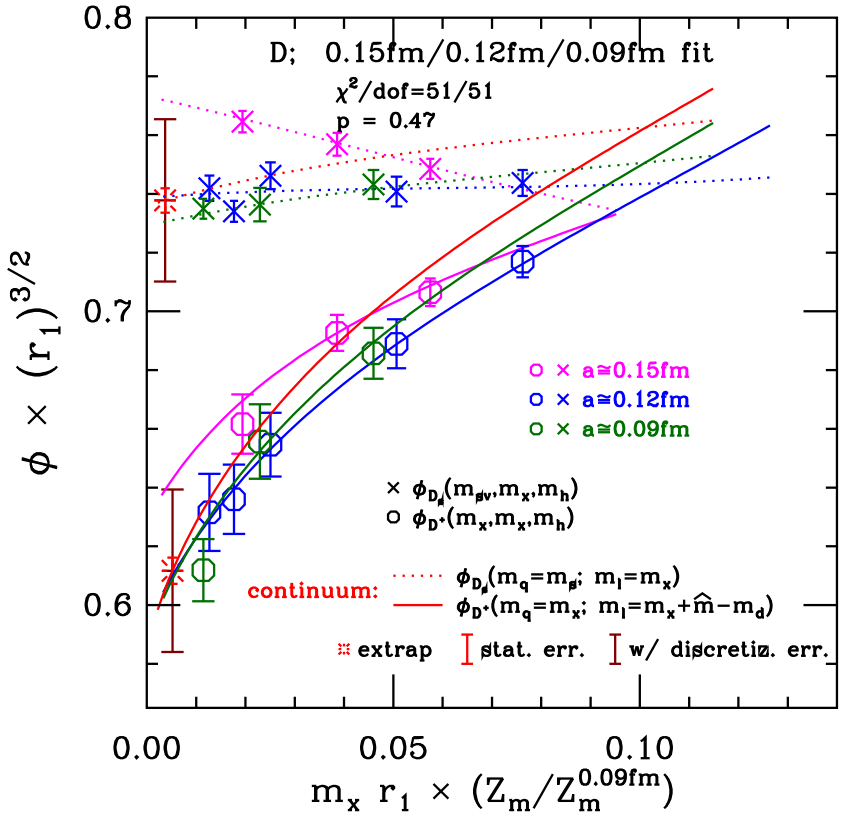

FIG. 4. Same as Fig. 3, but including points at $a \approx 0.15$ fm in the chiral-continuum fit.

[5] On the $a \approx 0.15$ fm ensembles, m_{s_v} is equal to the value of the strange sea quark mass m_h ($am_{s_v} = 0.0484$), but on the other two ensembles we take it lower than m_h, because m_h has been chosen somewhat larger than the physical strange mass. In the figure, $am_{s_v} = 0.415$ for the $a \approx 0.12$ fm ensembles and $am_{s_v} = 0.272$ for the $a \approx 0.09$ fm ensembles.

heavy and generic light quark discretization errors (as well as statistical errors, which are smaller). The consistency is reassuring.

As discussed in Sec. IV, we also examine Analysis II of the 2-point functions. Figure 5 shows the effect of using Analysis II in the chiral fits. The differences in the decay constant results between Fig. 3 and Fig. 5 are included in the decay-constant error budgets as a "fitting error". Note that the covariance matrix calculation in Analysis II results in an apparent underestimate of χ^2 (and, consequently, a high apparent p value). We believe that this stems from binning of the data to remove autocorrelation effects, which has the disadvantage of reducing the number of samples used to compute the covariance matrix. It is then difficult to determine small eigenvalues accurately. Indeed the eigenvalues of the (normalized) correlation matrix tend to have a lower bound of $\sim 10^{-4}$ to 10^{-3} with this approach, whereas they typically go down to 10^{-5} in Analysis I. [Recall that in Analysis I we keep all samples, and deal with autocorrelation effects by Eq. (4.13).] Nevertheless, the difficulty with small eigenvalues explains only a small fraction of the difference between the results from Analyses I and II. For example, f_D is changed by only 0.2 MeV when we smooth eigenvalues from Analysis I that are less than 10^{-3}, following the method of Ref. [96]. This may be compared to the total difference between f_D in Analyses I and II, which is 1.7 MeV.

C. Chiral fits and extrapolations for the B system

Results for the B system closely resemble those for the D system in most respects. One important difference is that the signal-to-noise ratio is worse for the B system because the mass difference that controls the noise, $2m_B - m_{\eta_b} - m_\pi$, increases with the mass of the heavy quark [97]. Therefore, the preferred fit in Analysis I for the charm case (1 simple exponential + 1 oscillating exponential at large $t_{\rm min}$) is too noisy here, and we must use fits with an extra excited state and smaller $t_{\rm min}$ (see Sec. IV B). Consequently, our B-system results have larger statistical errors. On the other hand, heavy-quark discretization errors are smaller in the B system. In the HQET analysis of discretization effects they appear in the heavy-quark expansion, which works better for B's to begin with [63].

Figure 6 shows, for unitary points only, our central chiral fit for the B system. This is based on Analysis I of the 2-point functions. As in Fig. 3, the red lines (solid for ϕ_{B^+}, dotted for ϕ_{B_s}) show the effect of extrapolation to the continuum and setting the strange quark mass to its physical value m_s. For the solid red line, the light sea mass is

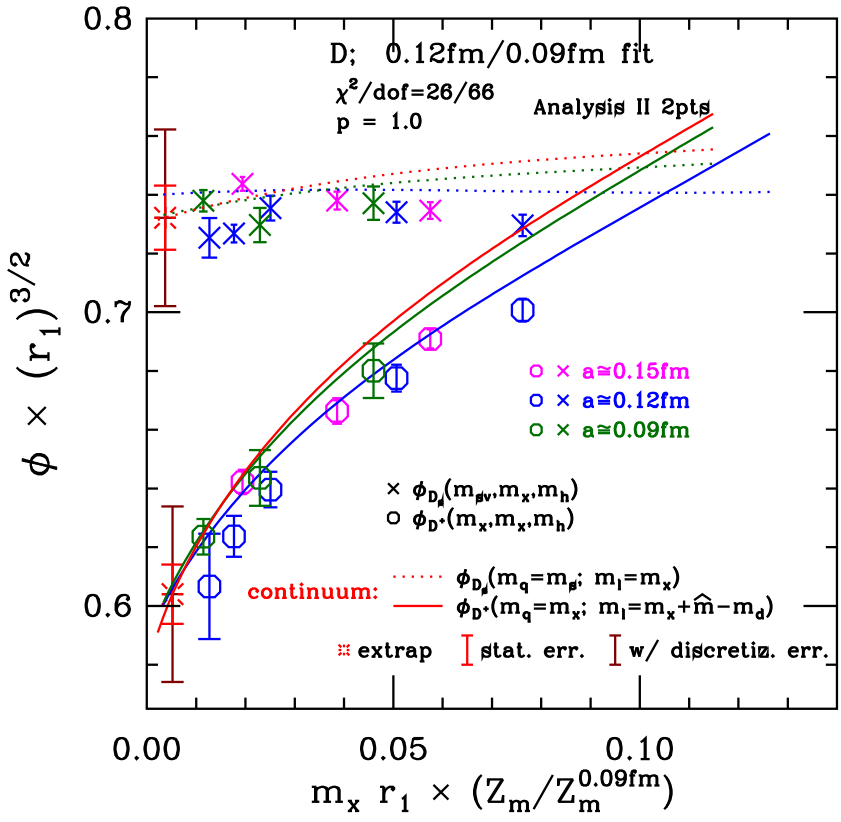

FIG. 5. Same as Fig. 3, but using Analysis II of the 2-point function.

again shifted slightly, but now $m_l = m_x + \hat{m} - m_u$, so that it takes its proper mass when $m_x = m_u$. The bursts show the final results, and come from setting $m_x = m_u$ for ϕ_{B^+} and $m_x = \hat{m}$ for ϕ_{B_s}. As before, the smaller, bright red, error bars, show purely statistical errors, and the larger, dark red, error bars come from the fit with Bayesian priors and include heavy-quark and generic light-quark discretization errors as well as statistical errors.

In Fig. 6, the $a \approx 0.15$ fm data are both noisy and far from those of the finer lattice spacings. Therefore, these ensembles are again dropped from the central fit. Figure 7 shows the effect of including the $a \approx 0.15$ fm points. Note that the resulting continuum-extrapolated line for ϕ_{B_s} (dotted red line) now has what appears to be a rather unphysical shape, showing a significant initial increase as the light sea-quark mass is decreased, starting at the right side of the graph. There are several possible causes for the large discretization effects at $a \approx 0.15$ fm. These include heavy quark effects (aM_H takes its largest value in our analysis, ~ 4, on these points), light quark taste violations ($a \approx 0.15$ fm ensembles are often excluded from light quark analyses [98] because of large a^4 corrections), and the fact that the improved gauge action does not remove $O(\alpha_s a^2)$ errors due to quark loops. In addition, there is the simple problem of the large statistical noise for B system, which is worst at the coarsest lattice spacing, as seen clearly in Fig. 7. The end result is that the differences caused by including the $a \approx 0.15$ fm points in the standard (Bayesian) fit is 10 to 20% larger than the dark red error bars in Fig. 6, and 40 to 60% larger than discretization errors estimated by removing the statistical errors from the dark red bars. Because the trend for $a \approx 0.15$ fm is so different from the other spacings, and because of the unphysical behavior when these points are included in the fit, we believe this difference overestimates the true discretization error. Nevertheless, to be conservative, we increase the discretization error estimate to take into account the effect of including the $a \approx 0.15$ fm ensembles, as described in Sec. VII.

Figure 8 shows the effect of using Analysis II of the correlation functions. In order to make these comparisons as direct as possible, we first turn off all the Bayesian discretization terms in the fits. Compared to the results from Fig. 6, this fit gives a value of f_{B_s} about 1 MeV higher and a value of f_{B^+} about 2 MeV lower. These differences are included in our estimate of the fitting errors due to excited state contamination in Sec. VII.

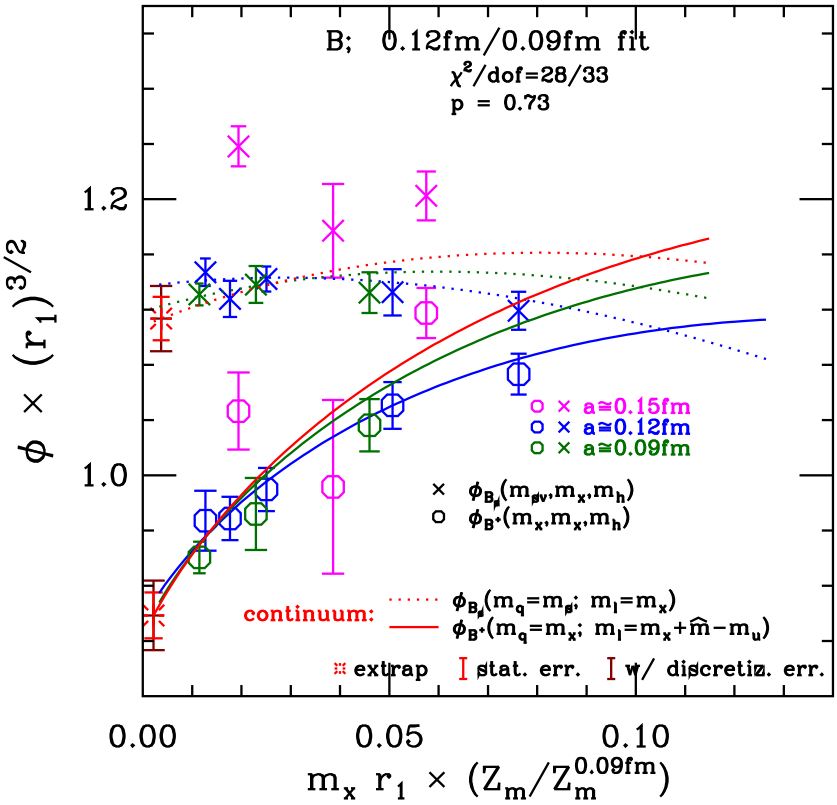

FIG. 6. Central chiral fit for the B system, with data from Analysis I of the 2-point functions. Only (approximately) unitary points are shown. Data from ensembles at $a \approx 0.15$ fm, $a \approx 0.12$ fm, and $a \approx 0.09$ fm are shown, but the $a \approx 0.15$ fm ensembles are not included in the fit. The bursts show extrapolated values for ϕ_{B_s} and ϕ_{B^+}, with the purely statistical errors in bright red and the statistical plus discretization errors in darker red. The physical strange-quark mass corresponds to an abscissa value of $m_x \approx 0.1$.

VII. ESTIMATION OF SYSTEMATIC ERRORS

In this section, we present a careful, quantitative accounting for the uncertainties in our calculation. We consider in turn discretization errors, fitting errors, errors from inputs r_1 and quark-mass tuning, renormalization, and finite-volume effects. Table XIII details our error budget.

A. Heavy-quark and generic light-quark discretization effects

As described in Sec. VI and Appendix A, we parameterize possible heavy-quark and generic light-quark discretization effects and follow a Bayesian approach in including such effects in our chiral fitting function. Consequently, the raw "statistical" error that comes from our fits is not a pure statistical error but includes an estimate of the errors coming from the discretization effects. This inclusive error is shown with the dark red error bars in the plots in Sec. VI. For the D system, it is listed in the first line of Table XIII.

In the B system, the effect on the continuum-extrapolated results caused by including the the $a \approx 0.15$ fm data can be somewhat larger than the discretization error estimated in the Bayesian approach. To be conservative, we therefore replace the Bayesian estimates in such cases with the difference between a fit with and without the $a \approx 0.15$ fm ensembles included. (These comparison fits do not themselves include the Bayesian discretization error terms.) The pure statistical error is then added in quadrature to the difference to get the "statistics $\oplus$ discretization" error shown for f_{B^+} and f_{B_s} in Table XIII. (For the ratio f_{B_s}/f_{B^+}, the Bayesian estimate was larger than the error determined this way, so we use the former.) For comparison, the Bayesian-determined errors for f_{B^+} and f_{B_s} are 5.5 and 5.1 MeV, respectively.

For informational purposes, it is useful to break down this inclusive error into its component parts, at least approximately. We can see what errors to expect and, hence, target for improvement in future simulations. In particular, with our current actions, the light-quark and heavy-quark discretization errors should behave differently as a function of lattice spacing, with heavy-quark errors decreasing more slowly as a is reduced. To extract the pure statistical errors, we rerun the fits with all the Bayesian discretization terms set to zero. We then find the pure heavy-quark (or pure light-quark) discretization contributions, by turning back on the heavy-quark (light-quark) terms, and then

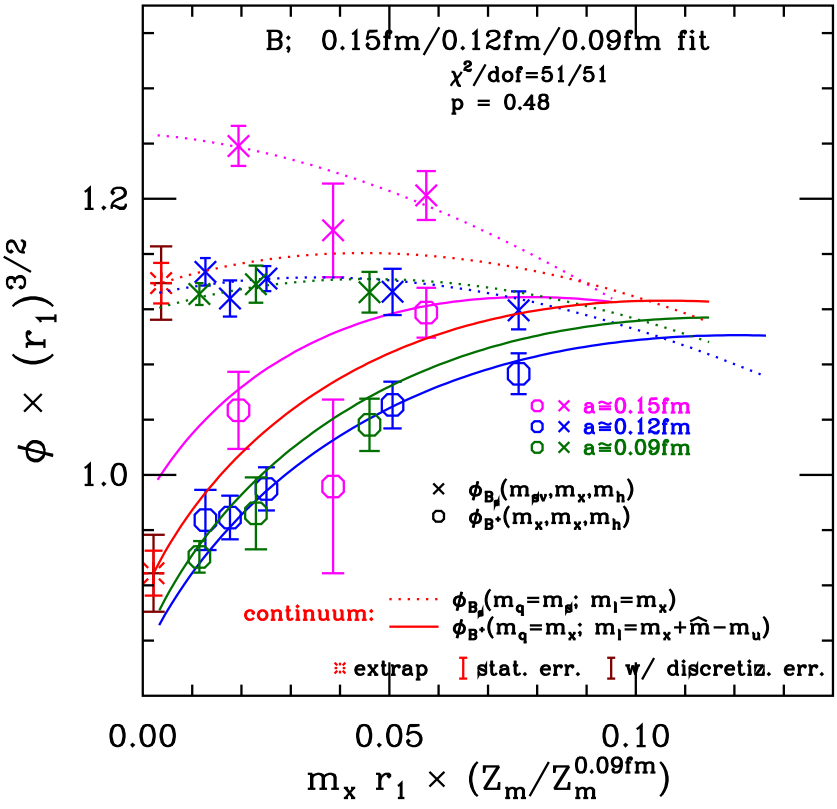

FIG. 7. Same as Fig. 6, but including points at $a \approx 0.15$ fm in the fit.

subtracting in quadrature the pure statistical errors from the resulting raw errors. These individual errors are shown in Table XIII in parentheses. Note that the total error at the bottom of the table includes the error on the first line, not the sum of the three errors in parentheses, when these differ. Note also that the discretization errors are similar to what we would have obtained with less sophisticated power counting.

B. Chiral extrapolation and taste-violating light-quark discretization effects

As described in Sec. VI, we modify the chiral fit function in a variety of ways to estimate the error associated with the chiral extrapolation:

χ1. Set the chiral coupling f to f_K instead of f_π.

χ2. Allow the chiral coupling f to be a Bayesian fit parameter, with prior value f_π and prior width equal to $f_K - f_\pi$.

χ3. Replace the H-H^*-π coupling g_π (which is 0.51 in the central fit) with 0.31 or 0.71, which are the extremes of the range discussed in Sec. VI.

χ4. Allow g_π to be a constrained fit parameter, with prior value 0.51 and prior width 0.20.

χ5. Fix to zero those NNLO analytic terms [Q_2 and/or Q_4 in Eq. (6.15)] that may be eliminated without making the fit unacceptably poor.

χ6. Use the chiral function without hyperfine and flavor splittings, *i.e.*, use Eq. (6.2) instead of Eq. (6.20).

χ7. Use combinations of modifications χ1 and χ3 or modifications χ2 and χ3. These choices can produce significantly larger deviations since changes in g_π have a similar effect on the fit function as changes in f.

These modifications typically change the decay constant by 1–3 MeV, and the ratios by 1–1.5%. We take the chiral extrapolation error of a given quantity to be the largest change (of either sign) under the above modifications, and

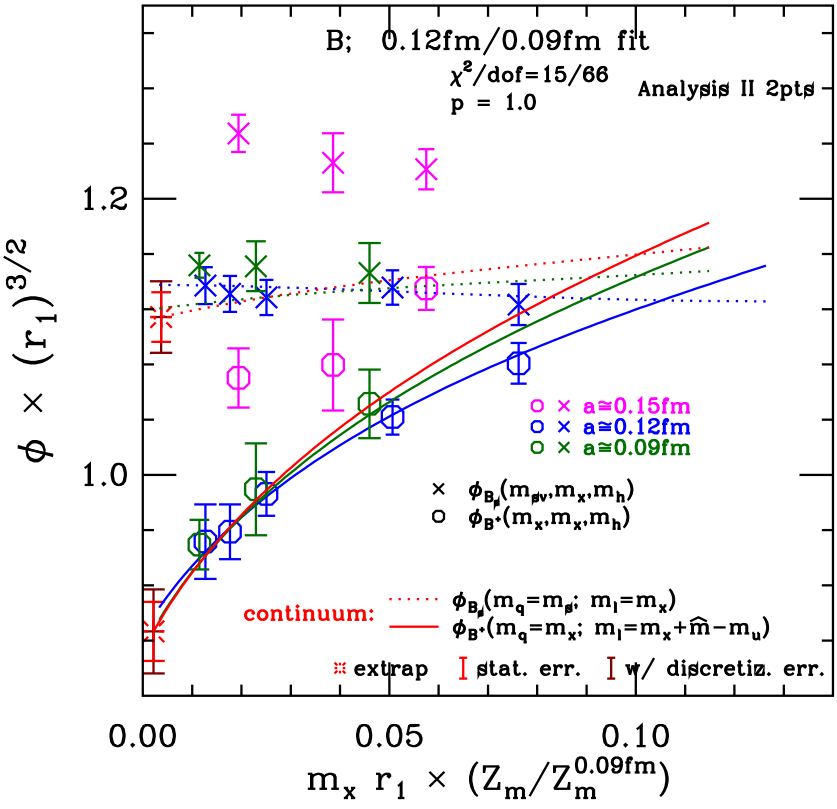

FIG. 8. Same as Fig. 6, but using Analysis II of the 2-point functions.

TABLE XIII. Total error budget for the heavy-light decay constants. Uncertainties are in MeV for decay constants. The total combines errors in quadrature. The first row includes statistics, heavy-quark discretization errors, and generic light-quark discretization errors, as explained in the text. Errors in parentheses are approximate sub-parts of errors that are computed in combination.

Source	f_{D^+} (MeV)	f_{D_s} (MeV)	f_{D_s}/f_{D^+}	f_{B^+} (MeV)	f_{B_s} (MeV)	f_{B_s}/f_{B^+}
Statistics ⊕ discretization	9. 2	8. 9	0. 014	5. 8	6. 0	0. 013
(statistics)	(2. 3)	(2. 3)	(0. 005)	(3. 6)	(3. 4)	(0. 010)
(heavy-quark disc.)	(8. 2)	(8. 3)	(0. 007)	(3. 8)	(4. 3)	(0. 004)
(light-quark disc.)	(2. 9)	(1. 5)	(0. 012)	(2. 5)	(2. 5)	(0. 007)
Chiral extrapolation	3. 2	2. 2	0. 014	2. 9	2. 8	0. 014
Two-point functions	3. 3	1. 6	0. 013	3. 0	4. 1	0. 015
Scale (r_1)	1. 0	1. 0	0. 001	1. 0	1. 4	0. 001
Light quark masses	0. 3	1. 4	0. 005	0. 1	1. 3	0. 006
Heavy quark tuning	2. 8	2. 8	0. 003	3. 9	3. 9	0. 005
u_0 adjustment	1. 8	2. 0	0. 001	2. 5	2. 8	0. 001
Finite volume	0. 6	0. 0	0. 003	0. 5	0. 1	0. 003
$Z_{V^4_{QQ}}$ and $Z_{V^4_{qq}}$	2. 8	3. 4	0. 000	2. 6	3. 1	0. 000
Higher-order $\rho^{Qq}_{A_4}$	1. 5	1. 8	0. 001	1. 4	1. 7	0. 001
Total Error	11. 3	10. 8	0. 025	9. 1	10. 0	0. 026

list it in Table XIII. In several cases, (f_{D^+}, f_{D_s}/f_{D^+}, and f_{B_s}/f_{B^+}) the largest change comes from modification $\chi 6$, eliminating the heavy-light splittings. The fit without the splittings is shown for the D system in Fig. 9. It may be compared to Fig. 3 to see the effects: the curvature at small mass for ϕ_{D^+} is slightly greater without the splittings, which results in a decrease of f_{D^+} of 3.2 MeV. Note that the p values of the two fits are almost identical, so the goodness-of-fit cannot be used to choose one version of the chiral extrapolation over the other.

Modifications of f and/or g_π produce the largest changes in the other quantities, namely f_{D_s}, f_{B^+} and f_{B_s}. In particular, putting $f = f_K$ and $g_\pi = 0.31$ results in an increase of +2.9 for f_{B^+} and +2.8 MeV for f_{B_s}. The modified fit is shown in Fig. 10, and may be compared with Fig. 6 to see the effects of the changes. Increasing f and decreasing g_π both suppress the chiral logarithms [*cf.* Eq. (6.20)] and give fit functions with less curvature and smaller slope at low quark mass.

In Sec. VI A, we argued that the fact that the chiral power counting is at best marginally applicable in the neighborhood of M_K is not a problem for the chiral extrapolation. To test this, we remove the largest two valence quark masses from each ensemble, and repeat the analysis. The heaviest valence masses are then $0.73m_s$ on the $a \approx 0.09$ fm ensembles and $0.58m_s$ on the $a \approx 0.12$ fm ensembles. For all quantities, the differences in final results from the central analysis are comparable to or less than the purely statistical errors, and always significantly less than the chiral error determined by the comparisons $\chi 1$–$\chi 7$ above. Furthermore, the chiral fit parameters never change by more than the statistical errors.

Since the rSχPT fit functions in Eqs. (6.2) and (6.20) explicitly include one-loop discretization effects coming from taste violations in the (rooted) staggered light quark action, the chiral error estimates we describe here inherently include taste-violating discretization errors. However, it seems unlikely that the current data can accurately distinguish between such taste-violating errors of order $\alpha_s^2 a^2$ and generic light-quark discretization effects of order $\alpha_s a^2$, or even heavy-quark discretization effects. Indeed, the taste-violating LEC L_a [*cf.* Eq. (6.12)] is not well constrained by our fits and is consistent with zero within large errors. The central fits give

$$L_a = +0.6 \pm 6.5 \qquad (D \text{ system}), \tag{7.1}$$

$$L_a = -1.9 \pm 8.8 \qquad (B \text{ system}), \tag{7.2}$$

where the error is the raw statistical error. (Note that we do not constrain L_a by any prior width.) The errors in L_a decrease by about 10% if Bayesian parameters for generic light-quark errors are removed, and an additional 10% if the parameters for heavy-quark errors are removed. Thus, there is "cross talk" between various error sources, making it difficult to completely distinguish the various types of discretization errors. Future work, with more and finer lattice spacings, should make a cleaner separation possible.

C. Fitting errors

The "fitting errors" are the errors introduced in the analysis of the two-point correlators. They represent the effects of various choices of fit ranges and fitting functions, and are an estimate of the systematic effect of the contamination by excited states. We compare results from the three choices of two-point fitting (see Sec. IV): Analysis I, Analysis II, and a modified Analysis I using 1 simple + 1 oscillating state, but values of $t_{\rm min}$ larger than those described in Sec. IV B.

Some of these differences may, in fact, be due simply to statistical effects, and hence already included in the statistical error. Figure 11 shows the differences between values of ϕ_{B_q} in Analyses I and II, divided by the average statistical error for each of the common partially quenched data points. Only 10 of 74 differences are greater than 1 statistical σ. Nevertheless, there appears to be some significant systematic trend in that 46 of 74 points are positive. To be conservative, we take the largest difference between the Analysis-I fits and the other two fits as the fitting error for each physical quantity, and list it in Table XIII. For f_{D_s} and f_{B_s}, the difference is largest for chiral fits based on 2-point Analysis II, while, for the other four quantities, the difference is largest for the modified Analysis I.

D. Scale uncertainty

We use the scale $r_1 = 0.3117(22)$ fm to tune the values of the quark masses and convert the decay constants into physical units (see Sec. III A). To find the scale errors on the final results, we shift r_1 to 0.3139 fm or 0.3095 fm and redo the analysis. Although ϕ_H scales like $r_1^{-3/2}$, the change in the results under a change in r_1 is smaller than pure dimensional analysis would imply, because our estimates of the physical light masses and the heavy-quark $\kappa_{\rm c}$ and $\kappa_{\rm b}$ also shift, producing partially compensating changes in ϕ_H. At $r_1 = 0.3139$ fm, we shift the light masses in Table XII upward by the scale error shown in that table. [The lattice light-quark masses scale like r_1^2, because they are approximately linear in the squared meson masses $(r_1 m_\pi)^2$ and $(r_1 m_K)^2$.] Similarly, we shift the tuned $\kappa_{\rm c}$ and $\kappa_{\rm b}$ downward by the scale error in Table V because the bare heavy quark mass increases with r_1. We then adjust $\phi_{B_{(s)}}$ and $\phi_{D_{(s)}}$ at each lattice spacing using Eq. (3.5) and the values of $d\phi/d\kappa$ given in Table V. Redoing the preferred

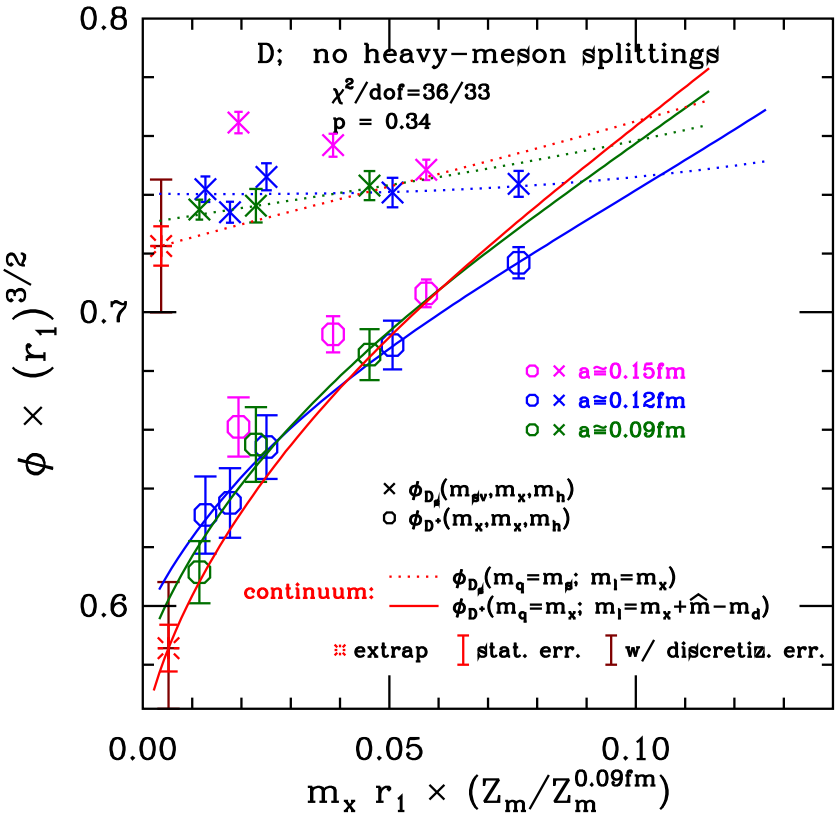

FIG. 9. Same as Fig. 3 but omitting heavy-light hyperfine and flavor splittings in the chiral fit function.

chiral fits shown in Figs. 3 and 6, extrapolating to the continuum, and plugging in the adjusted continuum light quark masses gives the scale error listed in Table XIII.

E. Light-quark mass determinations

To estimate the error from the light-quark mass determination, we follow a similar procedure to that in the scale-error case. We shift the continuum light quark masses in Table XII by the sum in quadrature of all errors except scale errors. This includes the statistical errors, the chiral errors and, where relevant, the electromagnetic errors. We then plug the new masses into the continuum-extrapolated chiral fits and take the difference from the central results to give the errors listed in Table XIII. The relative direction of shifts on different masses makes little difference in the size of the errors on the decay constants f_{D_s}, f_{D^+}, f_{B_s}, and f_{B^+}, since they are sensitive primarily to the valence quark masses. However, it does affect the error of the ratios f_{D_s}/f_{D^+} and f_{B_s}/f_{B^+}. The largest effect clearly occurs when the strange mass is shifted in the opposite direction from the lighter masses. To be conservative, we take the size of change of the ratios in this case as the error, but this is almost certainly an overestimate because the statistical and chiral extrapolation errors on the light quark masses are positively correlated between the strange mass and the other masses.

Note that the errors from the light-quark masses in Table XIII are much larger for f_{D_s} and f_{B_s} than for f_{D^+} and f_{B^+}. That simply reflects the facts that the decay constants have a nonzero limit when the quark masses vanish, and that the dependence on the quark masses is reasonably linear. Thus a given percent error in the strange mass produces a much larger percent difference in f_{D_s} and f_{B_s}, than the same percent error in the d or u mass does in f_{D^+} and f_{B^+}.

F. Bottom and charm quark mass determinations

The propagation of statistical errors in the tuned κ_c and κ_b to the decay constants is complicated by the fact that the independent errors at each lattice spacing affect the final results in a nontrivial way through the continuum and

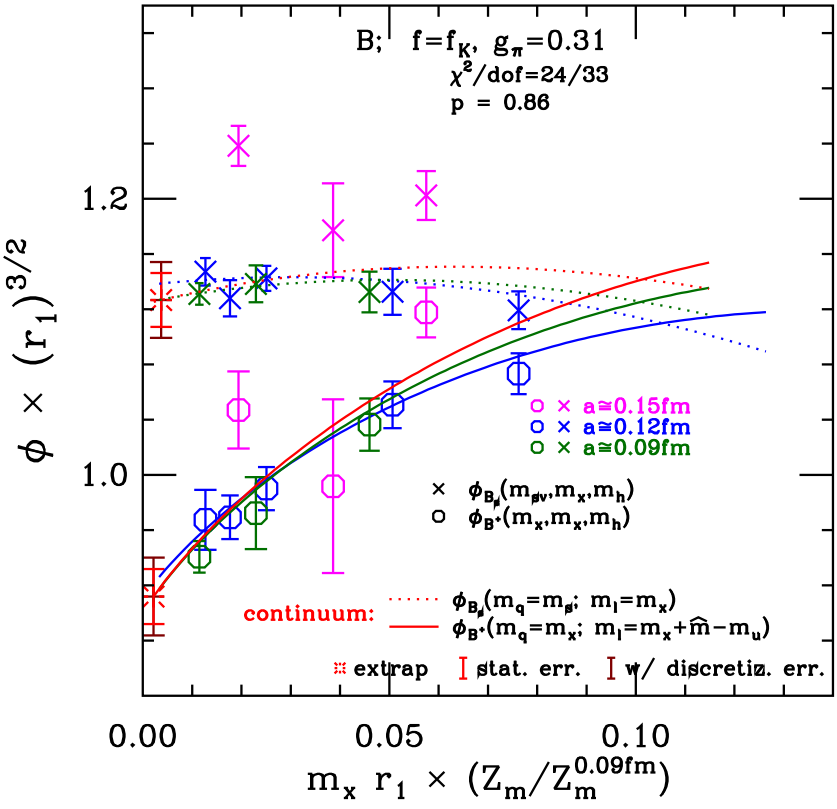

FIG. 10. Same as Fig. 6 but with $f = f_K$ and $g_\pi = 0.31$ in the chiral fit function.

chiral extrapolations. At each lattice spacing, we choose 200 gaussian-distributed ensembles of trial κ values with central value equal to the tuned values, and standard deviation equal to the statistical error, taken from Table V. For a given choice of trial κ values at each lattice spacing, we produce an adjusted trial data sample by shifting the ϕ_H values according to Eq. (3.5), but with the trial values replacing the tuned values. We then perform the complete chiral fit and extrapolation procedure on each of the 200 trial data sets. The standard deviation over trials of a given decay constant or decay constant ratio is taken to be the heavy quark tuning error, and is listed in Table XIII.

G. Tadpole factor (u_0) adjustment

In order to improve the convergence of lattice perturbation theory, we use tadpole-improved actions for the gluons, light quarks, and heavy quarks [79]. For the gluon and sea-quark actions we take the tadpole factor u_0 from the average plaquette. On the $a \approx 0.15$ fm and $a \approx 0.09$ fm lattices we use the same choice for the light valence and heavy-quark actions. On the $a \approx 0.12$ fm lattices, however, we use the tadpole factor u_0 taken from the Landau link in the valence-quark action and in the clover term in the heavy-quark action. This results in a slight mismatch between the light valence and sea-quark actions on these ensembles, and also affects the values obtained for the tuned bottom- and charm-quark masses κ_b and κ_c. The difference between u_0 obtained from the average plaquette and the Landau link is approximately 3–4% on the $a \approx 0.12$ fm ensembles.

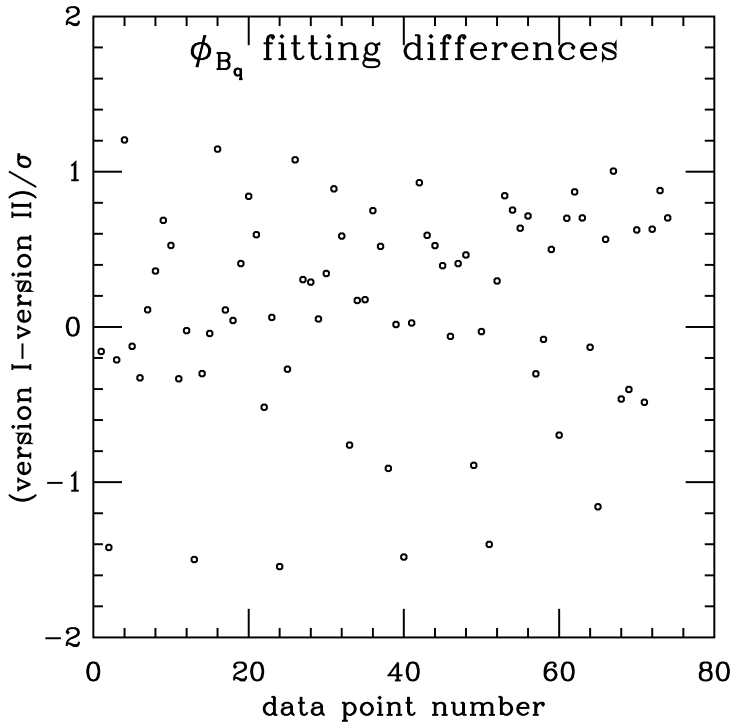

FIG. 11. Difference of ϕ_{B_q} values from Analyses I and II, divided by the average statistical error at each of the common valence and sea mass points. The order along the abscissa is arbitrary.

We propagate this difference through the chiral/continuum extrapolation as follows. First, we compute the heavy-strange meson decay amplitudes ϕ_{B_s} and ϕ_{D_s} with both choices for u_0 on the ensemble with $am_l/am_h = 0.01/0.05$, $a \approx 0.12$ fm. For each choice of u_0, we compute ϕ_{B_s} and ϕ_{D_s} directly at the tuned values of κ_b and κ_c, thereby avoiding an interpolation in κ. Next, we renormalize the lattice decay amplitudes using the nonperturbative, flavor-diagonal current renormalization factors $Z_{V^4_{qq}}$ and $Z_{V^4_{QQ}}$ obtained for each case. (We neglect the slight difference in the perturbative correction $\rho_{A^4_{Qq}}$.) Then, we calculate the ratio of the renormalized decay amplitudes, finding no difference within errors:

$$\phi_c^{\text{plaquette}}/\phi_c^{\text{Landau}} = 1.005(13), \tag{7.3}$$

$$\phi_b^{\text{plaquette}}/\phi_b^{\text{Landau}} = 1.014(20). \tag{7.4}$$

As expected, the u_0 dependence from the bare current and renormalization factors mostly cancels. Finally, we repeat the chiral/continuum extrapolation shifting ϕ_c and ϕ_b on the $a \approx 0.12$ fm ensembles by the statistical errors reported in Eqs. (7.3)–(7.4). We find that these percent-level errors in ϕ_c and ϕ_b lead to approximately 1% errors in the extrapolated decay constants and approximately 0.1% errors in the decay-constant ratios. These errors are listed as "u_0 adjustment" in the error budget in Table XIII.

H. Heavy-light current renormalization

There are two sources of systematic error in our heavy-light current renormalization. The first is due to the perturbative calculation of $\rho_{A^4_{Qq}}$ and the second is due to the nonperturbative calculation of $Z_{V^4_{QQ}}$ and $Z_{V^4_{qq}}$.

The perturbative calculation of $\rho_{A^4_{Qq}}$ has been carried out to one-loop order. Since $\rho_{A^4_{Qq}}$ is defined from a ratio of renormalization factors [see Eq. (2.5)], its perturbative corrections are small by construction. Indeed, as can be seen from the results for $\rho_{A^4_{Qq}}$ given in Table VIII, we observe very small corrections. For bottom they range from 0.3% at $a \approx 0.09$ fm to 0.8% at $a \approx 0.12$ fm and 2.8% at $a \approx 0.15$ fm. For charm they range from less than 0.08% at $a \approx 0.09$ fm to 0.4% at $a \approx 0.12$ fm and 0.6% at $a \approx 0.15$ fm. As shown in Ref. [46] the perturbative corrections to the ρ-factors for the spatial currents, while still small, tend to be bigger than those for the temporal currents A^4 and V^4. We therefore estimate the error due to neglecting higher order terms as $\rho^{[1]}_{V^1_{Qq}}\,\alpha_s^2$. We take α_s at $a \approx 0.09$ fm and $\rho^{[1]}_{V^1_{Qq}} \approx 0.1$, which is the largest one-loop coefficient for $\rho_{V^1_{Qq}}$ in the mass range $m_Q a \leq 3$. This procedure yields a systematic error of 0.7%, which we take for both charm and bottom decay constants.

The decay constant ratios f_{B_s}/f_{B^+} and f_{D_s}/f_{D^+} depend on the corresponding ratios of $\rho_{A^4_{Qs}}/\rho_{A^4_{Qq}}$. These ratios differ from unity only because of the small variation of the $\rho_{A^4_{Qq}}$ with light valence mass, which is described in Sec. V. We take the variation of the $\rho_{A^4_{Qq}}$ with light valence mass at $a \approx 0.09$ fm as the error. This yields an error of 0.1% for both bottom and charm.

The dominant corrections in the heavy-light renormalization factor as defined in Eq. (2.5) are due to $Z_{V^4_{QQ}}$ and $Z_{V^4_{qq}}$ which are calculated nonperturbatively. The values (and errors) for $Z_{V^4_{qq}}$ and $Z_{V^4_{QQ}}$ are listed in Tables IX and XI, respectively. To obtain the error in $Z_{V^4_{Qq}} = \sqrt{Z_{V^4_{qq}}\,Z_{V^4_{QQ}}}$ we add the statistical errors in $Z_{V^4_{qq}}$ and $Z_{V^4_{QQ}}$ in quadrature. The error on $Z_{V^4_{Qq}}$ is dominated by the error on $Z_{V^4_{qq}}$. The errors are largest, 1.3%, on the $a \approx 0.09$ fm ensemble and they are about the same for both charm and bottom on the two finest ensembles used to obtain our main decay constant results. Hence we use 1.3% as our estimate for the uncertainty in $Z_{V^4_{Qq}}$.

I. Finite volume effects

To study finite volume effects, we use the chiral fit function with heavy-light hyperfine and flavor splittings included (Eq. (6.20)), since the effects are known to be larger with the splittings than without [82]. The central fit includes the (one-loop) finite volume corrections, Eq. (6.21), on the lattice data, and then takes the infinite volume limit when extracting the final results for the decay constants. We then take the larger of the following two values as our estimate of the finite volume error:

V1. The difference between the central result and the result from a chiral fit in which the finite volume corrections are omitted.

V2. The largest finite volume correction to the relevant data points, as determined by the central fit. For ϕ_{D^+} and ϕ_{B^+}, the "relevant data points" are the ones on each ensemble with the lightest valence mass, *i.e.*, those closest to the chirally extrapolated point. For ϕ_{D_s} and ϕ_{B_s}, the relevant points are the ones on each ensemble with valence mass closest to m_s.

Method V1 gives a larger difference for ϕ_{D_s} and ϕ_{B_s}; method V2 for ϕ_{D^+} and ϕ_{B^+} and the ratios. The resulting values are shown in Table XIII. Note that our choices are conservative because we correct for the (one-loop) finite volume errors, but nevertheless take the full size of these effects as our error.

VIII. RESULTS AND CONCLUSIONS

After adding the error estimates described in the previous section in quadrature, we obtain:

$$f_{B^+} = 196.9(9.1)\ \text{MeV}, \tag{8.1}$$
$$f_{B_s} = 242.0(10.0)\ \text{MeV}, \tag{8.2}$$
$$f_{B_s}/f_{B^+} = 1.229(0.026), \tag{8.3}$$
$$f_{D^+} = 218.9(11.3)\ \text{MeV}, \tag{8.4}$$
$$f_{D_s} = 260.1(10.8)\ \text{MeV}, \tag{8.5}$$
$$f_{D_s}/f_{D^+} = 1.188(0.025). \tag{8.6}$$

Since our most reliable method of determining discretization errors combines them with statistical errors, we do not quote separate statistical and systematic errors.

Figure 12 shows a comparison of our results for charmed decay constants with other lattice QCD calculations and with experiment. Our results agree with the only other three-flavor lattice QCD determination from the HPQCD collaboration [99], which is obtained with HISQ staggered valence quarks and asqtad staggered sea quarks. (The difference in f_{D_s} is a bit greater than 1σ.) They are also consistent with the two-flavor results of the ETM Collaboration using twisted-mass Wilson fermions [100], although the ETM error budget does not include an estimate of the uncertainty due to quenching the strange quark. One can also compare with "experimental" determinations of f_D and f_{D_s} if one assumes CKM unitarity to obtain the matrix elements $|V_{cd}|$ and $|V_{cs}|$. For the D meson, Rosner and Stone combine CLEO's measurement of branching fraction $\mathcal{B}(D^+ \to \mu^+\nu)$ [101] with the latest determination of $|V_{cd}|$ from the PDG [54] to obtain $f_D = 206.7(8.9)$ MeV [53]. For the D_s meson, they average CLEO and Belle results for $\mathcal{B}(D_s^+ \to \mu^+\nu)$ [102, 103] with CLEO and BABAR results for $\mathcal{B}(D_s^+ \to \tau^+\nu)$ [102, 104–106] to obtain a combined average for the two decay channels of $f_{D_s} = 257.5(6.1)$ MeV [53]. The Heavy Flavor Averaging Group obtains a similar average, $f_{D_s} = 257.3(5.3)$ MeV [107]. Our results are consistent with these values, confirming Standard Model expectations at the $\sim 5\%$ level.

Figure 13 shows a similar comparison of our results for bottom meson decay constants with other lattice QCD calculations. Our results agree with the published three-flavor determination using NRQCD b-quarks and Asqtad staggered light quarks of the HPQCD collaboration [109], but are only marginally consistent with HPQCD's more recent calculation of f_{B_s} using HISQ light valence quarks [108]. Our results are also consistent with the two-flavor results of the ETM collaboration [100], who use Wilson heavy quarks and interpolate between the charm-mass region and the static limit to obtain results for bottom. Further, our result for the ratio f_{B_s}/f_B also agrees with the significantly less precise three-flavor determination using static b-quarks and domain-wall light quarks by the RBC and UKQCD Collaborations [110].

For the D system the largest uncertainties in our current calculation stem from heavy-quark discretization, while the chiral extrapolation, the Z_V factors, excited states, heavy-quark tuning, and the chiral-continuum extrapolation play important but subdominant roles. For the B system, heavy-quark tuning, statistics, and excited states are the sources of the largest errors, while the Z_V factors and the chiral-continuum extrapolation (incorporating our estimate of heavy-quark discretization effects) are next in size. Recall that a novel feature of our work is the treatment of heavy-quark discretization effects, via the functions f_i in Eq. (2.4), and priors constraining the chiral-continuum fits to follow this form. At tree level, we have explicit calculations of the mismatch, some of which appeared already in Ref. [36] and all of which are compiled in Ref. [63]. Beyond the tree level, the continuum and static limits can be used to constrain the functional form. That said, the theoretical guidance of the priors cannot be highly effective in an analysis, such as this, with only two lattice spacings. Indeed, the quoted heavy-quark discretization errors are similar to less sophisticated power-counting estimates.

While completing this analysis, we have begun runs to generate data that will address the main sources of uncertainty reported here. The new data set will contain four times the configurations used here to reduce the statistical errors

in the correlation functions and, thus, directly improve the decay amplitudes, the determinations of the hopping-parameters κ_c and κ_b, and the renormalization factors $Z_{V^4_{qq}}$ and $Z_{V^4_{QQ}}$, all of which feed into the decay constant. Our new data will also encompass two finer lattice spacings of $a \approx 0.06$ fm and $a \approx 0.045$ fm, in order to explicitly reduce light- and heavy-quark discretization errors and better control the continuum extrapolation. With four lattice spacings, our new method of heavy-quark discretization priors will be put to a more stringent test. The new runs will also include light valence- and sea-quark masses down to $\sim m_s/20$ in order to better control the chiral extrapolation

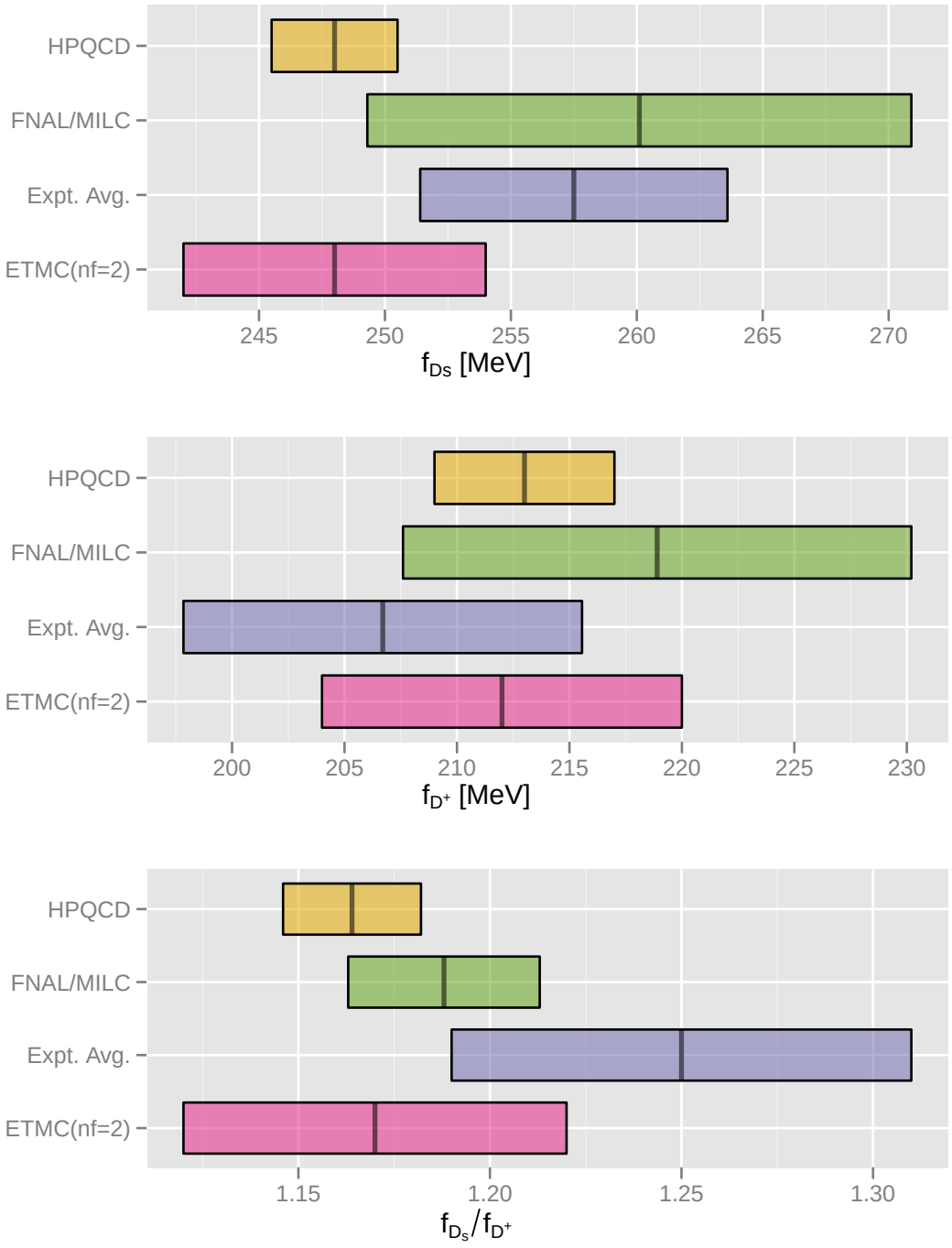

FIG. 12. Comparison of f_D and f_{D_s} with other two- and three-flavor lattice QCD calculations and with experiment. Results shown come from Refs. [53, 99–106]. The HPQCD f_D value is computed from their update to f_{D_s} and their earlier result for the ratio f_{D_s}/f_D.

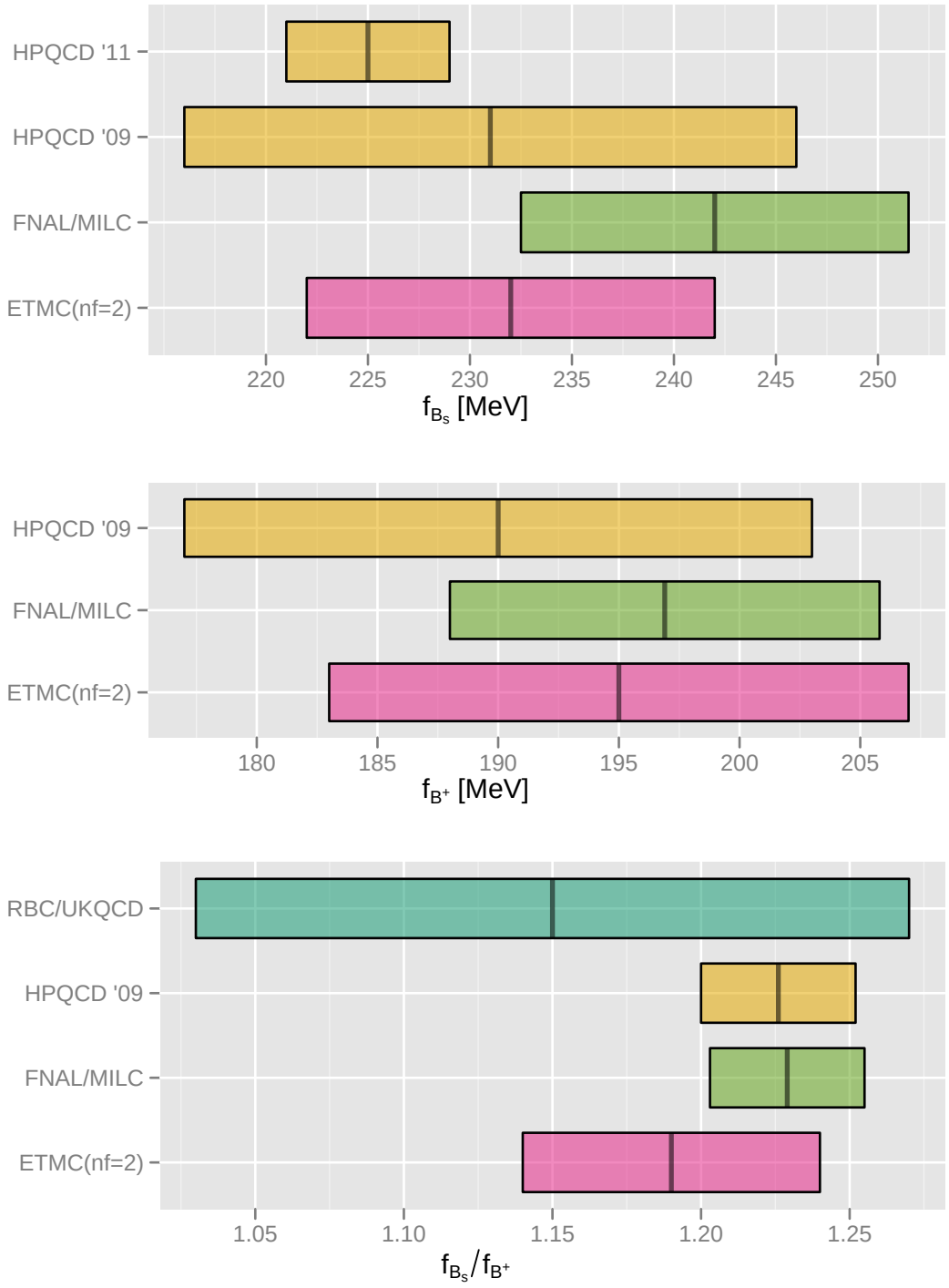

FIG. 13. Comparison of f_B and f_{B_s} with other two- and three-flavor lattice QCD calculations. Results shown come from Refs. [100, 108–110]. In the case of f_{B_s} HPQCD has two separate calculations using NRQCD b quarks and using HISQ b quarks; we show both the published NRQCD result (HPQCD '09) and the more recent HISQ result (HPQCD '11) in the plot above.

to the physical d and u quark masses.

In order to reduce errors further, we will have to eliminate the errors from the matching factors and from quenching the charmed quark. The MILC Collaboration [111] is generating ensembles with 2+1+1 flavors of sea quarks with the HISQ action, with plans to provide a range of lattice spacings and sea quark masses equal to or more extensive than the 2+1 asqtad ensembles. Use of the HISQ action for the charm valence quark will allow us to further reduce many of the uncertainties, and provides the particularly nice advantage that one can use the local pseudoscalar density without multiplicative renormalization to obtain the continuum matrix element [112]. In several years, once the full suite of HISQ ensembles with several sea-quark masses and lattice spacings has been analyzed, we expect to obtain percent-level errors for both B- and D-meson decay constants. This will enable precise tests of the Standard Model and may help to reveal the presence of new physics in the quark-flavor sector.

ACKNOWLEDGMENTS

We thank David Lin for his finite-volume chiral-log *Mathematica* code, upon which our own code is based. Computations for this work were carried out with resources provided by the USQCD Collaboration, the Argonne Leadership Computing Facility, the National Energy Research Scientific Computing Center, and the Los Alamos National Laboratory, which are funded by the Office of Science of the U.S. Department of Energy; and with resources provided by the National Institute for Computational Science, the Pittsburgh Supercomputer Center, the San Diego Supercomputer Center, and the Texas Advanced Computing Center, which are funded through the National Science Foundation's Teragrid/XSEDE Program. This work was supported in part by the U.S. Department of Energy under Grants No. DE-FC02-06ER41446 (C.D., L.L., M.B.O.), No. DE-FG02-91ER40661 (S.G.), No. DE-FG02-91ER40677 (C.M.B, R.T.E., E.D.F., E.G., R.J., A.X.K.), No. DE-FG02-91ER40628 (C.B), No. DE-FG02-04ER-41298 (D.T.); by the National Science Foundation under Grants No. PHY-0555243, No. PHY-0757333, No. PHY-0703296 (C.D., L.L., M.B.O.), No. PHY-0757035 (R.S.), No. PHY-0704171 (J.E.H.); by the URA Visiting Scholars' program (C.M.B., R.T.E., E.G., M.B.O.); by the Fermilab Fellowship in Theoretical Physics (C.M.B.); by the M. Hildred Blewett Fellowship of the American Physical Society (E.D.F.); and by the Science and Technology Facilities Council and the Scottish Universities Physics Alliance (J.L.). This manuscript has been co-authored by employees of Brookhaven Science Associates, LLC, under Contract No. DE-AC02-98CH10886 with the U.S. Department of Energy. R.S.V. acknowledges support from BNL via the Goldhaber Distinguished Fellowship. Fermilab is operated by Fermi Research Alliance, LLC, under Contract No. DE-AC02-07CH11359 with the United States Department of Energy.

Appendix A: Heavy-quark Discretization Effects

We are using the heavy-quark Lagrangian as given in [36], with $\kappa_t = \kappa_s$ (or, equivalently, $\zeta = 1$), $r_s = 1$, and $c_B = c_E = c_{\rm SW}$. This amounts to the Sheikholeslami-Wohlert Lagrangian [35] for Wilson fermions [62]. The current has a heavy quark of this type, rotated as in Eq. (4.2) (*cf.* Eqs. (7.8)–(7.10) of Ref. [36]), and a staggered light quark. At the tree level, the heavy-quark rotation is the same no matter what the other quark is. The discretization effects are estimated from a (continuum) effective field theory [39–41], as shown explicitly for decay constants in Eqs. (8.7)–(8.12) of Ref. [39].

1. Theory

Both QCD and lattice gauge theory can be described via

$$\mathcal{L}_{\rm QCD} \doteq \mathcal{L}_{\rm HQET} = \sum_i \mathcal{C}_i^{\rm cont}(m_Q)\mathcal{O}_i, \tag{A1}$$

$$\mathcal{L}_{\rm LGT} \doteq \mathcal{L}_{{\rm HQET}(m_0 a)} = \sum_i \mathcal{C}_i^{\rm lat}(m_Q, m_0 a)\mathcal{O}_i, \tag{A2}$$

where the $\mathcal{C}_i$ are short-distance coefficients and the $\mathcal{O}_i$ are operators describing the long-distance physics. The coefficients have dimension $4 - \dim \mathcal{O}_i$. For lattice gauge theory. they depend on $m_0 a$, which is a ratio of short distances a and $1/m_Q$. The effective-theory operators $\mathcal{O}_i$ in Eqs. (A1) and (A2) are the same.

The error from each term is simply the difference

$$\texttt{error}_i = \left| \left[\mathcal{C}_i^{\rm lat}(m_Q, m_0 a) - \mathcal{C}_i^{\rm cont}(m_Q) \right] \mathcal{O}_i \right| . \tag{A3}$$

The relative error in our matrix elements can be estimated by setting $\langle \mathcal{O}_i \rangle \sim \Lambda_{\rm QCD}^{\dim \mathcal{O}_i - 4}$; choices for the QCD scale $\Lambda_{\rm QCD}$ are discussed below. The coefficient mismatch can be written

$$\mathcal{C}_i^{\rm lat}(m_Q, m_0 a) - \mathcal{C}_i^{\rm cont}(m_Q) = a^{\dim \mathcal{O}_i - 4} f_i(m_0 a). \tag{A4}$$

This recovers the usual counting of powers of a (familiar from Symanzik [37, 38]), but maintaining the full $m_0 a$ dependence. The final expression for the discretization errors is then

$$\texttt{error}_i \propto f_i(m_0 a)(a\Lambda_{\rm QCD})^{\dim \mathcal{O}_i - 4}. \tag{A5}$$

For Wilson fermions, $\lim_{m_0 a \to 0} f_i =$ constant (whereas in lattice NRQCD without fine tuning this is not the case). We have explicit calculations of the f_i for the $O(a)$ and $O(a^2)$ errors at the tree level [36, 63]. The next subsection discusses how to use them to guide a continuum-limit extrapolation the $O(\alpha_s a)$ and $O(a^2)$ errors.

Equations (A1) and (A2) can be generalized to currents. For the axial-vector current,

$$\mathcal{A}^\mu \doteq C_{A_\perp}^{\rm cont}(m_Q)\bar{q} i\gamma_\perp^\mu \gamma_5 h_v - C_{A_\parallel}^{\rm cont}(m_Q) v^\mu \bar{q}\gamma_5 h_v - \sum_i B_{Ai}^{\rm cont}(m_Q)\mathcal{Q}_{Ai}^\mu, \tag{A6}$$

$$A_{\rm lat}^\mu \doteq C_{A_\perp}^{\rm lat}(m_Q, m_0 a)\bar{q} i\gamma_\perp^\mu \gamma_5 h_v - C_{A_\parallel}^{\rm lat}(m_Q, m_0 a) v^\mu \bar{q}\gamma_5 h_v - \sum_i B_{Ai}^{\rm lat}(m_Q, m_0 a)\mathcal{Q}_{Ai}^\mu, \tag{A7}$$

and $\doteq$ again means in the sense of matrix elements. Here v^μ selects the temporal component and $\perp$ the spatial, and the list of dimension-4 operators $\mathcal{Q}$ can be found in Refs. [40].

The matrix element of the temporal component of the axial-vector current [*cf.* Eq. (4.7)] is normalized by multiplying with $Z_{A^4} = C_{A_\parallel}^{\rm cont}/C_{A_\parallel}^{\rm lat}$. The current mismatch then leads to errors

$$a^{\dim \mathcal{Q}_i - 3} f_i(m_0 a) = Z_{A^4} B_{Ai}^{\rm lat} - B_{Ai}^{\rm cont}, \tag{A8}$$

with the sum running over the two operators $\mathcal{Q}$ that point in the temporal direction [40].

2. Error Estimation

The total error from heavy-quark discretization effects is then

$$\texttt{error} = \sum_i z_i \, (a\Lambda_{\rm QCD})^{s_i} f_i(m_0 a) \tag{A9}$$

where the sum runs over Lagrangian operators $\mathcal{O}_i$ of dimension 5 and 6 and current operators $\mathcal{Q}_i$ of dimension 4 and 5, $s_i = \dim \mathcal{O}_i - 4$ or $\dim \mathcal{Q}_i - 3$, and the z_i are unknown coefficients. The functions f_i (summarized below) have been computed for $\mathrm{O}(a^2)$ and estimated for $\mathrm{O}(\alpha_s a)$. We omit contributions of order $\alpha_s^l a^2$, whether from extra operators or from iterating to second order operators with coefficients of order $\alpha_s a$.

In the past, we have taken a very conservative $\Lambda_{\rm QCD} = 700$ MeV and assumed a Gaussian distribution for the z_i centered on 0 and of width 1. This amounts to treating the discretization errors as independent and adding them in quadrature. It also implicitly assumes that the data have nothing to say about the size or relative importance of the terms.

Here, however, we incorporate these errors into the chiral-continuum extrapolation, discussed in Sec. VI. This means that the z_i are now constrained fit parameters, with prior constraints discussed in Sec. VI.

The f_i are collected next.

a. $\mathrm{O}(a^2)$ *errors*

We start with these, because explicit expressions for the functions $f_i(m_0 a)$ are available. The Lagrangian leads to two bilinears, $\bar{h}\boldsymbol{D}\cdot\boldsymbol{E}h$ and $\bar{h}i\boldsymbol{\Sigma}\cdot[\boldsymbol{D}\times\boldsymbol{E}]h$, and many four-quark operators. At the tree level the coefficients of all four-quark operators vanish. At the tree level the coefficients of the two bilinears are the same, and the mismatch function is

$$f_E(m_0 a) = \frac{1}{8m_E^2 a^2} - \frac{1}{2(2m_2 a)^2}. \tag{A10}$$

Using explicit expressions for $1/m_2$ [36] and $1/m_E^2$ [63], one finds

$$f_E(m_0a) = \frac{1}{2}\left[\frac{c_E(1+m_0a)-1}{m_0a(2+m_0a)(1+m_0a)} - \frac{1}{4(1+m_0a)^2}\right]. \tag{A11}$$

We are using $c_E = 1$, so

$$f_E(m_0a) = \frac{2+3m_0a}{8(2+m_0a)(1+m_0a)^2}. \tag{A12}$$

With no further assumptions, this term enters twice independently, so we take the width of this prior to be $\sqrt{2}$ rather than 1.

The current leads to three more terms with non-zero coefficients, $\bar{q}\Gamma \boldsymbol{D}^2 h$, $\bar{q}\Gamma i\boldsymbol{\Sigma}\cdot\boldsymbol{B}h$, and $\bar{q}\Gamma\boldsymbol{\alpha}\cdot\boldsymbol{E}h$, which can be deduced from Eq. (A17) of Ref. [36]. Their coefficients can be read off from Eq. (A19). When $c_B = r_s$ the first two share the same coefficient

$$\begin{aligned} f_X(m_0a) &= \frac{1}{8m_X^2a^2} - \frac{\zeta d_1(1+m_0a)}{m_0a(2+m_0a)} - \frac{1}{2(2m_2a)^2}, \\ &= \frac{1}{2}\left[\frac{1}{(2+m_0a)(1+m_0a)} + \frac{1}{2(1+m_0a)} - \frac{1}{4(1+m_0a)^2} - \frac{1}{(2+m_0a)^2}\right], \\ &= \frac{1}{2}\left[\frac{1}{2(1+m_0a)} - \left(\frac{m_0a}{2(2+m_0a)(1+m_0a)}\right)^2\right], \end{aligned} \tag{A13}$$

where the last term on the second line comes from using the tree-level d_1 (as we do in the simulations). Because of the two-fold appearance, we again take the prior width to be $\sqrt{2}$.

For $\bar{q}\Gamma\boldsymbol{\alpha}\cdot\boldsymbol{E}h$

$$\begin{aligned} f_Y(m_0a) &= \frac{1}{2}\left[\frac{d_1}{m_2a} - \frac{\zeta(1-c_E)(1+m_0a)}{m_0a(2+m_0a)}\right], \\ &= \frac{2+4m_0a+(m_0a)^2}{4(1+m_0a)^2(2+m_0a)^2}, \end{aligned} \tag{A14}$$

where the last line reflects the choices made for c_E and d_1.

b. $\mathrm{O}(\alpha_s a)$ and $\mathrm{O}(a^3)$ errors

Here the mismatch functions $f_i(m_0a)$ start at order α_s, and we do not have explicit expressions for them. We take unimproved tree-level coefficients as a guide to the combinatoric factors and the asymptotic behavior as $m_0a \to 0$ and $m_0a \to \infty$.

The Lagrangian leads to two bilinears, the kinetic energy $\mathcal{O}_2 = \bar{h}\boldsymbol{D}^2h$ and the chromomagnetic moment $\mathcal{O}_B = \bar{h}i\boldsymbol{\Sigma}\cdot\boldsymbol{B}h$. We match the former nonperturbatively, by identifying the meson's kinetic mass with the physical mass; the discretization error f_2 stems, therefore, from discretization effects in M_2.

The computed kinetic meson mass is

$$M_2 = m_2(\kappa) + \text{continuum binding energy} + \delta M_2, \tag{A15}$$

where [58]

$$\delta M_2 = \frac{\bar{\Lambda}^2}{6m_Q}\left[5\left(\frac{m_2^3}{m_4^3} - 1\right) + 4w_4(m_2a)^3\right], \tag{A16}$$

and m_2, m_4, and w_4 are functions of m_0a and, hence, κ. (See Refs. [36, 63] for explicit expressions.) Equating M_2 to a physical meson mass means that we choose κ such that $m_2(\kappa) + \delta M_2 = m_Q$, thereby making in ϕ a relative error

$$\texttt{error}_2 = \bar{\Lambda}\left(\frac{1}{2m_2} - \frac{1}{2m_Q}\right) = \bar{\Lambda}\left(\frac{1}{2m_Q - 2\delta M_2} - \frac{1}{2m_Q}\right) \approx \bar{\Lambda}\frac{\delta M_2}{2m_Q^2}. \tag{A17}$$

The right-most expression is $(a\bar{\Lambda})^3\, f_2(m_0 a)$, $f_2 = [\,]/12(m_2 a)^3$, where $[\,]$ is the bracket in Eq. (A16). It is formally smaller than the other errors considered here—f_2 is of order 1 for all $m_0 a$. Numerically, however, it is not much smaller.

At the tree level the chromomagnetic mismatch is

$$f_B^{[0]}(m_0 a) = \frac{c_B - 1}{2(1 + m_0 a)}. \tag{A18}$$

This has the right asymptotic behavior in both limits, so our Ansatz for the one-loop mismatch function is simply

$$f_B(m_0 a) = \frac{\alpha_s}{2(1 + m_0 a)}, \tag{A19}$$

and $\texttt{error}_B$ is this function multiplied by $a\Lambda$. We take $\alpha_s = 0.288$ on the $a \approx 0.12$ fm ensembles, which is the value determined for α_V from the plaquette [79] with one-loop running to scale $q^* = 2.5/a$. On other ensembles, α_s is found by assuming that the measured average taste splitting goes like $\alpha_s^2 a^2$ (with a determined from r_1/a). This gives α_s values that track $\alpha_V(q^* = 2.5/a)$ quite well, which is why we make that q^* choice. The results are rather insensitive to the details here. For example, using $\alpha_s = 0.325$ on the $a \approx 0.12$ fm ensembles, which corresponds to $q^* = 2.0/a$, increases the error estimate by less than 0.6 MeV for f_{D^+}, and less than 0.25 MeV for f_{B^+}.

The current leads to one more term, with tree-level mismatch function

$$f_3^{[0]}(m_0 a) = \frac{m_0 a}{2(2 + m_0 a)(1 + m_0 a)} - d_1, \tag{A20}$$

and the tree-level d_1 is chosen so that $f_3^{[0]} = 0$. As with the mismatch function f_B, we would like to anticipate $f_3^{[1]}$ by setting $d_1^{[1]} = 0$ and multiplying the rest with α_s. But it is not generic that this vanishes as $m_0 a \to 0$. Therefore, we take

$$f_3(m_0 a) = \frac{\alpha_s}{2(2 + m_0 a)}, \tag{A21}$$

which has the right asymptotic behavior. We take the prior width as $\sqrt{2}$, because A^4 has two such corrections [40].

3. Dispersion relation, Eq. (3.1)

We take a similar approach to the dispersion relation, Eq. (3.1), with the difference that we now know the sign of the leading effect.

The tree-level functions are

$$a_4^{[0]} = \frac{1}{(m_2^{[0]} a)^2} - \frac{m_1^{[0]} a}{(m_4^{[0]} a)^3}, \tag{A22}$$

$$a_{4'}^{[0]} = m_1^{[0]} a\, w_4^{[0]}. \tag{A23}$$

The binding energy enters A_4 and $A_{4'}$ via the meson's kinetic energy. Hence, the binding contributions are

$$A_4' = \frac{3 m_1^{[0]} a}{m_2^{[0]} a\, (m_4^{[0]} a)^3} - \frac{2}{(m_2^{[0]} a)^3} -]\frac{1}{(m_4^{[0]} a)^3}, \tag{A24}$$

$$A_{4'}' = w_4^{[0]} \left(1 - \frac{m_1^{[0]} a}{m_2^{[0]} a}\right), \tag{A25}$$

and in Eq. (3.4) the binding energy floats within a Gaussian prior described by $(\bar{\Lambda}, \sigma_{\bar{\Lambda}}) = (600, 400)$ MeV. This choice conservatively brackets the binding energy of a heavy-strange meson. For the higher-order perturbative contribution to the coefficients, we take the Ansätze based on the asymptotic behavior:

$$a_4^{[1]} = \frac{y_4 + z_4 \ln(1 + m_0 a)}{(1 + m_0 a)^2}, \tag{A26}$$

$$a_{4'}^{[1]} = \frac{y_{4'} m_0 a + z_{4'} \ln(1 + m_0 a)}{1 + m_0 a}, \tag{A27}$$

where the ys and zs float within Gaussian priors described by $(y_4, \sigma_{y_4}) = (3, 5)$, $(z_4, \sigma_{z_4}) = (1, 2)$, $(y_{4'}, \sigma_{y_{4'}}) = (0, 0)$, and $(z_{4'}, \sigma_{z_{4'}}) = (0, 2)$. The terms proportional to y_i stem from the $m_0 a \to 0$ limit, in which the renormalization of m_4 must coincide with that of m_1, and $a_4 = m_1 a\, w_4$ must vanish like $m_0 a$. The terms proportional to z_i stem from the $m_0 a \to \infty$ limit, where the static limit is obtained. Except for $y_{4'}$, the numerical values have been chosen consistent with one-loop experience for m_1 and m_2 [113]. We have set $y_{4'} \equiv 0$, because at small $m_0 a$ it is indistinguishable from the other term in $a_{4'}^{[1]}$, and our range of $m_0 a$ does not reach far into the region $m_0 a \gg 1$.

Appendix B: Two point fit results from Analysis I

TABLE XIV. Heavy-light pseudoscalar meson masses and renormalized decay amplitudes obtained from Analysis I fits of the charm correlators at lattice spacing $a \approx 0.09$ fm.

am_l/am_s	am_q	aM_H	$a^{3/2}\phi_H$	χ^2/dof	p
0.0031/0.031	0.0031	0.7523(0.0016)	0.0857(0.0015)	58/48	0.23
0.0031/0.031	0.0044	0.7553(0.0014)	0.0873(0.0013)	56/48	0.28
0.0031/0.031	0.0062	0.7589(0.0011)	0.0890(0.0011)	55/48	0.33
0.0031/0.031	0.0087	0.7634(0.0009)	0.0910(0.0009)	53/48	0.38
0.0031/0.031	0.0124	0.7699(0.0007)	0.0936(0.0007)	53/48	0.41
0.0031/0.031	0.0186	0.7807(0.0005)	0.0978(0.0006)	52/48	0.44
0.0031/0.031	0.0272	0.7954(0.0004)	0.1030(0.0005)	50/48	0.5
0.0031/0.031	0.031	0.8018(0.0004)	0.1052(0.0004)	50/48	0.5
0.0062/0.031	0.0031	0.7541(0.0030)	0.0875(0.0027)	56/48	0.37
0.0062/0.031	0.0044	0.7577(0.0023)	0.0899(0.0021)	52/48	0.49
0.0062/0.031	0.0062	0.7613(0.0019)	0.0917(0.0018)	50/48	0.58
0.0062/0.031	0.0087	0.7654(0.0015)	0.0933(0.0015)	58/51	0.43
0.0062/0.031	0.0124	0.7712(0.0012)	0.0952(0.0012)	52/48	0.48
0.0062/0.031	0.0186	0.7810(0.0009)	0.0985(0.0010)	56/48	0.37
0.0062/0.031	0.0272	0.7952(0.0006)	0.1032(0.0008)	59/48	0.28
0.0062/0.031	0.031	0.8015(0.0005)	0.1052(0.0007)	60/48	0.25
0.0124/0.031	0.0031	0.7551(0.0038)	0.0930(0.0036)	60/48	0.27
0.0124/0.031	0.0042	0.7554(0.0031)	0.0926(0.0028)	65/48	0.15
0.0124/0.031	0.0062	0.7574(0.0023)	0.0929(0.0021)	65/48	0.16
0.0124/0.031	0.0087	0.7608(0.0017)	0.0938(0.0015)	59/48	0.28
0.0124/0.031	0.0124	0.7666(0.0013)	0.0957(0.0012)	49/48	0.63
0.0124/0.031	0.0186	0.7766(0.0008)	0.0991(0.0009)	42/48	0.85
0.0124/0.031	0.0272	0.7907(0.0006)	0.1038(0.0007)	48/48	0.64
0.0124/0.031	0.031	0.7969(0.0005)	0.1058(0.0006)	53/48	0.47

TABLE XV. Heavy-light pseudoscalar meson masses and renormalized decay amplitudes obtained from Analysis I fits of the charm correlators at lattice spacing $a \approx 0.12$ fm.

am_l/am_s	am_q	aM_H	$a^{3/2}\phi_H$	χ^2/dof	p
0.005/0.050	0.005	0.9943(0.0032)	0.1436(0.0030)	30/30	0.52
0.005/0.050	0.007	0.9977(0.0024)	0.1453(0.0024)	29/30	0.6
0.005/0.050	0.01	1.0026(0.0018)	0.1477(0.0019)	28/30	0.64
0.005/0.050	0.014	1.0090(0.0016)	0.1508(0.0017)	28/30	0.64
0.005/0.050	0.02	1.0186(0.0013)	0.1551(0.0015)	29/30	0.58
0.005/0.050	0.03	1.0345(0.0010)	0.1620(0.0012)	33/30	0.42
0.005/0.050	0.0415	1.0526(0.0008)	0.1694(0.0010)	36/30	0.27
0.007/0.050	0.005	0.9948(0.0035)	0.1442(0.0035)	17/30	0.98
0.007/0.050	0.007	0.9975(0.0027)	0.1455(0.0028)	19/30	0.95
0.007/0.050	0.01	1.0019(0.0021)	0.1476(0.0021)	22/30	0.89
0.007/0.050	0.014	1.0081(0.0016)	0.1504(0.0017)	24/30	0.83
0.007/0.050	0.02	1.0178(0.0012)	0.1547(0.0014)	23/30	0.85
0.007/0.050	0.03	1.0338(0.0009)	0.1615(0.0010)	20/30	0.94
0.007/0.050	0.0415	1.0520(0.0007)	0.1687(0.0008)	19/30	0.95
0.010/0.050	0.005	0.9958(0.0039)	0.1461(0.0041)	15/30	0.99
0.010/0.050	0.007	1.0000(0.0031)	0.1486(0.0032)	20/30	0.94
0.010/0.050	0.01	1.0057(0.0024)	0.1516(0.0026)	26/30	0.75
0.010/0.050	0.014	1.0126(0.0019)	0.1549(0.0021)	29/27	0.41
0.010/0.050	0.02	1.0226(0.0015)	0.1594(0.0017)	33/30	0.39
0.010/0.050	0.03	1.0387(0.0011)	0.1662(0.0014)	31/30	0.5
0.010/0.050	0.0415	1.0567(0.0008)	0.1733(0.0011)	27/30	0.68
0.020/0.050	0.005	0.9942(0.0046)	0.1537(0.0050)	49/30	0.036
0.020/0.050	0.007	0.9959(0.0036)	0.1533(0.0039)	49/30	0.036
0.020/0.050	0.01	0.9987(0.0027)	0.1532(0.0031)	48/30	0.051
0.020/0.050	0.014	1.0037(0.0021)	0.1543(0.0024)	45/30	0.075
0.020/0.050	0.02	1.0124(0.0016)	0.1575(0.0019)	43/30	0.11
0.020/0.050	0.03	1.0274(0.0011)	0.1632(0.0014)	37/30	0.27
0.020/0.050	0.0415	1.0447(0.0009)	0.1695(0.0012)	32/30	0.48
0.030/0.050	0.005	0.9830(0.0042)	0.1475(0.0042)	33/30	0.39
0.030/0.050	0.007	0.9853(0.0033)	0.1485(0.0033)	33/30	0.4
0.030/0.050	0.01	0.9897(0.0025)	0.1505(0.0025)	32/30	0.47
0.030/0.050	0.014	0.9960(0.0020)	0.1534(0.0020)	31/30	0.53
0.030/0.050	0.02	1.0054(0.0015)	0.1574(0.0016)	32/30	0.46
0.030/0.050	0.03	1.0205(0.0011)	0.1633(0.0012)	37/30	0.27
0.030/0.050	0.0415	1.0376(0.0009)	0.1695(0.0010)	40/30	0.15

TABLE XVI. Heavy-light pseudoscalar meson masses and renormalized decay amplitudes obtained from Analysis I fits of the charm correlators at lattice spacing $a \approx 0.15$ fm.

am_l/am_s	am_q	aM_H	$a^{3/2}\phi_H$	χ^2/dof	p
0.0097/0.0484	0.0048	1.1659(0.0044)	0.1979(0.0052)	20/20	0.5
0.0097/0.0484	0.007	1.1710(0.0034)	0.2017(0.0040)	22/20	0.37
0.0097/0.0484	0.0097	1.1768(0.0027)	0.2054(0.0032)	25/20	0.26
0.0097/0.0484	0.0194	1.1951(0.0016)	0.2159(0.0020)	25/20	0.26
0.0097/0.0484	0.029	1.2117(0.0012)	0.2242(0.0015)	20/20	0.51
0.0097/0.0484	0.0484	1.2432(0.0009)	0.2385(0.0012)	15/20	0.79
0.0194/0.0484	0.0048	1.1726(0.0046)	0.2106(0.0052)	23/20	0.35
0.0194/0.0484	0.007	1.1749(0.0036)	0.2105(0.0041)	23/20	0.35
0.0194/0.0484	0.0097	1.1785(0.0028)	0.2113(0.0031)	23/20	0.32
0.0194/0.0484	0.0194	1.1935(0.0016)	0.2174(0.0020)	30/20	0.092
0.0194/0.0484	0.029	1.2091(0.0013)	0.2244(0.0016)	32/20	0.055
0.0194/0.0484	0.0484	1.2400(0.0010)	0.2381(0.0013)	27/20	0.17
0.0290/0.0484	0.0048	1.1613(0.0044)	0.1975(0.0049)	17/20	0.72
0.0290/0.0484	0.007	1.1660(0.0034)	0.2010(0.0040)	18/20	0.64
0.0290/0.0484	0.0097	1.1717(0.0026)	0.2049(0.0031)	21/20	0.47
0.0290/0.0484	0.0194	1.1896(0.0015)	0.2151(0.0019)	24/20	0.3
0.0290/0.0484	0.029	1.2058(0.0011)	0.2229(0.0015)	23/20	0.32
0.0290/0.0484	0.0484	1.2368(0.0008)	0.2364(0.0011)	20/20	0.49

TABLE XVII. Heavy-light pseudoscalar meson masses and renormalized decay amplitudes obtained from Analysis I fits of the bottom correlators at lattice spacing $a \approx 0.09$ fm.

am_l/am_s	am_q	aM_H	$a^{3/2}\phi_H$	χ^2/dof	p
0.0031/0.031	0.0031	1.6509(0.0018)	0.1359(0.0016)	41/39	0.48
0.0031/0.031	0.0044	1.6532(0.0016)	0.1378(0.0015)	40/39	0.51
0.0031/0.031	0.0062	1.6562(0.0015)	0.1402(0.0014)	40/39	0.49
0.0031/0.031	0.0087	1.6601(0.0013)	0.1433(0.0014)	42/39	0.42
0.0031/0.031	0.0124	1.6659(0.0012)	0.1475(0.0013)	45/39	0.31
0.0031/0.031	0.0186	1.6752(0.0011)	0.1542(0.0012)	47/39	0.23
0.0031/0.031	0.0272	1.6879(0.0009)	0.1628(0.0011)	49/39	0.19
0.0031/0.031	0.031	1.6934(0.0009)	0.1664(0.0011)	49/39	0.18
0.0062/0.031	0.0031	1.6539(0.0046)	0.1358(0.0051)	40/39	0.56
0.0062/0.031	0.0044	1.6557(0.0039)	0.1377(0.0044)	37/39	0.68
0.0062/0.031	0.0062	1.6584(0.0032)	0.1402(0.0037)	34/39	0.77
0.0062/0.031	0.0087	1.6620(0.0027)	0.1434(0.0031)	34/39	0.8
0.0062/0.031	0.0124	1.6675(0.0022)	0.1480(0.0026)	36/39	0.72
0.0062/0.031	0.0186	1.6767(0.0018)	0.1550(0.0022)	41/39	0.53
0.0062/0.031	0.0272	1.6892(0.0014)	0.1637(0.0019)	45/39	0.37
0.0062/0.031	0.031	1.6946(0.0014)	0.1672(0.0018)	45/39	0.35
0.0124/0.031	0.0031	1.6532(0.0036)	0.1387(0.0038)	52/39	0.16
0.0124/0.031	0.0042	1.6550(0.0033)	0.1407(0.0034)	48/39	0.27
0.0124/0.031	0.0062	1.6576(0.0030)	0.1432(0.0031)	40/39	0.55
0.0124/0.031	0.0087	1.6606(0.0027)	0.1456(0.0029)	35/39	0.77
0.0124/0.031	0.0124	1.6650(0.0024)	0.1488(0.0027)	33/39	0.84
0.0124/0.031	0.0186	1.6730(0.0019)	0.1544(0.0023)	36/39	0.73
0.0124/0.031	0.0272	1.6847(0.0016)	0.1623(0.0021)	42/39	0.48
0.0124/0.031	0.031	1.6900(0.0015)	0.1657(0.0020)	45/39	0.38

TABLE XVIII. Heavy-light pseudoscalar meson masses and renormalized decay amplitudes obtained from Analysis I fits of the bottom correlators at lattice spacing $a \approx 0.12$ fm.

am_l/am_s	am_q	aM_H	$a^{3/2}\phi_H$	χ^2/dof	p
0.005/0.050	0.005	1.9170(0.0044)	0.2236(0.0050)	45/27	0.03
0.005/0.050	0.007	1.9197(0.0039)	0.2263(0.0046)	46/27	0.022
0.005/0.050	0.01	1.9235(0.0033)	0.2300(0.0040)	46/27	0.021
0.005/0.050	0.014	1.9287(0.0029)	0.2347(0.0036)	45/27	0.027
0.005/0.050	0.02	1.9367(0.0024)	0.2418(0.0031)	43/27	0.046
0.005/0.050	0.03	1.9503(0.0020)	0.2532(0.0026)	39/27	0.096
0.005/0.050	0.0415	1.9657(0.0017)	0.2654(0.0023)	36/27	0.17
0.007/0.050	0.005	1.9147(0.0036)	0.2224(0.0039)	37/27	0.12
0.007/0.050	0.007	1.9177(0.0033)	0.2254(0.0037)	35/27	0.17
0.007/0.050	0.01	1.9219(0.0030)	0.2292(0.0036)	34/27	0.2
0.007/0.050	0.014	1.9272(0.0028)	0.2337(0.0037)	35/27	0.19
0.007/0.050	0.02	1.9351(0.0026)	0.2401(0.0037)	36/27	0.15
0.007/0.050	0.03	1.9485(0.0022)	0.2508(0.0035)	38/27	0.096
0.007/0.050	0.0415	1.9638(0.0019)	0.2628(0.0031)	40/27	0.07
0.010/0.050	0.005	1.9182(0.0047)	0.2254(0.0047)	30/27	0.4
0.010/0.050	0.007	1.9207(0.0041)	0.2284(0.0042)	32/27	0.29
0.010/0.050	0.01	1.9250(0.0035)	0.2328(0.0037)	36/27	0.18
0.010/0.050	0.014	1.9307(0.0030)	0.2383(0.0033)	39/27	0.097
0.010/0.050	0.02	1.9391(0.0025)	0.2457(0.0028)	43/27	0.048
0.010/0.050	0.03	1.9527(0.0020)	0.2569(0.0024)	47/27	0.02
0.010/0.050	0.0415	1.9682(0.0017)	0.2689(0.0021)	51/27	0.0092
0.020/0.050	0.005	1.9136(0.0060)	0.2278(0.0069)	33/27	0.27
0.020/0.050	0.007	1.9163(0.0050)	0.2305(0.0059)	33/27	0.28
0.020/0.050	0.01	1.9200(0.0042)	0.2340(0.0050)	31/27	0.36
0.020/0.050	0.014	1.9249(0.0036)	0.2381(0.0043)	29/27	0.47
0.020/0.050	0.02	1.9322(0.0031)	0.2437(0.0039)	28/27	0.52
0.020/0.050	0.03	1.9445(0.0027)	0.2526(0.0038)	30/27	0.42
0.020/0.050	0.0415	1.9590(0.0025)	0.2627(0.0039)	33/27	0.3
0.030/0.050	0.005	1.9030(0.0058)	0.2196(0.0073)	38/27	0.12
0.030/0.050	0.007	1.9058(0.0049)	0.2223(0.0064)	32/27	0.29
0.030/0.050	0.01	1.9099(0.0041)	0.2258(0.0056)	27/27	0.56
0.030/0.050	0.014	1.9155(0.0034)	0.2306(0.0048)	23/27	0.74
0.030/0.050	0.02	1.9239(0.0028)	0.2376(0.0040)	22/27	0.77
0.030/0.050	0.03	1.9372(0.0022)	0.2479(0.0034)	25/27	0.64
0.030/0.050	0.0415	1.9518(0.0019)	0.2585(0.0032)	28/27	0.49

TABLE XIX. Heavy-light pseudoscalar meson masses and renormalized decay amplitudes obtained from Analysis I fits of the bottom correlators at lattice spacing $a \approx 0.15$ fm.

am_l/am_s	am_q	aM_H	$a^{3/2}\phi_H$	χ^2/dof	p
0.0097/0.0484	0.0048	2.2553(0.0071)	0.3311(0.0115)	36/25	0.097
0.0097/0.0484	0.007	2.2576(0.0061)	0.3341(0.0102)	37/25	0.09
0.0097/0.0484	0.0097	2.2611(0.0052)	0.3389(0.0089)	36/25	0.1
0.0097/0.0484	0.0194	2.2757(0.0036)	0.3568(0.0063)	34/25	0.16
0.0097/0.0484	0.029	2.2901(0.0030)	0.3727(0.0053)	33/25	0.16
0.0097/0.0484	0.0484	2.3175(0.0023)	0.4002(0.0046)	35/25	0.12
0.0194/0.0484	0.0048	2.2296(0.0175)	0.2743(0.0416)	32/25	0.2
0.0194/0.0484	0.007	2.2349(0.0142)	0.2823(0.0357)	34/25	0.15
0.0194/0.0484	0.0097	2.2416(0.0118)	0.2917(0.0309)	36/25	0.1
0.0194/0.0484	0.0194	2.2639(0.0072)	0.3243(0.0202)	36/25	0.1
0.0194/0.0484	0.029	2.2819(0.0054)	0.3482(0.0152)	30/25	0.27
0.0194/0.0484	0.0484	2.3124(0.0038)	0.3839(0.0109)	24/25	0.59
0.0290/0.0484	0.0048	2.2402(0.0073)	0.3101(0.0123)	29/25	0.32
0.0290/0.0484	0.007	2.2464(0.0061)	0.3199(0.0104)	30/25	0.28
0.0290/0.0484	0.0097	2.2524(0.0052)	0.3289(0.0089)	31/25	0.25
0.0290/0.0484	0.0194	2.2695(0.0036)	0.3502(0.0066)	27/25	0.42
0.0290/0.0484	0.029	2.2847(0.0030)	0.3665(0.0058)	21/25	0.72
0.0290/0.0484	0.0484	2.3125(0.0025)	0.3939(0.0057)	18/25	0.87

[1] M. Bona *et al.* (UTfit), Phys. Lett. **B687**, 61 (2010), arXiv:0908.3470 [hep-ph].
[2] A. Lenz *et al.* (CKMfitter), Phys. Rev. **D83**, 036004 (2011), arXiv:1008.1593 [hep-ph].
[3] E. Lunghi and A. Soni, Phys. Lett. **B697**, 323 (2011), arXiv:1010.6069 [hep-ph].
[4] J. Laiho, E. Lunghi, and R. Van de Water, PoS **FPCP2010**, 040 (2010), arXiv:1102.3917 [hep-ph].
[5] K. Hara *et al.* (Belle), Phys. Rev. **D82**, 071101 (2010), arXiv:1006.4201 [hep-ex].
[6] P. del Amo Sanchez *et al.* (BaBar)(2010), arXiv:1008.0104 [hep-ex].
[7] M. Masuzawa, in *Proceedings of IPAC 2010*, edited by K. Oide (2010) `http://accelconf.web.cern.ch/AccelConf/IPAC10/`.
[8] T. Iijima, "Search for Charged Higgs in $B \to \tau\nu$ and $D \to \tau\nu$ Decays," (2009), `http://kds.kek.jp/materialDisplay.py?contribId=5&sessionId=2&materialId=slides&confId=2865`.
[9] B. O'Leary *et al.* (SuperB)(2010), arXiv:1008.1541 [hep-ex].
[10] M. E. Biagini *et al.* (SuperB)(2010), arXiv:1009.6178 [physics.acc-ph].
[11] E. Lunghi and A. Soni, Phys. Rev. Lett. **104**, 251802 (2010), arXiv:0912.0002 [hep-ph].
[12] C. T. H. Davies *et al.* (HPQCD, MILC, and Fermilab Lattice), Phys. Rev. Lett. **92**, 022001 (2004), arXiv:hep-lat/0304004.
[13] L. Susskind, Phys. Rev. **D16**, 3031 (1977).
[14] H. S. Sharatchandra, H. J. Thun, and P. Weisz, Nucl. Phys. **B192**, 205 (1981).
[15] C. Aubin *et al.* (MILC), Phys. Rev. **D70**, 114501 (2004), arXiv:hep-lat/0407028 [hep-lat].
[16] I. F. Allison *et al.* (HPQCD), Phys. Rev. Lett. **94**, 172001 (2005), arXiv:hep-lat/0411027.
[17] S. Prelovšek, Phys. Rev. **D73**, 014506 (2006), arXiv:hep-lat/0510080.
[18] C. Bernard, Phys. Rev. **D73**, 114503 (2006), arXiv:hep-lat/0603011.
[19] C. Bernard, C. E. DeTar, Z. Fu, and S. Prelovšek, Phys. Rev. **D76**, 094504 (2007), arXiv:0707.2402 [hep-lat].
[20] C. Aubin, J. Laiho, and R. S. Van de Water, Phys. Rev. **D77**, 114501 (2008), arXiv:0803.0129 [hep-lat].
[21] C. Bernard, M. Golterman, and Y. Shamir, Phys. Rev. **D73**, 114511 (2006), arXiv:hep-lat/0604017 [hep-lat].
[22] Y. Shamir, Phys. Rev. **D71**, 034509 (2005), arXiv:hep-lat/0412014.
[23] Y. Shamir, Phys. Rev. **D75**, 054503 (2007), arXiv:hep-lat/0607007.
[24] C. Bernard, M. Golterman, and Y. Shamir, Phys. Rev. **D77**, 074505 (2008), arXiv:0712.2560 [hep-lat].
[25] W.-J. Lee and S. R. Sharpe, Phys. Rev. **D60**, 114503 (1999), arXiv:hep-lat/9905023.
[26] C. Aubin and C. Bernard, Phys. Rev. **D68**, 034014 (2003), hep-lat/0304014.
[27] S. R. Sharpe and R. S. Van de Water, Phys. Rev. **D71**, 114505 (2005), arXiv:hep-lat/0409018.
[28] S. R. Sharpe, PoS **LAT2006**, 022 (2006), arXiv:hep-lat/0610094.
[29] A. S. Kronfeld, PoS **LAT2007**, 016 (2007), arXiv:0711.0699 [hep-lat].
[30] M. Golterman, PoS **CONFINEMENT8**, 014 (2008), arXiv:0812.3110 [hep-ph].
[31] A. Bazavov *et al.*, Rev. Mod. Phys. **82**, 1349 (2010), arXiv:0903.3598 [hep-lat].
[32] G. C. Donald, C. T. H. Davies, E. Follana, and A. S. Kronfeld, Phys. Rev. **D84**, 054501 (2011), arXiv:1106.2412 [hep-lat].
[33] J. Laiho, E. Lunghi, and R. S. Van de Water, Phys. Rev. **D81**, 034503 (2010), arXiv:0910.2928 [hep-ph].
[34] C. W. Bernard *et al.*, Phys. Rev. **D64**, 054506 (2001), arXiv:hep-lat/0104002.
[35] B. Sheikholeslami and R. Wohlert, Nucl. Phys. **B259**, 572 (1985).
[36] A. X. El-Khadra, A. S. Kronfeld, and P. B. Mackenzie, Phys. Rev. **D55**, 3933 (1997), arXiv:hep-lat/9604004.
[37] K. Symanzik, Nucl. Phys. **B226**, 187 (1983).
[38] K. Symanzik, Nucl. Phys. **B226**, 205 (1983).
[39] A. S. Kronfeld, Phys. Rev. **D62**, 014505 (2000), arXiv:hep-lat/0002008.
[40] J. Harada *et al.*, Phys. Rev. **D65**, 094513 (2002), [Erratum-ibid. **D71**, 019903 (2005)], arXiv:hep-lat/0112044.
[41] J. Harada *et al.*, Phys. Rev. **D65**, 094514 (2002), arXiv:hep-lat/0112045.
[42] C. Aubin and C. Bernard, Phys. Rev. **D73**, 014515 (2006), arXiv:hep-lat/0510088.
[43] J. Laiho and R. S. Van de Water, Phys. Rev. **D73**, 054501 (2006), arXiv:hep-lat/0512007.
[44] C. Aubin and C. Bernard, Phys. Rev. **D76**, 014002 (2007), arXiv:0704.0795 [hep-lat].
[45] A. X. El-Khadra, A. S. Kronfeld, P. B. Mackenzie, S. M. Ryan, and J. N. Simone, Phys. Rev. **D64**, 014502 (2001), arXiv:hep-ph/0101023.
[46] A. X. El-Khadra, E. Gámiz, A. S. Kronfeld, and M. A. Nobes, PoS **LAT2007**, 242 (2007), arXiv:0710.1437 [hep-lat].
[47] C. Aubin *et al.* (Fermilab Lattice and MILC), Phys. Rev. Lett. **95**, 122002 (2005), arXiv:hep-lat/0506030.
[48] C. Bernard *et al.* (Fermilab Lattice and MILC), PoS **LAT2006**, 094 (2006).
[49] C. Bernard *et al.* (Fermilab Lattice and MILC), PoS **LAT2007**, 370 (2007).
[50] C. Bernard *et al.* (Fermilab Lattice and MILC), PoS **LATTICE2008**, 278 (2008), arXiv:0904.1895 [hep-lat].
[51] A. Bazavov *et al.* (Fermilab Lattice and MILC), PoS **LAT2009**, 249 (2009), arXiv:0912.5221 [hep-lat].
[52] J. Simone *et al.* (Fermilab Lattice and MILC), PoS **LATTICE2010**, 317 (2010).
[53] J. L. Rosner and S. Stone(2010), in Ref. [54], arXiv:1002.1655 [hep-ex].
[54] K. Nakamura *et al.* (Particle Data Group), J. Phys. **G37**, 075021 (2010), and 2011 partial update for the 2012 edition.
[55] C. Aubin *et al.* (Fermilab Lattice and MILC), Phys. Rev. Lett. **94**, 011601 (2005), arXiv:hep-ph/0408306.
[56] C. Bernard *et al.* (Fermilab Lattice and MILC), Phys. Rev. **D79**, 014506 (2009), arXiv:0808.2519 [hep-lat].
[57] J. A. Bailey *et al.* (Fermilab Lattice and MILC), Phys. Rev. **D79**, 054507 (2009), arXiv:0811.3640 [hep-lat].
[58] C. Bernard *et al.* (Fermilab Lattice and MILC), Phys. Rev. **D83**, 034503 (2011), arXiv:1003.1937 [hep-lat].

[59] G. P. Lepage, Phys. Rev. **D59**, 074502 (1999), arXiv:hep-lat/9809157.
[60] M. Lüscher and P. Weisz, Phys. Lett. **B158**, 250 (1985).
[61] Z. Hao, G. M. von Hippel, R. R. Horgan, Q. J. Mason, and H. D. Trottier, Phys. Rev. **D76**, 034507 (2007), arXiv:0705.4660 [hep-lat].
[62] K. G. Wilson, "Quarks and Strings on a Lattice," in *New Phenomena In Subnuclear Physics*, edited by A. Zichichi (Plenum, New York, 1975) p. 69, cLNS-321.
[63] M. B. Oktay and A. S. Kronfeld, Phys. Rev. **D78**, 014504 (2008), arXiv:0803.0523 [hep-lat].
[64] H.-W. Lin and N. Christ, Phys. Rev. **D76**, 074506 (2007), arXiv:hep-lat/0608005.
[65] G. P. Lepage, L. Magnea, C. Nakhleh, U. Magnea, and K. Hornbostel, Phys. Rev. **D46**, 4052 (1992), arXiv:hep-lat/9205007.
[66] R. Sommer, Nucl. Phys. **B411**, 839 (1994), arXiv:hep-lat/9310022.
[67] C. W. Bernard *et al.*, Phys. Rev. **D62**, 034503 (2000), arXiv:hep-lat/0002028.
[68] C. R. Allton(1996), hep-lat/9610016.
[69] A. Bazavov *et al.* (MILC), PoS **CD09**, 007 (2009), arXiv:0910.2966 [hep-ph].
[70] C. T. H. Davies, E. Follana, I. D. Kendall, G. P. Lepage, and C. McNeile (HPQCD), Phys. Rev. **D81**, 034506 (2010), arXiv:0910.1229 [hep-lat].
[71] G. P. Lepage *et al.*, Nucl. Phys. Proc. Suppl. **106**, 12 (2002), arXiv:hep-lat/0110175.
[72] C. Morningstar, Nucl. Phys. Proc. Suppl. **109A**, 185 (2002), arXiv:hep-lat/0112023.
[73] A. S. Kronfeld, Nucl. Phys. Proc. Suppl. **53**, 401 (1997), arXiv:hep-lat/9608139.
[74] N. Kawamoto and J. Smit, Nucl. Phys. **B192**, 100 (1981).
[75] J. L. Richardson, Phys. Lett. **B82**, 272 (1979).
[76] D. P. Menscher, "Charmonium and Charmed Mesons with Improved Lattice QCD," (2005), PhD thesis.
[77] M. Wingate, J. Shigemitsu, C. T. H. Davies, G. P. Lepage, and H. D. Trottier, Phys. Rev. **D67**, 054505 (2003), arXiv:hep-lat/0211014.
[78] M. D. Pierro and E. Eichten, Phys. Rev. **D64**, 114004 (2001), hep-ph/0104208, `http://arxiv.org/abs/hep-ph/0104208`.
[79] G. P. Lepage and P. B. Mackenzie, Phys. Rev. **D48**, 2250 (1993), arXiv:hep-lat/9209022.
[80] Q. Mason *et al.* (HPQCD), Phys. Rev. Lett. **95**, 052002 (2005), arXiv:hep-lat/0503005.
[81] K. Hornbostel, G. P. Lepage, and C. Morningstar, Phys. Rev. **D67**, 034023 (2003), arXiv:hep-ph/0208224.
[82] D. Arndt and C. J. D. Lin, Phys. Rev. **D70**, 014503 (2004), arXiv:hep-lat/0403012.
[83] C. Bernard (MILC), Phys. Rev. **D65**, 054031 (2002), arXiv:hep-lat/0111051.
[84] A. S. Kronfeld and S. M. Ryan, Phys. Lett. **B543**, 59 (2002), arXiv:hep-ph/0206058.
[85] C. G. Boyd and B. Grinstein, Nucl. Phys. **B442**, 205 (1995), arXiv:hep-ph/9402340.
[86] I. W. Stewart, Nucl. Phys. **B529**, 62 (1998), arXiv:hep-ph/9803227.
[87] D. Bećirević, S. Prelovšek, and J. Zupan, Phys. Rev. **D68**, 074003 (2003), arXiv:hep-lat/0305001.
[88] C. Bernard *et al.* (MILC), PoS **LATTICE2007**, 090 (2007), arXiv:0710.1118 [hep-lat].
[89] R. Casalbuoni *et al.*, Phys. Rept. **281**, 145 (1997), arXiv:hep-ph/9605342 [hep-ph].
[90] A. Anastassov *et al.* (CLEO), Phys. Rev. **D65**, 032003 (2002), arXiv:hep-ex/0108043.
[91] A. Abada *et al.*, Nucl. Phys. Proc. Suppl. **119**, 641 (2003), arXiv:hep-lat/0209092.
[92] M. C. Arnesen, B. Grinstein, I. Z. Rothstein, and I. W. Stewart, Phys. Rev. Lett. **95**, 071802 (2005), arXiv:hep-ph/0504209.
[93] H. Ohki, H. Matsufuru, and T. Onogi, Phys. Rev. **D77**, 094509 (2008), arXiv:0802.1563 [hep-lat].
[94] J. Bulava, M. A. Donnellan, and R. Sommer (ALPHA), PoS **LATTICE2010**, 303 (2010), arXiv:1011.4393 [hep-lat].
[95] C. Aubin *et al.* (HPQCD), Phys. Rev. **D70**, 031504 (2004), arXiv:hep-lat/0405022.
[96] C. Bernard *et al.* (MILC), Phys. Rev. **D66**, 094501 (2002), arXiv:hep-lat/0206016.
[97] G. P. Lepage, in *From actions to answers. Proceedings, Theoretical Advanced Study Institute in Elementary Particle Physics, Boulder, USA, June 5-30, 1989*, edited by T. A. DeGrand and D. Toussaint (World Scientific, 1989).
[98] A. Bazavov *et al.* (MILC), PoS **LATTICE2010**, 074 (2010), arXiv:1012.0868 [hep-lat].
[99] C. T. H. Davies, C. McNeile, E. Follana, G. P. Lepage, H. Na, *et al.* (HPQCD), Phys. Rev. **D82**, 114504 (2010), arXiv:1008.4018 [hep-lat].
[100] P. Dimopoulos *et al.* (ETM)(2011), arXiv:1107.1441 [hep-lat].
[101] B. I. Eisenstein *et al.* (CLEO), Phys. Rev. **D78**, 052003 (2008), arXiv:0806.2112 [hep-ex].
[102] J. P. Alexander *et al.* (CLEO), Phys. Rev. **D79**, 052001 (2009), arXiv:0901.1216 [hep-ex].
[103] L. Widhalm *et al.* (Belle), Phys. Rev. Lett. **100**, 241801 (2008), arXiv:0709.1340 [hep-ex].
[104] P. Naik *et al.* (CLEO), Phys. Rev. **D80**, 112004 (2009), arXiv:0910.3602 [hep-ex].
[105] P. U. E. Onyisi *et al.* (CLEO), Phys. Rev. **D79**, 052002 (2009), arXiv:0901.1147 [hep-ex].
[106] J. P. Lees *et al.* (BaBar), Phys. Rev. **D82**, 091103 (2010), arXiv:1003.3063 [hep-ex].
[107] D. Asner *et al.* (Heavy Flavor Averaging Group)(2010), `http://www.slac.stanford.edu/xorg/hfag/charm/CHARM10/f_ds/results_20jan11.html` with future updates at `http://www.slac.stanford.edu/xorg/hfag/charm/`, arXiv:1010.1589 [hep-ex].
[108] C. McNeile, C. T. H. Davies, E. Follana, K. Hornbostel, and G. P. Lepage (HPQCD)(2011), arXiv:1110.4510 [hep-lat].
[109] E. Gámiz, C. T. H. Davies, G. P. Lepage, J. Shigemitsu, and M. Wingate (HPQCD), Phys. Rev. **D80**, 014503 (2009), arXiv:0902.1815 [hep-lat].
[110] C. Albertus *et al.* (RBC and UKQCD), Phys. Rev. **D82**, 014505 (2010), arXiv:1001.2023 [hep-lat].
[111] A. Bazavov *et al.* (MILC), PoS **LATTICE2010**, 320 (2010), arXiv:1012.1265 [hep-lat].
[112] E. Follana, C. T. H. Davies, G. P. Lepage, and J. Shigemitsu (HPQCD), Phys. Rev. Lett. **100**, 062002 (2008),

arXiv:0706.1726 [hep-lat].
[113] B. P. G. Mertens, A. S. Kronfeld, and A. X. El-Khadra, Phys. Rev. **D58**, 034505 (1998), arXiv:hep-lat/9712024.